THE UNIVERSITY OF QUEENSLAND

AUSTRALIA

Mechanical and Microstructural Characterisation in the Processing of Biomedical Metallic Fine Tubes

Yaowu Zhang

Master of Materials Engineering

Bachelor of Materials Engineering

A thesis submitted for the degree of Doctor of Philosophy at

The University of Queensland in 2016

School of Mechanical and Mining Engineering

Abstract

Fine tube stents are used for maintaining localised flow in stenotic blood vessels. Elasticity and plasticity for expansion, rigidity for resisting bending under force and strength to prevent unexpected failure, are required properties of the tubes from which these stents are formed. Biomedical metastable β titanium alloys have been developed as implant materials for a large number of biomedical applications due to a combination of favourable characteristics, e.g. good biocompatibility, excellent toughness and corrosion resistance. A metastable β alloy, Ti-25Nb-3Mo-3Zr-2Sn, has been developed without toxic alloying elements, which is a promising candidate material for stent applications. Metallic materials used for stents are commonly not biodegradable and implanted in the vessel permanently, which may provoke in-stent restenosis and stent thrombosis. In order to remove the implanted materials after service, biodegradable materials, absorbed by the body slowly, are also a field of research interest. Magnesium alloys have been used in studies for biomedical stent applications as a new biodegradable material. Magnesium stents can reopen the blocked blood vessels temporarily before degrading in physiological environments. In addition to the biodegradable characteristics, their mechanical properties are reasonable. The Mg-3Al-1Zn (AZ31) alloy is the subject of some research on the processing of biomedical magnesium alloys as it is a commonly available commercial alloy. Consequently, the Ti-25Nb-3Mo-3Zr-2Sn alloy and the AZ31 magnesium alloy have been used in this thesis to investigate the evolution of mechanical properties and microstructure in the processing of fine tubes.

The deformation mechanisms during cold deformation of metastable β titanium alloys are mainly associated with martensitic phase transformations and mechanical twinning. It has been reported that stress-induced phase transformations and $\{112\}\langle 111\rangle$, $\{332\}\langle 113\rangle$ twinning modes may be activated under different stress states in metastable β titanium alloys. They can exhibit varying elasticity, Young's modulus and strain hardening behaviour. Because the martensitic start temperature is below room temperature for most metastable β titanium alloys, the α″ martensitic transformation can easily occur under a small amount of external stress. Mechanical twins were reported to hinder slip and dislocation motion thereby increasing the strain hardening rate. The development of β and α″ texture during processing is another critical influence on the mechanical properties of fine tubes. Therefore, studies on the martensitic transformation, mechanical twins and texture evolution is of significance in order to understand the processing of β titanium fine tubes.

Magnesium alloys deform through the formation of a large amount of mechanical twins due to the relatively low critical stress to activate twinning in comparison with $\langle c + a \rangle$ slip. There are typically two primary mechanical twinning modes for magnesium alloys, $\{10\bar{1}2\}$ extension twins and $\{10\bar{1}1\}$ contraction twins. Secondary twinning can be activated within reoriented and well-developed primary twins. Mechanical twinning may contribute to reorientations of the twinned grains, resulting in texture evolution. Thus, mechanical anisotropy of magnesium alloys has been frequently reported. Conversely, the activation of twins depends on the texture evolution in magnesium alloys. In this thesis, the activation of different twinning modes has been investigated to reveal the evolution of mechanical properties in the processing of magnesium fine tubes.

Cold rolling is a necessary process to fabricate fine tubes in view of the observed deterioration in performance and grain growth during annealing of fine grain metallic products. In this thesis, cold rolling and intermediate annealing were performed for the Ti-25Nb-3Mo-3Zr-2Sn fine tubes. Processing parameters (cross sectional reduction rate ε and wall thickness to diameter reduction rate Q) were used to analyse their influence on mechanical properties and microstructure. The evolution of strength, modulus, ductility and strain hardening rate during processing has been investigated via tensile tests of cold rolled and annealed fine tubes. Electron Back Scattered Diffraction (EBSD) was used to index and identify stress-induced martensitic phases, mechanical twins and orientation rotations of the β matrix and martensitic α″ phase. The volume fraction of martensitic α″ phase and matrix β phase were quantified using EBSD and their influence on the mechanical properties of the β titanium fine tubes have been studied. For AZ31 fine tubes, EBSD has also been used to identify the primary and secondary twins, as well as pole figures calculated from EBSD for investigating the texture evolution of both the magnesium and β titanium fine tubes during processing. However, fine martensite and secondary twins are difficult to be identified by EBSD, so transmission electron microscopy was used to observe these fine features in order to study the nucleation and growth of the α″ phase at high magnification. The orientation relationships between the phases has been studied to analyse their influence on the mechanical properties of the fine tubes.

Declaration by author

This thesis is composed of my original work, and contains no material previously published or written by another person except where due reference has been made in the text. I have clearly stated the contribution by others to jointly-authored works that I have included in my thesis.

I have clearly stated the contribution of others to my thesis as a whole, including statistical assistance, survey design, data analysis, significant technical procedures, professional editorial advice, and any other original research work used or reported in my thesis. The content of my thesis is the result of work I have carried out since the commencement of my research higher degree candidature and does not include a substantial part of work that has been submitted to qualify for the award of any other degree or diploma in any university or other tertiary institution. I have clearly stated which parts of my thesis, if any, have been submitted to qualify for another award.

I acknowledge that an electronic copy of my thesis must be lodged with the University Library and, subject to the policy and procedures of The University of Queensland, the thesis be made available for research and study in accordance with the Copyright Act 1968 unless a period of embargo has been approved by the Dean of the Graduate School.

I acknowledge that copyright of all material contained in my thesis resides with the copyright holder(s) of that material. Where appropriate I have obtained copyright permission from the copyright holder to reproduce material in this thesis.

Publications during candidature

Zhang, Y., Kent, D., Wang, G., St John, D., & Dargusch, M. (2015). Evolution of the microstructure and mechanical properties during fabrication of mini-tubes from a biomedical β-titanium alloy. *Journal of the Mechanical Behavior of Biomedical Materials*, 42(0), 207-218.

Zhang, Y., Kent, D., Wang, G., St John, D., & Dargusch, M. (2015). An investigation of the mechanical behaviour of fine tubes fabricated from a Ti–25Nb–3Mo–3Zr–2Sn alloy. *Materials & Design*, 85(0), 256-265.

Zhang, Y., Kent, D., Wang, G., St John, D., & Dargusch, M. (2014). The cold-rolling behaviour of AZ31 tubes for fabrication of biodegradable stents. *Journal of the Mechanical Behavior of Biomedical Materials*, 39(0), 292-303.

Zhang, Y., Kent, D., Wang, G., & Dargusch, M. Identification and analysis of twinning activity in the cold rolling of Mg-Al-Zn alloy mini tube. *Materials Characterization. (accepted)*

Publications included in this thesis

Zhang, Y., Kent, D., Wang, G., St John, D., & Dargusch, M. (2015). Evolution of the microstructure and mechanical properties during fabrication of mini-tubes from a biomedical β-titanium alloy. *Journal of the Mechanical Behavior of Biomedical Materials*, 42, 207-218. Incorporated as PAPER 1 in Chapter 3

Contributor	Statement of contribution
Yaowu Zhang	Designed study (70%) Data collection and analysis (80%) Wrote the paper (65%)
Damon Kent	Data collection and analysis (15%) Edited paper (15%)
Gui Wang	Designed study (20%) Edited paper (10%)
David St John	Edited paper (5%)

Matthew Dargusch	Designed study (10%) Edited paper (5%) Data interpretation (5%)

Zhang, Y., Kent, D., Wang, G., St John, D., & Dargusch, M. (2015). An investigation of the mechanical behaviour of fine tubes fabricated from a Ti–25Nb–3Mo–3Zr–2Sn alloy. *Materials & Design*, 85, 256-265. Incorporated as PAPER 2 in Chapter 3

Contributor	Statement of contribution
Yaowu Zhang	Designed study (70%) Data collection and analysis (80%) Wrote the paper (70%)
Damon Kent	Data collection and analysis (15%) Edited paper (15%)
Gui Wang	Designed study (20%) Edited paper (5%)
David St John	Edited paper (5%)
Matthew Dargusch	Designed study (10%) Edited paper (5%) Data interpretation (5%)

Zhang, Y., Kent, D., Wang, G., St John, D., & Dargusch, M. (2014). The cold-rolling behaviour of AZ31 tubes for fabrication of biodegradable stents. *Journal of the Mechanical Behavior of Biomedical Materials*, 39, 292-303. Incorporated as PAPER 3 in Chapter 3

Contributor	Statement of contribution
Yaowu Zhang	Designed study (70%) Data collection and analysis (80%) Wrote the paper (70%)
Damon Kent	Data collection and analysis (15%) Edited paper (15%)
Gui Wang	Designed study (20%)

	Edited paper (5%)
David St John	Edited paper (5%)
Matthew Dargusch	Designed study (10%) Edited paper (5%) Data interpretation (5%)

Zhang, Y., Kent, D., Wang, G., & Dargusch, M. Identification and analysis of twinning activity in the cold rolling of Mg-Al-Zn alloy mini tube. *Materials Characterization.* Incorporated as PAPER 4 in Chapter 3

Contributor	Statement of contribution
Yaowu Zhang	Designed study (80%) Data collection and analysis (95%) Wrote the paper (75%)
Damon Kent	Edited paper (15%)
Gui Wang	Designed study (10%) Edited paper (5%)
Matthew Dargusch	Designed study (10%) Edited paper (5%) Data interpretation (5%)

Contributions by others to the thesis

No contributions by others.

Statement of parts of the thesis submitted to qualify for the award of another degree

None.

Acknowledgements

There are many people to whom I would like to express my gratitude for their help in the pursuit of the research and preparation of this thesis. The completion of my thesis would not have been possible without their support.

The persons deserving of the most thanks is my supervisors, Assoc. Prof. Matthew Dargusch, Dr. Gui Wang and Dr. Damon Kent. I met Dr. Gui Wang and Assoc. Prof. Matthew Dargusch in one of their seminars at Northwestern Polytechnical University when I was in the graduate study. They offered me the opportunity to participate in research towards a PdD at the University of Queensland, one of the top universities in the world. I would like to thank Dr. Gui Wang, who provided invaluable advice and the well-designed experiments. I know that it would not have been possible to achieve my research targets in the 3-year candidature without his unwavering faith in my abilities and knowledge. I would like to thank Assoc. Prof. Matthew Dargusch. His constant support and encouragement enabled me to achieve my goals. I also wish to thank Dr. Damon Kent, who spent a lot of his valuable time on reading and commenting on my drafts. When I was struggling in operating transmission electron microscopy, he was there and provided a great help.

My thanks also go to my colleagues and good friends, Dr. Yao Xi and Hongyi Zhan, for sharing your valuable experiences and time. I always learn a lot from you.

I would also like to acknowledge Ms Brianne Mackinnon, Ms Katie Gollschewski and Ms Kristin Greer and to help on applications and other academic paperwork.

Finally, I would like to thank my wife Jiaqian and my parents for their understanding, patience and encouragement through all the challenging times.

Keywords

β titanium alloys, magnesium alloys, tube rolling, annealing, mechanical properties, martensitic transformation, twinning, microstructural characterisation

Australian and New Zealand Standard Research Classifications (ANZSRC)

091207, Metals and Alloy Materials, 70%

091399, Mechanical Engineering not elsewhere classified, 20%

091006, Manufacturing Processes and Technologies, 10%

Fields of Research (FoR) Classification

0912, Materials Engineering, 70%

0913, Mechanical Engineering, 20%

0910, Manufacturing Engineering, 10%

Table of Contents

Chapter 1 Introduction

1.1. Introduction to biomedical β titanium alloys

Metallic materials are widely used for biomedical applications such as vascular stents, joint prosthesis and dental prosthesis [1, 2]. Materials to be used as implants require superior mechanical properties, such as strength, ductility, elasticity and corrosion resistance [3, 4]. Titanium alloys meet all of these requirements and have good biomechanical and biochemical compatibilities and so are attractive materials for biomedical applications. Metastable β-Ti alloys have advantages over α and α+β alloys in biomedical applications because they have greater biocompatibility, lower modulus, high ductility and good mechanical processability, i.e. the superior elasticity effectively reduces the risk of damage to the stents as they are compressed during delivery into the body before being deployed in the target location [5, 6]. Therefore, metastable β Titanium alloys are attracting attentions for the applications of biomedical implants. Ti-Mo based alloys and Ti-Nb based alloys with high elasticity have been reported to be favourable for stent applications. Their superior elasticity lowers the risk of damage to the stent during inserting into the body and in service [7-12].

The alloying elements V, Ni and Al ions potentially release from titanium alloys and cause long-term health risks when using for biomedical applications. Research has widely attempted to overcome the concern of potential release of harmful ions [13, 14]. Considerable research has focused on new metastable β titanium alloys for biomedical applications which do not contain these elements [9, 11, 15, 16]. Ti-Nb-Sn, Ti-Nb-Zr, Ti-Nb-Mo Ti-Nb-Si and Ti-Nb-Ta-Mn alloys exhibit good elasticity and high strength [9-11]. Therefore, the Ti-Nb-based alloys are promising candidates for manufacturing biomedical stents. They have dominant β phase compositions, whilst other phases (α, ω and α″ phases) can form during deformation and heat treatments. [17-19].

A metastable β Ti alloy, Ti-25Nb-3Mo-3Zr-2Sn (wt.%), was developed by Yu et al. [20] and has been investigated as a promising material for biomedical applications [12, 18, 19, 21-23]. The Ti–25Nb–3Zr–3Mo–2Sn alloy has a low modulus, high strength and exhibits considerable plasticity and pseudoelastic character. In this thesis, the Ti-25Nb-3Zr-3Mo-2Sn alloy was evaluated for use in the fabrication of biomedical stents.

1.2. Introduction to biomedical magnesium alloys

Biodegradable implants should provide an appropriate mechanical strength when necessary and degrade at a rate similar to the formation of new tissues, thereby eliminating the need for an additional

removal operation. Biodegradable magnesium stents, on one hand, are capable of providing good mechanical properties and can achieve properties similar to conventional stents. On the other hand, they are able to temporarily open the blood vessels until they remodel and are then absorbed into the body, thereby reducing the likelihood of long-term complications or risks [24, 25]. Hence, magnesium alloys have been attracting increasing attention due to their promise in applications for biodegradable fine tube stents [1, 24]. Several magnesium alloys, such as AE21 (2 wt.% Al and 1wt.% rare earth elements) and WE43 (4 wt.% Y and 3 wt.% rare earth elements) have been investigated for use in biodegradable implants in recent years [1, 26]. Although there is still discussion on the addition of aluminium to bio-materials [27, 28], Mg-3Al-1Zn (AZ31) alloys are widely used for research on the processing of biomedical magnesium alloys as they are commonly available commercial alloys [29, 30]. The AZ31 alloy was used in this thesis to investigate the cold-rolling behaviour of magnesium tubes.

1.3. Microstructural evolution of β titanium alloys in the processing of fine tubes

Any permanent implant materials intended for use in stents need to be mechanically stable in biological environments for long periods, ideally for the lifetime of the patient. In order to fabricate mechanically-suitable β-Ti alloy fine tubes for stent applications, the microstructure evolution must be carefully controlled to obtain a suitable balance of mechanical properties.

The deformation mechanisms were reported to be plastic slip, mechanical twinning, stress-induced martensitic transformation and any combinations of these deformation modes [31-34]. The mechanical properties of metastable β-Ti alloys depend on the different deformation mechanisms [6]. Studies dedicated to improving their mechanical properties have focussed on understanding and controlling these deformation mechanisms [6, 35]. The dominant deformation mechanism changes from stress induced martensite to mechanical twinning to slip with increasing concentrations of the β phase stabilising elements [6].

The stress-induced martensitic α″ transformation can be activated under external stress for alloys which have a martensitic start temperature below room temperature as is the case for many of the metastable β titanium alloys [17, 36, 37]. It is well known that the martensitic α″ transformation depends on the β phase stability. The mechanism of deformation transitions from martensitic transformation to mechanical twinning, then to dislocation slip with the increasing β phase stability [38]. The elements Nb, Mo and Sn are β phase stabilisers which have a high degree of solubility in

the β phase and lower the β transit temperature. For binary Ti-Nb alloys, the least amount of Nb necessary in order to stabilise the β phase is ~38 wt.% [39]. The addition of Mo and Sn can facilitate stabilisation of the β phase at lower concentrations of Nb.

As Ti-25Nb-3Mo-3Zr-2Sn is a metastable β titanium alloy, stress-induced martensite α″ has been shown to form during deformation at room temperature [20, 23]. A portion of stress-induced martensite α″ reverts to the β phase when the external stress is released, while the remainder can readily decompose into the β phase by annealing. The stress-induced martensitic transformation can strongly influence the mechanical behaviours of the metastable β-Ti alloys both during processing and as a fine tube product. Neelakantan et al. [40] suggested that stress-induced martensite effects can be tailored to achieve improvements in the mechanical properties and performance of the metastable β-Ti alloys.

Another common deformation mechanism is mechanical twinning for β-Ti alloys which have low stacking fault energies [41]. In metastable β-Ti alloys, {112}⟨111⟩ and {332}⟨113⟩ twinning system have been reported [42, 43]. In comparison with {112}⟨111⟩, the {332}⟨113⟩ twinning mode has been more frequently reported in the β-Ti alloys with lower amounts of β phase stabilising elements. This mode of twinning has been observed in Ti-Mo alloys [44], Ti-V alloys [42], Ti-Nb alloys [45] and binary Ti-Cr [46] alloys, and has attracted attention as an important deformation mechanism which influences the mechanical properties of β-Ti alloys.

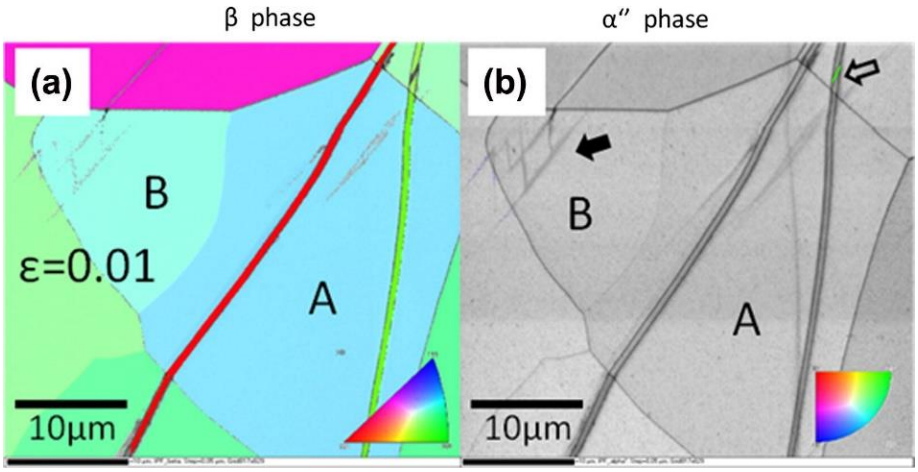

Fig. 1.1. EBSD superimposed band contrast and inverse pole figure maps showing complex deformation patterns within different grains at a strain of 0.01. (a) Two {332}⟨113⟩ twins with different orientations cross several grains. (b) Needle-like α″ martensite grains in the β matrix are indicated by a black arrow. A grain of α″ martensite within the twin band is indicated by an open arrow. [35]

The EBSD mapping in Fig. 1.1 was performed by Sun et al. [35] on specimens strained to 0.01 to highlight the complex patterns. Both $\{332\}\langle 113\rangle$ twins and SIM α'' plates were observed. Fig. 1.1a exhibits the two twinning systems activated in the early stage of plastic deformation. Small misorientations were observed when twins propagate through grain boundary which depends on the misorientation between the neighbouring grains. They measured the width of these twins ranging between between 600 and 800 nm. Fig. 1.1b shows α'' phase within the twin. This phenomenon of secondary α'' transformation was also reported in β-Ti alloys undergoing high levels of strain [47, 48].

A wide range of mechanical properties have been reported over the last decades due to the influence of different processing regimes and the large variety of compositions of the metastable β-Ti alloys. The stress and strain distributions during deformation vary for processing of bulk, plate or sheet materials and fine tubes. Several gaps exist in the current literature in the understanding of the role played by stress-induced martensitic transformation and mechanical twinning on the mechanical properties of β-Ti fine tubes. In the fabrication of fine tubes from metastable β-Ti alloys, processes of cold rolling/drawing and annealing are conducted to form the fine diameters/wall thicknesses. In this thesis, the cold rolling and annealing behaviours of Ti-25Nb-3Mo-3Zr-2Sn fine tubes were investigated during processing of fine tubes. The fine tubes exhibit different deformation mechanisms and mechanical properties with reductions in the diameter/wall thickness. The relationship between the evolution of microstructure and mechanical properties during processing of the tubes was investigated.

1.4. Microstructural evolution of Magnesium alloys in the processing of fine tubes

The hexagonal close-packed structure of magnesium alloys is associated with poor formability and restricts plastic deformation at room temperature [49, 50]. Fabrication of magnesium alloy tubes traditionally requires processing at elevated temperatures. However, this is not suitable for fabrication of magnesium fine tubes because grain growth at elevated temperatures leads to deterioration of the mechanical properties which cannot then be improved during consequent drawing processes [51, 52]. Therefore, cold rolling is a necessary process during manufacture of magnesium fine tubes [53].

Magnesium alloys exhibit a strong preference for mechanical twinning during cold deformation because the twinning has a lower threshold stress than that for $\langle c + a\rangle$ slip and there are a limited number of the slip systems. It is well known that there are typically two types of deformation twins,

$\{10\bar{1}2\}$ extension twins and $\{10\bar{1}1\}$ contraction twins [54]. $\{10\bar{1}2\}$ twinning is a common deformation mechanism in Mg alloys due to the low critical resolved shear stresses for this twinning mode. Extension twins are formed when there is an extension stress parallel to the c-axis which is generated at the onset of plastic deformation and contributes to the strain [55-57]. Contraction twins are generated when there is a contraction stress parallel to the c-axis at larger levels of deformation in order to relax the stress concentration [58, 59]. As well as the two types of primary twins, secondary twinning, such as $\{10\bar{1}1\}-\{10\bar{1}2\}$, $\{10\bar{1}2\}-\{10\bar{1}1\}$ and $\{10\bar{1}3\}-\{10\bar{1}2\}$ double twins, also can be activated within reoriented primary twins. Ma et al. reported a two-shear mode mechanism for twinning in a strongly textured Mg alloy for the nucleation of $\{10\bar{1}1\}-\{10\bar{1}2\}$ double twins [60]. The initial texture of Mg alloys plays an important role in the formation of different twinning modes and the activation of $\{10\bar{1}2\}$ extension twinning is largely dependent on the strain directions [61]. Xin et al. studied the formation mechanism of multiple twinning modes and $\{10\bar{1}2\}-\{10\bar{1}1\}$ secondary twins in the rolling of AZ31 Mg alloys [62, 63]. They concluded that multiple twinning modes could be activated in grains with the same orientations and that the activation of these complex twins were in accordance with the prediction of an effective Schmid factor.

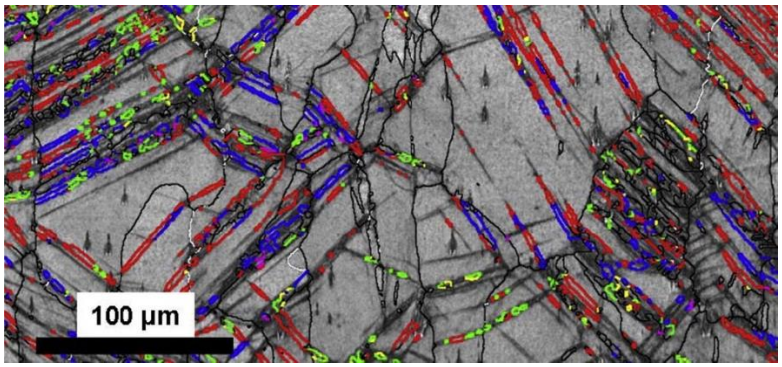

Fig. 1.2. EBSD maps of the microstructures produced by a tensile strain of 0.15 in AZ31 magnesium alloy. The $\{10\bar{1}1\}$ contraction twin boundaries are shown in red, the double twin boundaries rotated by 38 °in blue, by 30 °in red, by 66.5 °in yellow and by 69.9 °in green. The tensile axis is vertical on this figure. [64]

Typical microstructures are shown in Fig. 1.2 as determined by EBSD. The primary twins are outlined in red with the double twin boundaries rotated by 38 °in blue, by 30 °in red, by 66.5 °in yellow and by 69.9 ° in green, respectively. It is noted that all the secondary twins shown in Fig. 1.2. were originally primary twins. These twins were observed to convert into second generation twins by further straining after their formation.

The activation of twinning during deformation has a large effect on texture evolution due to the lattice reorientation, e.g. the lattice will rotate by 86.3 °through $\{10\bar{1}2\}$ twinning [65]. It has been observed that ~7% strain in twinning dominated deformation results in complete texture reorientation [66]. Thus, the twins are associated with the mechanical anisotropy of magnesium alloys [55-57]. During the processing of magnesium fine tubes, the activation of twins greatly depends on the texture [67-69]. Liu et al. [70, 71] studied the relationship between texture and deformation mode and concluded that the shape of the stress-strain curve is determined by the type of twinning that occurs and by when the twins are activated. Jiang, et al. [72] conducted a study to determine the twinning modes and texture development under different strain paths. Their conclusion was in accordance with that of Barnett et al. [73] who reported that the effect of mechanical twinning and corresponding texture development on the flow stress is more significant than the effects of grain size.

The effect of twins on the mechanical properties of Mg alloys has been extensively studied, e.g. Barnett studied twinning and ductility in Mg alloys and concluded that the ductility of Mg alloys is associated with the activation of different twinning modes [74, 75]. When Mg alloys are deformed in a direction favourable for $\{10\bar{1}2\}$ twinning, the yield strength will be reduced in comparison to with that in more unfavourable directions [76]. In addition, because twins tend to propagate through parent grains, the boundaries between twins and parent grains act as sub-boundaries that induce Hall-Petch strengthening during deformation [77]. Strain hardening behaviour can also be attributed to the influence of mechanical twinning. Knezevic et al. [78] reported that mechanical twins in AZ31 affected strain hardening and the main contribution to hardening comes from texture hardening. Rohatgi et al. [79] considered that the reason that twinning increases the strain hardening rate lies in the effective grain refinement that results from twinning. However, Barnett [73] provided another explanation that reorientation of the c-axes by ~86 ° has a more significant effect on the strain hardening produced by twinning.

Therefore, in order to understand and effectively utilise the evolution of microstructure and texture induced by twinning in cold rolled magnesium tubes, it is essential to obtain a comprehensive understanding of twinning modes and their impacts on processing and properties. The cold rolling behaviour of magnesium alloys has been investigated in recent years [50, 80]. However, most of the previous studies focused on the formation of twins in uniaxial deformation and only a few investigated twinning activity in the plane strain state, which is still not applicable to the characteristics of twins formed in cold rolled magnesium tubes. The nucleation and growth mechanism of primary and secondary twins, the formation and interaction of multiple twins and the

local strain accommodation at interfaces between the parent grain and twins remain unclear in the processing of cold rolled tubes. In this thesis, the mechanical properties of magnesium fine tubes was examined and twinning activity was investigated in regards to the morphology and orientation of twins during the process of cold rolling, in order to develop an understanding of how the different processing parameters influence the mechanical properties of the magnesium fine tubes.

1.5. Thesis outline

Although the application of β titanium alloys and magnesium alloys in biomedical stents is still under development. These alloys have exhibited advantages in processing and mechanical properties over that of traditional materials. In this thesis, a metastable β Ti-25Nb-3Mo-3Zr-2Sn alloy and Mg-3Al-1Zn alloy were used to assess the viability of these two alloy systems for biomedical fine tube stent applications. Despite extensive research on the deformation behaviour of the two alloys, little information is available on the processing of fine tubes in consideration of their differing stress states and varying processing parameters. This thesis aims to understand the relationship between the microstructural evolution and mechanical properties in the processing of biomedical metallic fine tubes. Varying processing parameters have been used in the production of the fine tubes and then corresponding observations of the microstructure and mechanical testing was performed. The results and findings in this thesis can be applied to the fabrication of fine tubes and the effects of processing on both the microstructural evolution and the mechanical behaviours to optimise the properties of the fine tubes.

A review of current literature is provided in Chapter 2 focussing on biomedical material selection, deformation mechanisms and their effects on mechanical properties. In particular, stress-induced martensitic transformations and mechanical twinning are the primary focus when investigating deformation in β titanium alloy tubes as the simultaneous activation of the two deformation mechanisms benefits the mechanical behaviour of fine tubes. In magnesium alloys, mechanical twinning is dominant during deformation and the different twinning types and their influence have been reviewed in this chapter.

The research findings during the candidature are presented as a series of publications in Chapter 3 including experimental methods, results, analysis and conclusions. These papers provide details of the experimental methods and the findings were presented in the results. The martensitic α″phase and {332}⟨113⟩ twins formed during cold rolling influence the mechanical properties of the β titanium

fine tubes. For the magnesium fine tubes, twinning modes were studied on a grain-by-grain basis and their effects on mechanical properties were analysed. Chapter 4 summarises the findings and proposes potential directions for future research on processing of metallic fine tubes.

Chapter 2 Literature Review

2.1. Fine tubes for application in stents

Stents are generally metallic fine tubes implanted in vessels to maintain localised flow in stenotic blood vessels and other passages for dilation [81, 82]. The principal advantage is that they are implanted directly through vessels instead of open operations. Currently, the implanting of various stents has been extensively used in clinical practice. Over one million stents are being implanted each year [83]. In view of the service circumstances of stents, the mechanical requirements mainly include elasticity, plasticity, rigidity and strength [84]. In this project, the processing of fine tubes for eligible stent materials was investigated, as well as the evolution of mechanical properties and deformation mechanisms in the processing.

2.1.1. Materials used in the fabrication of fine tubes

Implanted biomedical devices are mainly made of metals, polymers, ceramics and other composites [85]. Fig. 2.1 shows the typical tensile curves of polymers, metal and ceramics, where strength, Young's modulus and fracture toughness can be observed [86]. Ceramics have poor properties in ductility and plasticity, although they have good tensile strength. Fracture may occur even during low plastic deformation due to their low fracture toughness. As a result, ceramics is not an ideal materials used in fine tube stents. Another material, Polymers, have high ductility but low strength and Young's modulus. Therefore, it is also difficult to fabricate polymers fine tubes due to the both high flexibility and strength.

In comparison, metals are suitable materials for fabricating stents in terms of their mechanical properties. Currently, metals are commonly used in the manufacture of fine tube stents, including stainless steel, nitinol, titanium, magnesium alloys, platinum-iridium alloy, tantalum and cobalt-chrom alloy, [86]. Approximately 30 types of fine tube stents are available in clinical practice or in development [87]. Although new techniques for the installation of metallic stents are being developed rapidly, development in the fabrication of the fine tube for stent application lags behind. Thus, there is a need to discuss the candidate materials for fine tube stents and the corresponding fabrication research and the technology development process.

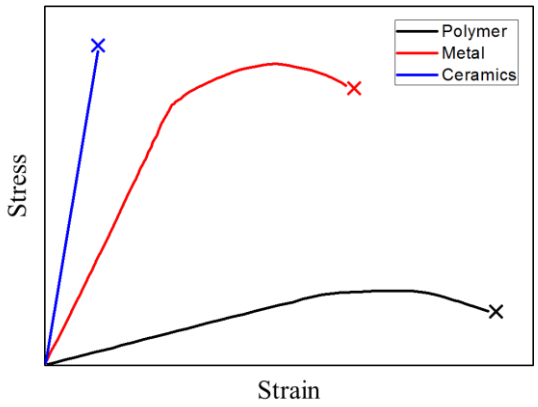

Fig. 2.1. Typical stress-strain curves of metals, ceramics, and polymers. The gradient of the straight line in the elastic deformation region represents the Young's modulus. [86]

2.1.2.1. Metastable β-titanium alloys

In comparison with the stainless steel and cobalt-chrome alloys with high elongation [88], titanium alloys have relatively low ductility, especially as cold rolled tubes. In addition, the cobalt-chrome alloys and stainless steel have superior radial and hoop strength, and their elastic moduli can reach approximately 200 GPa, which would bring negative effects when the fine tube stent goes through vessels with small diameters or with complicated structures. Another biomedical material, nitinol, with superior super-elasticity due to reversible phase transformation, has been widely studied as a candidate material of fine tube stents [2, 89]. However, hypersensitivity caused by the release of Ni ion remains a concern in terms of the biocompatibility of nitinol alloys [2]. It also has been reported that the rates of Ni ion release can increase significantly over time [90].

α + β titanium alloys composed of non-toxic elements were first developed for biomedical applications. However, they are too stiff to be delivered in to vessels and premature failure may occur for stent applications [85]. Because β phase has much lower elastic modulus than α phase and exhibits excellent toughness, corrosion resistance and biocompatibility, a series of metastable β-Ti alloys composed of non-toxic elements (Nb, Ta, Zr, Mo, etc) have been developed and are receiving increasing attention for stent applications [91]. Ti-V-based, Ti-Mo-based and Ti-Nb-based β alloys have been reported to display shape memory and superelastic behaviours [12, 92, 93], which are desirable characteristics for many biomedical applications. For the application of stents, the large elastic strains in β-Ti alloys reduce the risk of damage to the stent both during delivery into the body and after being deployed in the target location [94].

The potential release of harmful V and Al ions from Ti alloys used for biomedical applications has been reported and research has attempted to overcome their long-term health risks [14, 95]. Thus, considerable work has focused on new metastable β titanium alloys for biomedical applications which do not contain Ni, V and other harmful elements [15]. Ti-Nb-Sn, Ti-Nb-Zr, Ti-Nb-Mo, Ti-Nb-Si and Ti-Nb-Ta-Mn alloys exhibit good shape memory and super-elasticity [9-11]. Therefore, the Ti-Nb-based alloys are promising candidates for manufacture of biomedical stents. They have dominant β phase structures and other phases (such as, α, ω and α″) have been reported to form during deformation or heat treatments due to their metastability [18, 19].

A metastable β Ti alloy, Ti-25Nb-3Mo-3Zr-2Sn (wt.%), was developed by Yu et al. [20] and has been researched as a promising material for biomedical applications. The Ti-25Nb-3Zr-3Mo-2Sn alloy has low modulus, high strength and exhibits considerable plasticity and superelastic behaviour [96]. The alloying elements Zr and Sn have similar abilities to enhance strength and improve the plasticity of the β Ti alloys [97]. Binary Ti-Nb alloys with stable β phase structures exhibit undesirably high elastic moduli. Replacing some of the Nb with Zr reduces the elastic moduli to lower levels, but the Zr does not significantly affect the stability of the β phase. Additionally, the stabilising effect of Zr is much weaker than that of Sn in the Ti-Nb-Zr-Sn system [39]. The addition of Sn to the Ti-25Nb-3Zr-3Mo-2Sn alloy improves the stability of the β phase. Therefore, the biomedical Ti-25Nb-3Mo-3Zn-2Sn titanium alloy fine tube is one of the most promising candidates for the application of metallic stents with superior mechanical properties.

2.1.2.2. Magnesium alloys

Stents made of β-Ti alloys, stainless steel and cobalt-chrome alloys serve in the target location permanently after implanting even the stenosed vessels has recovered. This may cause long term issues, as reported in-stent restenosis and thrombosis [25]. Biodegradable stents can temporarily support the abnormal vessel, then be absorbed into the body until its remodelling. Therefore, biodegradable metallic stents are a promising alternative to permanent stents.

As promising candidate for biodegradable stents, Mg alloys have attracted interest due to their excellent biodegradability and biocompatibility [24, 98, 99]. Mg alloys have been used for biodegradable orthopedic implants [1], but their application to stents are still in experimental stage. Mg has the lowest density of all commercially utilised metals. Pure Mg does not meet the requirements for stents due to its poor mechanical and corrosion properties [100]. Thus, Mg alloys

has been targeted for stent applications. The general alloying elements for Mg alloys are Zn, Mn and rare-earth metals. Release of toxic degradation products from these stents as that in biomedical β-Ti alloys is not a concern because most of the alloying elements in Mg alloys are non-toxic in human bodies [101, 102]. AE21 and WE43 are two promising candidate materials reported for the development of stents [26, 102]. AE21 has alloying elements of aluminium and rare-earth metals, while WE43 is composed of yttrium, zirconium and rare-earth metals [26]. The alloying elements are reported to improve castability and resistance to pressure. However, the strength of the Mg alloys containing rare-earth elements is still low at ambient temperature. In clinical trials, a Lekton Magic stent made of WE43 alloy is a new developed Mg stent [102]. Biotronik undertook human trials on the Lekton Magic stent and the results indicated that it was implanted and was well tolerated [103]. Mg alloy fine tubes commonly have relatively low radial and hoop strength due to their low elastic modulus. Therefore, in order to provide an appropriate support to the vessel wall, the stent struts have to be wider, which increases the contact area with the vessel wall. Mg alloy fine tubes also may fracture due to their low ductility. As a result, the investigation and improvement of mechanical properties in Mg alloy fine tubes needs to focus on overcoming these disadvantages, in order to enhance their potential for use in stents.

2.1.2. Mechanical properties required for fine tubes

As mentioned in previous sections, a large number of studies about stents have been performed, mainly concerning material biocompatibility and the reactions between stents and tissues. Apart from the required biodegradability and biocompatibility, the biodegradable fine tubes for stent applications must have a minimum mechanical strength of 300 MPa and an minimum elongation of 15% [104]. However, there are few studies on the mechanical properties of fine tubes. Since the main functionality of stents is to reopen the stenosed vessels and poor mechanical properties will result in damage to the vessel or other complications, mechanical properties are always the focus in the development of fine tube stents.

The mechanical requirement for the fine tubes are good expandability, sufficient radial and hoop strength and sufficient ductility, which are detailed as follows:

- When the fine tube stent is deployed at the target location, the fine tubes should have the ability to undergo large plastic deformations.

- The fine tube stent should have the ability to overcome the forces imposed by the vessel wall and prevent it from collapsing.
- It should be flexible in order to pass through and move with the vessels.

For expandable stents, fine tubes should have sufficient hoop strength and radial strength [85]. For self-expanding stents, sufficient elasticity is required when delivery and then expanded at target location. Nitinol is a typical material used in the self-expanding stent. The alloy transfers to its martensitic phase when force is applied, while the force is released, the alloy are composed of austenitic phase. In current clinical practice, expandable stents are preferred due to the property.

Radial strength is an important mechanical property for fine tubes. It is known that the radial strength of the fine tubes is closely related with elastic modulus of the material. Therefore, the elastic modulus is an important property for candidate materials for fabrication of the fine tubes. Theoretically, fine tubes have similar radial strength when they are made of materials with similar elastic moduli. However, their radial strength is generally associated with other factors even though the same material was used to fabricate the fine tube stent. This highlights the importance of the processing that can further optimise the mechanical properties of the fine tubes.

Therefore, it is believed that an appropriate combination of materials and mechanical properties can enable excellent elastic performance as well as improved strength. Fine tubes with good strength and elasticity allow the fabrication of stents with a smaller contact area with the vessel wall, which is desirable for stents, especially when used in small vessels.

2.2. Deformation mechanisms in metastable β-Ti alloys

2.2.1. Phase transformations and stability of β phase

The β phase stability is a critical parameter in β-Ti alloys in terms of their mechanical properties. Metastable β-Ti alloys deform through different mechanisms from dislocation slip to mechanical twinning then to stress-induced martensitic transformation or combinations of these with the decreasing β phase stability [38, 45].

According to a previous report [105], a typical sequence of cold deformation mechanisms for β-Ti alloys is as follows: Initiation of SIM transformation in the elastic region, continuing formation of

SIM and the beginning of plastic deformation simultaneously (at ~7%-10%), intersecting of the deformation-induced products (10%), the formation of secondary martensite laths between the primary laths (20%) and formation of mechanical twins (35%).

Athermal martensite forms on quenching from a high temperature phase, inducing a phase transformation triggered by the coordinated production of stacking faults. This process has been described by Grosdidier et al. for a variety of high temperature phases and martensitic crystal structures [106]. The martensitic phase formed during quenching undergoes only incomplete transformation, as it is arrested by the adjoining high temperature phase, which remains when quenching to room temperature for sufficiently high levels of β stabilising elements. On the other hand, the metastable β phase can be transformed into α″ orthorhombic martensite at room temperature by providing an extra amount of energy by mechanical deformation. Stress-induced martensitic (SIM) transformation is a common phenomena in deformed metastable β-Ti alloys [107, 108] . The transformation from metastable β phase to martensite occurs athermally or under the influence of stress depending on alloy composition and deformation temperature, which determines the susceptibility for SIM transformations [23].

The metastable β phase can also partially transform into the ω phase during the quenching processes. The ω phase transformation depends on cooling rate and composition of alloys. It has been observed in various β-Ti alloys, water quenched from the β field. The ω phase transformation is activated at a similar temperature with the initial temperature of martensitic transformation. The formation of the ω phase is a diffusionless transformation and the ω phase has a similar composition with that of β phase. According to the study by Duerig [94], the trigger stress to activate martensitic transformation in a Ti-10V-2Fe-3Al alloy decreases with an increasing volume fraction of ω phase. The decreasing trigger stress for the martensitic transformation at room temperature is believed to be associated with the presence of ω phase. It was explained that the ω phase decreases the dislocations mobility and increases the internal stresses in a material, supporting the martensitic transformation [109].

Table 2.1 Critical content in β-stabilising elements to retain the β phase after quenching

β alloys	Isomorph					Eutectoid					
Alloying element	Mo	V	W	Nb	Ta	Fe	Cr	Cu	Ni	Co	Mn
Critical content (wt.%)	11.0	15.0	22.5	36.0	45.0	3.5	6.5	13.0	9.0	7.0	6.5

Alloying is one of the most common and effective methods to change the stabilisation of the β phase [110, 111]. For concentrations of stabilising alloying elements higher than a critical content (Table 2.1), the β phase is retained in a metastable state after quenching. The β phase stability affects its propensity to transform into martensite during deformation.

Among the potential compositions, Ti-Nb based alloys are the most common biomedical candidate materials because of the combination of good biocompatibility and mechanical properties as detailed in the last section [93, 112]. Depending on the Nb content, binary Ti-Nb alloys can display a fully α″ martensitic microstructure at room temperature and thus exhibit shape memory properties [12, 113]. If the Nb content is high, the microstructure is fully β at room temperature and the alloys can display a SIM transformation leading to superelastic properties. However, Tahara et al. reported that for superelasticity in Ni-free β Ti alloys, the critical stress for dislocation slip and the functional stability are much lower than these in Ti-Ni alloys [114]. However, Adding alloying elements, such as Mo, Sn, Al, Ta and Zr can increase critical stress for slip and the functional stability. The mechanical strength and the elasticity were also reported to be improved to some extent [115-118].

Martensitic transformation can be activated in the metastable β grains in Ti-Nb-Si alloys. The element Zr shows similar mechanical and chemical properties because they belong to the same group in the periodic table. Investigations have shown the effectiveness of Zr addition in reducing the modulus without changing β phase stability.

Combined alloying with Zr and Sn can result in a very good combination of strength and Young's modulus, because it is reported that martensitic transformation was depressed and β transit temperatures was increased by adding Zr and Sn. Sn has a beneficial role in stabilising the β phase and suppressing the intermediate ω phase. The yield strength and elongation is decreased when Nb content was increased in β-Ti alloys due to solid solution hardening caused by Nb content. Lower Nb content can minimise the segregation effects and is known to decrease the β phase stability thereby leading to unexpected metastable phase transformations such as β to martensitic α″ or β to ω during quenching or under the influence of stress.

Paradkar et al. [119] reported that the trigger stress required for the transformation of β phase to martensitic phase was reduced in a Ti-15Al-12Nb alloy by increasing Nb content. Generally, Ti-Nb alloys containing 14-28 wt.% Nb are known to undergo partial SIM transformation resulting in a two-phase microstructure prior to the onset of plastic deformation [120].

2.2.2. α″ martensitic transformation in β titanium alloys

2.2.2.1. Mechanisms of martensitic transformation

In β-Ti alloys, the lattice parameters of martensitic phase depend on the solute concentration. The β phase in solute-lean alloys tends to transform hcp martensitic phases at high temperatures, while in solute-rich alloys, orthorhombic martensitic phase is easier to be formed from β phase after water quenching [121]. Martensitic transformations are usually described using characteristic temperatures, austenite start (As) and austenite finish (Af) temperatures, martensite start (Ms), martensite finish (Mf), , respectively [122]. These temperatures have been evaluated in previous reports by dynamic mechanical analysis for different applied static stresses, and the martensitic transformation is generally observed through reduction of the dynamic elastic modulus. Therefore, the β transit and the Ms temperature are two critical parameters in terms of elasticity and other mechanical properties. In α and α+β Ti alloys, the martensitic transformation from β phase takes place after water quenching at a high temperature above β transit temperature, while in metastable β-Ti alloys, Ms temperature is below room temperature and martensitic transformation can be activated under and external stress with critical levels of stabilising elements.

When determining the potential for SIM transformation in β-Ti alloys, the molybdenum equivalency, Moeq, and the martensite start temperature, Ms, are both considered to depend on alloy composition according to equation 2.1 and 2.2 respectively [1, 11], where the coefficients are the amount of each β-stabilising element in weight percent (wt.%). It has been demonstrated that for values of Mo_{eq} higher than 8 wt.%, the β phase will be in a metastable state and is likely to transform into α″ phase under applied stress [123].

Equation 2.1

$$Mo_{eq} = 1.00[Mo] + 0.28[Nb] + 0.22[Ta] + 0.67[V] + 1.60[Cr] + 2.90[Fe] - 1.00[Al]$$

Equation 2.2

$$Ms = 1156 - 150[Fe] - 96[Cr] - 49[Mo] - 37[V] - 17[Nb] - 7[Zr] + 15[Al]$$

Kuan et al. observed plate-shaped SIM α″ phase during tensile deformation and the habit plane of $\{554\}$ was determined using XRD method for Ti-Nb binary alloys [124]. The martensitic

transformation can significantly influence the mechanical behaviour of β-Ti alloys. If the trigger stress is lower than the yield stress of the parent β phase, the tensile stress-strain curve presents a typical double yielding phenomenon (as shown in Fig. 2.2 [119]) [125], which will be detailed in section 2.2.2.2.

A three step deformation sequence of martensitic transformation was established in previous studies [5]. Firstly, the β phase is elastically deformed up to ~ 2.5% of strain. Secondly, the deformation is accommodated by the SIM α″ transformation, which is elastically deformed up to ~ 5%. For strains greater than 5%, both the residual β phase and α″ phase start deform plastically [126]. Several studies have investigated the effect of the martensitic transformation on mechanical behaviours of metastable β-Ti alloys [127-129]. Baker [130] observed its influence on potential strain recovery. Then, Duerig et al. [127] performed experiments involving the evolution of β phase microstructures. Strain recovery has been observed when temperature was raised up to the As. the material through the austenitic start temperature. It is also reported that effective suppression of the martensitic transformation makes possible alternative deformation related strengthening mechanisms.

2.2.2.2. Trigger stress for activating martensitic transformation

Previous studies have attempted to estimate the trigger stress for activating SIM transformation by stress-strain curves. It is demonstrated in Fig. 2.2. The intersection of tangent lines of elastic stage curve and of extended elastic curve was considered to be the trigger stress [119].

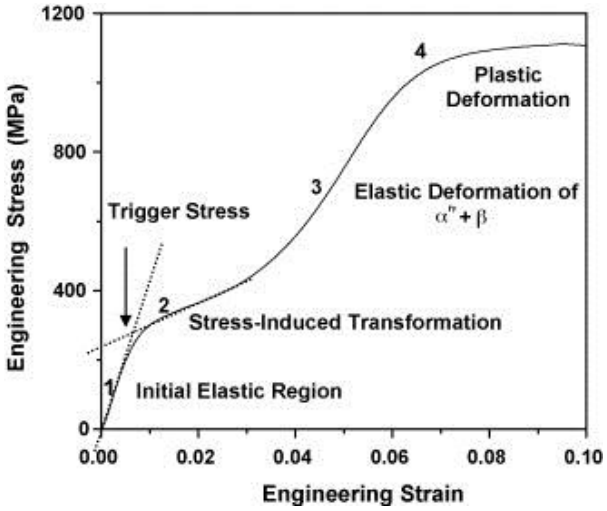

Fig. 2.2. Trigger stress obtained from double yielding stress-strain curve. [119]

Paradkar et al. ascribed the trigger stress behaviours to the phase transformation of β to martensitic phase transformation [119]. Major factors associated with trigger stress to activate SIM transformation are reported to be experimental temperatures, grain sizes and composition of the alloys [119, 120]. The trigger stress was lowered when temperature was raised up to the room temperature, then it increased with further increasing temperature according to the experiment performed using a Ti-V-Fe-Al alloy [119].

The conclusions about the influence of grain size on the trigger stress available in references are contradictory. Grosdidier et al [131] reported that increases in the β grain size decrease trigger stress in a Ti-Mo-Al-Zr alloy at a constant temperature [106]. However, a contradictory result was reported by Gil and Planell [132] that the increasing grain size increased the trigger stres. Bhattacharjee et al obtained a similar conclusion [120]. The following study [119] showed that trigger stress-grain size curve exhibits a U shape. Trigger stress are also related to the strain rate, Sadeghpour et al. observed the SIM transformation in a Ti-4Al-7Mo-3V-3Cr alloy with varying strain rates [105]. The results showed that both trigger stress for SIM formation and yield strength increase linearly with the logarithm of strain rate, but it was noted that the volume fraction of deformation-induced products were independent of the strain rate.

2.2.2.3. Identification of α″ phase

The martensitic α″ phase has a c-centred orthorhombic structure and the orientation relationship between β and α″ phase is described in the literature as a Burgers type except for uncompleted shear and atomic shuffle from the β to the hexagonal α phase [133]. The Burgers orientation relationships for the β to α″ transformation are $(\bar{1}10)\beta//(001)\alpha''$ and $[111]\beta//[110]\alpha''$ [38]. An illustration of the correspondence between the β phase structure and the α″ martensitic structure is presented in the Fig. 2.3 [134]. By application of the Burger orientation relationship, each β grain is decomposed into several possible α″ variants by application of six possible lattice correspondences, leading to a α″ self-accommodating microstructure at room-temperature and potential superelasticity [135, 136].

Fig. 2.3 a and b show the unit cells of β and α″, respectively [23, 134]. The crystal structure of β is bcc with a lattice parameter of a_β = 3.3065 Å in a Ti-5Mo-5Al-3Zr alloy. A face-centred tetragonal unit cell can be selected from four bcc unit cells, as outlined in Fig. 2.3 a. During the β to α″ transformation, the face-centred tetragonal unit cell is changed into an orthorhombic lattice as shown

in Fig. 2.3 b with parameters of $a_{\alpha''}$ = 3.152 Å, $b_{\alpha''}$ = 4.854 Å and $c_{\alpha''}$ = 4.642 Å, calculated for the orthorhombic α″ phase [23].

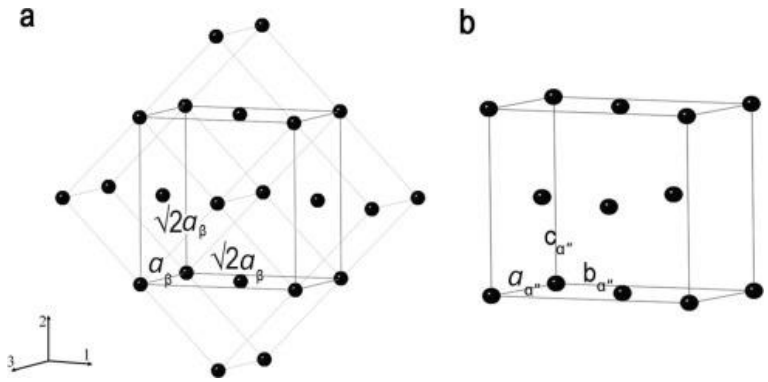

Fig. 2.3. (a) The crystal structure of β with a = 3.3065 Å showing a face-centred tetragonal unit cell selected from four bcc unit cells, and (b) the unit cell of α″ with the lattice parameters of a = 3.152 Å, b = 4.854 Å and c = 4.642 Å. [23, 134]

Fig. 2.4 a and b exhibit typical bright field and dark field TEM figures of α″ phase, respectively, formed at a strain of 0.4 in a Ti-Mo-Zr-Al alloy [137]. A needle-shaped α″ phase had a thickness of 100±10 nm and its length was 1±0.4 μm. Martensitic transformation was also conformed by the selected area diffreaction in Fig. 2.4c. The dashed lines appeared to shear the acicular α″ plates into shorter pieces as shown in Fig. 2.4a and b, which indicate that α″ laths divided the β grains and themselves into much smaller domains, significantly accelerating the grain refinement process in SIM β-Ti alloys

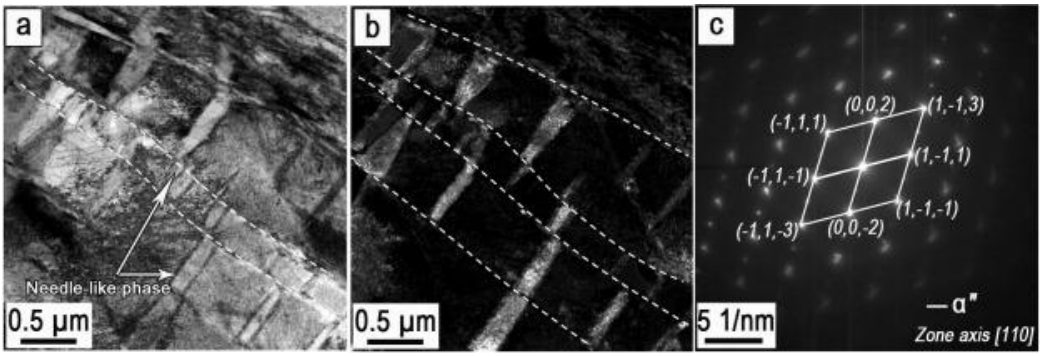

Fig. 2.4. (a) Bright and (b) dark field TEM figures of a Ti-Mo-Zr-Al alloy at a strain of 0.4, showing the needle shaped α″ identified in the SAD pattern in (c), and its shearing along the dashed lines [137].

Strain recovery in the metastable β-Ti alloys results from the fact that there is one unique path for the inverse transformation upon heating, which means that each of the six α″ variants can only transform into the same unique parent crystal. The crystallographic orientation of the parent phase based on α″ was calculated in a previous report using electron backscattered diffraction [138]. Electron backscattered diffraction measurements are commonly used to determine the crystallographic orientation of phases and the orientation relationships between phases in phase transformations. The method to calculate the orientation of the parent phase involves applying the orientation relationship to each variant of α″ martensite.

Fig. 2.5 shows EBSD maps of a Ti-Nb-Ta sample and the corresponding X-ray diffractogram [134]. The sample in Fig. 2.5a was in annealed condition, only β phase was identified by the diffractogram (Fig. 2.5b). Fig. 2.5c shows the same area as that in Fig. 2.5a after a compression stain of 0.35. The grain morphology is quite different to that in Figure Fig. 2.5a due to the thin metallic layer formed during the deformation. The diffractogram (Fig. 2.5d) indicates that samples contain β phase and α″ martensitic phase. Inverse pole figures (Fig. 2.5c) show the grain boundaries and martensite-parent grain interfaces in the deformed sample. In the grains, microstructures composed of laths and needles were frequently observed. Fig. 2.5c and d indicate that β phase has been partially transformed into α″ martensite when the alloy is deformed. Generally, the indexation rate for deformed β-Ti alloys are largely reduced due to the lattice distortion around the martensite-parent grain interfaces and inside the martensite phase, while other reports attribute the reduced indexation rate to nano-sized α″ microstructures [138, 139]. A mix of the different possible variants of α″ was observed in deformed β-Ti alloys. Bertrand et al. reported that different variants of α″ can be activated in the same β grains during deformation [140]. In addition, it was reported that a small amount of ω phase was detected in some alloys, but it cannot be confirmed by EBSD due to its nanometric size and coherence with the β phase [141].

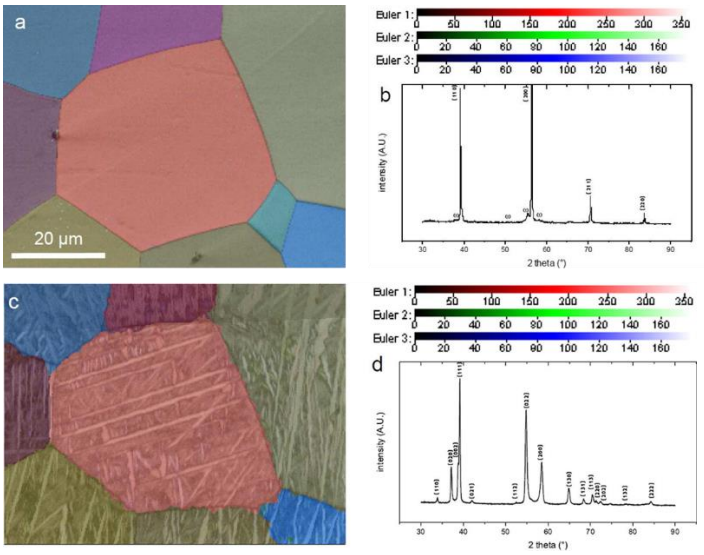

Fig. 2.5. (a) EBSD mapping of annealed samples, only β phase was observed, (b) corresponding X-ray diffractogram of (a), (c) inverse pole figures obtained from indexation on the β phase and SIM α″ phase at the same area as in (a), (d) corresponding X-ray diffractogram of (c). [134]

It is difficult to index nano-sized SIM α″ laths by EBSD to determine their orientations. However, Bertrand et al. [134] reported a method to calculate the crystallographic orientation of parent phase from the martensitic microstructure by indexing electron backscattered patterns without indexation of the martensite in the β to orthorhombic α″ martensitic transformation. In their experiment, the real orientation of the parent phase was obtained via simulation of the electron backscattered patterns.

Recently, in situ experiments have been carried out to characterise the reversible SIM transformation after the release of the stress [142, 143]. Al-Zain et al. and Tahara et al. performed in situ X-ray diffraction studies on Ti-26Nb and Ti-13Nb-4Mo alloys (at%) and detected the SIM α″ phase transformation [144, 145]. The α″ phase is shown to be formed from 0.2% to 2.5% of strain and to be partially reversible after unloading from 2.5% strain [144-146]. These experiments were performed using a deformation of 2.5% which was followed by unloading. On the other hand, cycles of loading-unloading to obtain a small amount of plastic deformation were performed to obtain more precise characterisation of the SIM transformation. Strain values at which the transformation starts and finishes, reversibility of the transformation and mechanisms of elasticity and plasticity were studied by this method [147-149]. Typical diffraction peaks for the β and α″ phases were clearly observed during loading and unloading. The reversible martensitic transformation was demonstrated. In addition, variations in the β and α″ crystal structures were characterised for both loading and unloading conditions.

2.2.2.4. Martensitic transformation and nano-sized α″ martensite

Reversible martensitic transformation has been widely studied because of the development of metastable β-Ti alloys with high strength and low elastic modulus [150, 151]. The metastable β-Ti alloys have been reported to exhibit a specific nonlinear tensile stress-strain curve in elastic stage. The reversible SIM transformation exhibited in metastable β-type titanium alloys could be influenced by changes in composition and materials processing. This behaviour is believed to be associated with the reversible SIM transformation [152, 153].

A nano-sized SIM transformation occurred in a Ti-Nb-Zr-Sn alloy which was different to the conventional self-accommodating twinned structures. The SIM α″ phase with nano-sized morphology has also been reported during tensile loading in Ti-24Nb-4Zr-8Sn alloys [154, 155]. It could be inferred from the findings that the formation of nano-sized martensite is a common phenomenon in metastable β-Ti alloys, resulting in both high strength and low elastic modulus.

The formation of martensite under externally applied loading is an important deformation mode in metastable β-Ti alloys and is associated with specific mechanical properties as follows [5]:

- When transformation-induced plasticity is activated, elongation increases significant and SIM transformation is activated.
- Reversible martensitic transformation in metastable β-Ti alloys exhibits shape memory effects and allow peculiar properties.
- Strains can be recovered on release of external stress when elastic martensite is formed mechanically. This phenomenon is called superelasticity in metastable β-Ti alloys.

2.2.2.5. Martensitic transformation and heat treatments on β titanium alloys

Titanium alloys are often subject to heat treatments, a key process toward obtaining the desired microstructure and mechanical properties via allowing the constituents to dissolve into the solid solution during homogenisation or reversibility of stress induced α″ phase to β phase [156, 157]. Heat treatment is considered to be one of the key factors to control the SIM transformation by changing the phase stability and Ms temperature. An appropriate heat treatment on β-Ti alloys can lead to enhanced the β phase metastability and varying trigger stress on deformation at room temperature

[158]. The supersaturation provides is necessary to elicit phase transformation during the subsequent mechanical deformation.

During heat treatment, the control of β grain growth is essential, especially for the processing of β-Ti fine tubes since the grain size stongly influence the mechanical properties of metastable β-Ti alloys [159]. Generally, the tensile strength of an annealed β-Ti alloy decreases with an increase in annealing temperature, while the ductility increases. For example, Fan et al. reported that a Ti-7Mo-3Nb-3Cr-3Al alloy exhibits no strength advantage after heat treatment, but can achieve high ductility following annealing treatments [160]. Cold deformation and interstitial annealing can increase elasticity. Wang et al. contribute the improvement to the decreased grain sizes and increased dislocations [161]. Zhang et al. and Kim et al. reported that fine α phase and fine thermal ω precipitates potentially formed by heat treatments enhanced shape memory the characterisation [162, 163].

2.2.3. Twinning activity in β titanium alloys

2.2.3.1. Overview of twins

Designing alloys on the basis of Mo_{eq} and martensite start temperature is confined to prediction of SIM transformation. However, it is also used to predict the occurrence of twinning, which is another important deformation mechanism in metastable β-Ti alloys. Generally twinning is an important deformation mechanism in hcp structure due to the low crystal symmetry. In body-centred-cubic (bcc) metals and face-centred-cubic (fcc) metals, twinning is also a commonly observed deformation mechanism [164]. In bcc structures, $\{332\}\langle 113\rangle$ is a most frequently reported twinning mode. $\{112\}\langle 111\rangle$ twinning mode has also been observed in metastable alloys [42, 43]. Table 2.2 shows the 12 variants in each twinning mode [45]. Research involving the twinning mechanism has been widely performed due to its importance to the mechanical properties of β-Ti alloys.

The nucleation and growth of twins is responsible for the complex nature of twinning mechanism. Two traditional explanations of the twinning mechanism are shear by stress and dislocation dissociation. The shear mechanism involves external stress or internal strain applied to the crystal, while the dislocation mechanism is associated with the nucleation and movement of partial dislocations. However, these two approaches do not adequately explain the twinning process. As a result, a shuffle mechanism for bcc lattice structures and a mechanism of random activation of partials in fcc metals have been proposed [165]. The twin formation energy of bcc structures is generally

higher than that of fcc metals [166], indicating that twin formation in bcc crystals is more difficult than in fcc crystals. However, deformation twinning in fcc metals is less frequently observed under normal deformation conditions due to the relatively high stacking fault energies in fcc metals. Conversely, $\{112\}\langle 111\rangle$ and $\{332\}\langle 113\rangle$ twins have been frequently observed in bcc β-Ti alloys [167]. The shuffle mechanism is commonly ascribed to $\{112\}\langle 111\rangle$ and $\{332\}\langle 113\rangle$ twins. It was reported that the twins can form through a repeated shuffle sequence by overcoming an energy barrier [167].

Table 2.2 12 variants of $\{332\}\langle 113\rangle$ and $\{112\}\langle 111\rangle$ twinning modes. [45]

$\{112\}\langle 111\rangle$ twinning mode	$\{332\}\langle 113\rangle$ twinning mode
$(112)[\bar{1}\bar{1}1]$	$\{332\}\langle 11\bar{3}\rangle$
$(121)[\bar{1}1\bar{1}]$	$\{332\}\langle 1\bar{3}1\rangle$
$(211)[1\bar{1}\bar{1}]$	$\{332\}\langle \bar{3}11\rangle$
$(\bar{1}12)[1\bar{1}\bar{1}]$	$\{33\bar{2}\}\langle 1\bar{1}\bar{3}\rangle$
$(\bar{1}21)[11\bar{1}]$	$\{3\bar{2}3\}\langle 131\rangle$
$(\bar{2}11)[\bar{1}\bar{1}\bar{1}]$	$\{2\bar{3}3\}\langle \bar{3}\bar{1}1\rangle$
$(1\bar{1}2)[\bar{1}11]$	$\{\bar{3}32\}\langle \bar{1}1\bar{3}\rangle$
$(1\bar{2}1)[\bar{1}\bar{1}\bar{1}]$	$\{\bar{3}23\}\langle \bar{1}\bar{3}1\rangle$
$(2\bar{1}1)[11\bar{1}]$	$\{\bar{2}33\}\langle 311\rangle$
$(11\bar{2})[\bar{1}\bar{1}\bar{1}]$	$\{33\bar{2}\}\langle 113\rangle$
$(12\bar{1})[\bar{1}11]$	$\{32\bar{3}\}\langle 1\bar{3}\bar{1}\rangle$
$(21\bar{1})[1\bar{1}1]$	$\{23\bar{3}\}\langle \bar{3}1\bar{1}\rangle$

2.2.3.2. $\{332\}\langle 113\rangle$ twinning mode

In comparison with $\{112\}\langle 111\rangle$ twinning, the $\{332\}\langle 113\rangle$ twinning mode has been more frequently reported in β-Ti alloys with lower amounts of β phase stabilising elements such as reduced Nb and Sn [6, 168-170]. This twinning mode was first confirmed in the 1970s in a Ti-15Mo-6Zr-4Sn alloy (wt.%) [47]. It is considered as an important deformation mode in addition to the SIM transformation [35]. However, $\{332\}\langle 113\rangle$ twinning has not been reported as a major twinning mode in other bcc metals. This is because $\{332\}\langle 113\rangle$ twinning is not the most favourable twinning mode in bcc metals and alloys because one-half of the atoms must shuffle after the twinning shear to form the $\{332\}\langle 113\rangle$ twin [171]. Such additional movement of atoms is not required in $\{112\}\langle 111\rangle$ twinning. For the $\{332\}\langle 113\rangle$ twinning, the decrease of the β phase stabilising alloy elements causes a decrease in the

shear modulus $c'((c_{11}-c_{12})/2)$, which reflects the resistance to shear of $\{011\}$ β planes along $\langle 011\rangle$ β directions. Several models of the movement of atoms required in $\{332\}\langle 113\rangle$ twinning have been reported [172, 173], and it has been considered that instability of the metastable β-Ti phase allows complex movement of atoms and facilitates $\{332\}\langle 113\rangle$ twinning [174]. Tobe et al. [41] studied $\{332\}\langle 113\rangle$ twinning and compared it with other twinning modes by taking account of the shear and shuffle mechanisms of the twinning modes, and concluded that lattice instability lowers the possibility of $\{112\}\langle 111\rangle$ twinning because additional shuffling to form the $\{112\}\langle 111\rangle$ twins is caused by the lattice modulation. Therefore, $\{332\}\langle 113\rangle$ twinning of the bcc structure was reported as the most likely twinning mode due to the required lower magnitude of shuffle in comparison with the other twinning modes. The lattice modulation plays an important role in facilitating the formation of the $\{332\}\langle 113\rangle$ twins and in suppressing the formation of the $\{112\}\langle 111\rangle$ twins.

$\{332\}\langle 113\rangle$ twinning has been reported in metastable β-Ti alloys [42, 44-46, 95], and has attracted attention as an important deformation mechanism. Hanada et al. [42] observed $\{332\}\langle 113\rangle$ twins in various β-Ti alloys and reported that twins were associated with the stability of β phase. They also concluded that the $\{332\}\langle 113\rangle$ twinning was associated with strain hardening behaviour due to the following features [174].

- The accumulation of dislocations in twinned area and neighbouring area between twins and parent grains,
- Frequent twin intersections between secondary twins and primary twins,

2.2.3.3. Twinning identification

$\{332\}\langle 113\rangle$ twinning can be characterised by optical microscope and TEM observations. The former has lower resolution and cannot identify twins directly. The latter has a high resolution but can only observe a small and highly localised area. In comparison, EBSD analysis provides a better method for twin identification. This method has been widely used in analysing deformation twined structures in twinning-induced plasticity steels [175-177], magnesium alloys [178-180] and twinning in β-Ti alloys [45, 170]. Kuramoto et al. [170] indentified $\{332\}\langle 113\rangle$ twins in a deformed metastable Ti-Nb-Ta-Zr β-Ti alloy using EBSD. Bertrand et al. [45] determined different twinning modes using EBSD, $\{112\}\langle 111\rangle$ and $\{332\}\langle 113\rangle$ twinning were identified in a Ti-Nb-Ta β-Ti alloy in a cyclic tensile testing.

Twin formation in β-Ti alloys is dependent on grain orientation. Materials deformed by $\{332\}\langle113\rangle$ twinning form distinct areas depending on the deformation directions. In general, the twins form in a lattice with the deformation direction close to the $\langle111\rangle$ direction. The orientation dependence of twinning can be described using Schmid factor (SF) [45, 62, 178]. The formular to calculate SF is shown as:

$$SF = \cos\lambda \cos\phi \qquad \text{Equation 2.3}$$

where λ and ϕ are the angles between the tensile direction and the normal to the twinning plane and the twinning direction, respectively.

The SF is initially proposed to predict slip systems. Then twinning mode was also anylysed by the SF for hcp or bcc structured materials [45, 47]. Bertrand et al. [45] studied the selection of twinning systems in β-Ti alloys. The results indicated and $\{332\}\langle113\rangle$ and $\{112\}\langle111\rangle$ twins obeyed SF in the β-Ti alloys. The highest value of SFs was generally selected when twinning was activated. When calculated SFs were close for the two twinning systems, $\{112\}\langle111\rangle$ twinning tends to be activated, while $\{332\}\langle113\rangle$ twinning can be activated with a higher SF value exclusively. Preferential selection of twinning variants also depends on the existence of crystallographic texture. However, other factors (such as local stress concentrations and geometric constraints between neighbouring grains) should also be considered in the formation of twins. The two factors are believed not to obey the Schmid's law. Min et al. reported that the two factors contribute to the activation of twinning systems even at a very low SFs [181, 182].

2.2.3.4. Other deformation mechanisms associated with $\{332\}\langle113\rangle$ twinning

It also has been reported that the $\{332\}\langle113\rangle$ twinning is associated with the stress-induced ω phase transformation [183, 184]. After conducting a systematic study between $\{332\}\langle113\rangle$ twins and plate-like ω phase in a metastable β-Ti alloy, Hanada et al. [38] concluded that single variant of plate-shaped ω phase was generated with a special orientation relationship with the β phase matrix and $\{332\}\langle113\rangle$ twinning for low contents of Nb in Ti-Nb alloys, while deformation results in only $\{332\}\langle113\rangle$ mechanical twins by increasing Nb content [42]. Zhao et al. also reported $\{332\}\langle113\rangle$ mechanical twinning in a series of metastable β Ti-18V and Ti-22V alloys during cold rolling, but plate-shaped stress-induced ω phases were not observed [185].

The relations between ω phase transformation and twinning are conflicting. Some reports considered that it may be related to the amount of oxygen content in β titanium alloys [42]. Decreasing oxygen content can enhance the ω phase transformation in β titanium alloys [186]. Plastic behaviour of metastable β-Ti alloys with different levels of oxygen have been studied by Wang et al. They reported that the β-Ti alloys with low levels of oxygen tend to deform through martensitic transformation, whereas alloys with high levels of oxygen deform through mechanical twinning [125].

Increasing the oxygen concentration increases yield strength and decreases elastic modulus and, but does not reduce the ductility significantly for the β-Ti alloy [125]. A combination of mechanical {332}⟨113⟩ twins and ω-phase is an effective approach for enhancing ductility in β-Ti alloys [35]. Merteleur et al. and Sun et al. [35, 187] reported a Ti-12Mo alloy that exhibited a considerable balance between strength and ductility due to a combination of different deformation mechanisms.

Dislocation slip is another deformation mode associated with twinning. It can be activated in alloys with high β phase stability, and results in superior yield strength and reduced ductility. Therefore, the high yield strength alloys are mainly dominated by dislocation slip, and alloys showing large uniform elongation typically deform by {332}⟨113⟩ twinning with significant strain hardening. Min et al. reported that a combination of {332}⟨113⟩ twinning and dislocation slip caused by solidification segregation of alloying elements, resulting in heterogeneous distribution of Mo, Zr, and Fe, was effective for achieving high strength and good ductility in Ti-Mo-Zr and Ti-Mo-Fe alloys [181, 182, 188].

2.2.4. Mechanical properties of β-Ti alloys

2.2.4.1. Effects of stress-induced α″ martensite on mechanical properties

A low Young's modulus of approximately 38 GPa were observed to occur in metastable β Ti alloy undergoing stress-induced α″ martensitic transformation during cold rolling [37, 48]. Based on observations of the preferred texture development of ⟨010⟩ α″ and ⟨110⟩ β, the low modulus was associated with the anisotropic elastic modulus of α″ with an orthorhombic crystal structure, although there was no available data regarding the elastic moduli of an α″ single crystal. The low elastic modulus is contribute to be due to the easy movement of α″ interfaces under applied stress.

It was reported that the SIM transformation may occur during elastic deformation of the β phase. Therefore, the trigger stress for activating the α″ phase does not represent the yield strength for the alloys. These alloys exhibit the double yielding phenomenon was observed in these alloys during tensile tests as shown in Fig. 2.2, where the first yielding point indicates the critical stress required to activate an α″ phase transformation.

Hao et al. studied a Ti-24Nb-4Zr-7.9Sn alloy. This alloy exhibited a stress-strain curve with non-linear shape in elastic stage. The maximum recoverable strain in this alloy can achieve up to 3.3% and its modulus was very low [32, 153, 189]. Due to the non-linear shape in tensile stress-strain curves, a tangent modulus was defined as the slope of tensile curves at very beginning stage. This result also implies that α″ may be induced at a stress below those estimated from a stress-strain curve, which is the reason that an exact trigger stress to SIM α″ transformation is difficult to determine in these alloys.

Some previous work tried to stabilise SIM α″ by cyclic deformation and severe deformation [38, 146, 190]. It has been accepted that the stabilisation is due to the interruption of the reverse martensitic transformation by dislocations introduced during prior plastic deformation. Hanada et al. [107] attempted to estimate the real Young's modulus by stabilising the stress induced α″ martensite in a β Ti alloy with strong ⟨010⟩ α″ and ⟨110⟩ β textures through heavy rolling. When complete α″ stabilisation is obtained, no martensitic transformation would be induced and no interface of existing martensite plates would move. The elastic moduli of ⟨010⟩ α″ and ⟨110⟩ β obtained in the rolled β-Ti alloy exhibited a low low value, which is favourable for implant materials.

2.2.4.2. Strain hardening behaviour of β-Ti alloys

An true stress-true strain curve for a Ti-Mo alloy is presented in Fig. 2.6 obtained by Sun et al [35]. The tensile curve shows much larger strain hardening rate than that of traditional titanium alloys. A strain hardening rate-true strain curve was also presented in Fig. 2.6. From the elastic limit, first increase of the strain hardening rate was observed which went up to 2000 MPa according to literature [187, 191]. For this type of strain hardening curve, typical three stages are defined. Stage I is related to the traditional elastic and plastic transition. Strain hardening rate largely increased in stage II, then decreased in Stage III. The two deformation modes, twinning and martensitic transformation, were reported to occur in the stage III [187]. The selection of activated deformation mechanisms in Stage II

is important for the evolution of the deformation modes to exhibit unconventional strain hardening rate and the superior ductility of SIM β-Ti alloys.

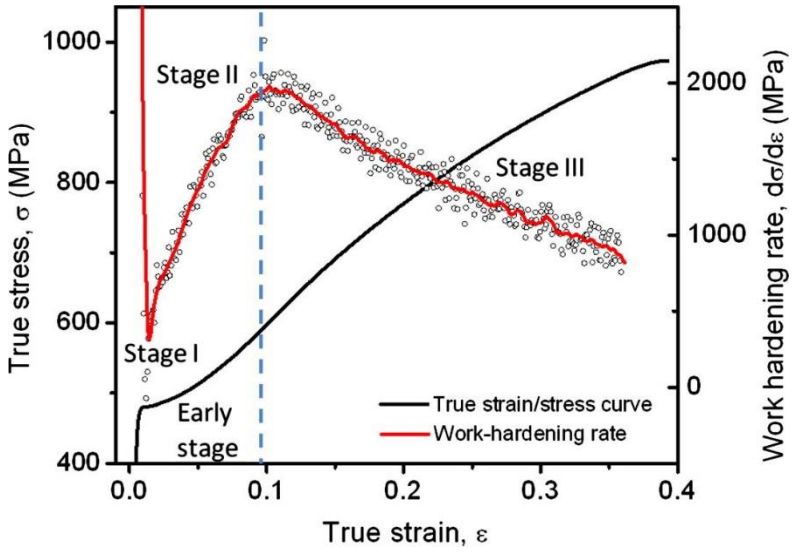

Fig. 2.6 Tensile curve of a Ti-12Mo alloy in black line. The read trace shows corresponding strain hardening rate-true strain curve. [35]

2.2.4.3. Anisotropic moduli in β-Ti alloys

The modulus, elasticity and mechanical strength is strongly orientation dependent. Tensile tests on metastable β-Ti alloys showed that samples with ⟨100⟩ and ⟨111⟩ textures had a classic elastic deformation behaviour, while samples with ⟨110⟩ texture exhibits a superelastic behaviour [192]. Morris et al. reported that trigger stress for phase transformation was beyond yield strength when loading is along the ⟨100⟩ and ⟨111⟩ directions [193].

Matsumoto et al. [194] and Jung et al. [195] investigated the influence of α″ martensitic transformation on the elastic modulus in metastable β Ti-33.6%Nb-4%Sn alloy. They found that cold rolling led to a low modulus and explained that the low modulus is related to ⟨110⟩ β and ⟨100⟩ α″ texture formation along the rolling direction. Therefore, they concluded that the second method to further decrease the modulus is to use stress-induced α″ martensitic transformation apart from modifying the alloy composition of a single β phase.

Several studies on the elastic moduli of single crystals are helpful in tailoring desired elasticity. Tane et al. [196] concluded that Young;s modulus was increased when texture develop from ⟨100⟩ to ⟨110⟩, then to ⟨111⟩ directions. Similar elastic anisotropy was reported in Ti-Nb-Al, Ti-24Nb-4Zr-8Sn and Ti-Mo-Zr-Al alloys [113, 197, 198].

Jung et al. [199] investigated the mechanical properties of severely deformed Ti-25Nb-11Sn rods and found that the rods were composed of single β phase, exhibiting low modulus and high strength. The alloy had a strong ⟨110⟩ texture along the deformation direction. According to Zhang et al. [113], the elastic moduli of Ti-24Nb-4Zr-8Sn have Young's moduli in ⟨100⟩, ⟨110⟩ and ⟨111⟩ of 27.1 GPa, 56.3 GPa and 88.1 GPa, respectively. Therefore, the utilisation of ⟨100⟩ deformation texture is promising for the application of β-Ti alloys to biomedical applications.

Zhang et al. and Lee et al. found that decreasing electron-to-atom ratio in metastable β-Ti alloys leads to a decreased Young's modulus [113, 198]. Therefore, the control of crystal orientations in low e/a single crystals or of deformation textures in low e/a polycrystals is a promising method to develop new β-Ti alloys with low Young's modulus. Lee et al. summarized the data on the Young's modulus of single β crystals, and claimed that low modulus was strongly related to low electron to atom ratio, e/a, ranging from 4.1 to 4.8 [198]. Therefore, ⟨100⟩ textured β Ti alloy with a low e/a ratio as a material with lowest Young's modulus.

2.2.4.4. Size effect on mechanical properties

In single phase polycrystalline metallic alloys, the yield stress of alloys depends on grain size according to the following Hall-Petch equation, where σ_i and k are material parameters and D is the grain size [200].

$$\sigma_y = \sigma_i + k/\sqrt{D} \qquad \text{Equation 2.4}$$

There have been some efforts to apply the Hall-Petch relation to the β-Ti alloys [201-203]. In these studies, the grain size of the matrix phase was used. However, in alloys experiencing martensitic transformation, grain sizes of different phases play a role in controlling the overall friction stress. For example, a Ti-Nb-Al-Zr alloy undergoing SIM transformation during mechanical testing was investigated [204]. Two-phase microstructures consisting of β and martensite α″ phases were observed prior to plastic deformation in this case. The real yield strength deviated from the results

calculated by the Hall-Petch equation using the β grain size phase. This indicates that σ_i and k determined by using the grain size of one of the phases are not strictly independent of grain size, in the view of the assumptions in equation 2.4. Fan et al. [205] proposed a modified Hall-Petch relationship for two-phase alloys, which has been shown to be valid for several different materials, including some β-Ti alloys. The applicability of the Hall-Petch relationship for metastable β-Ti alloys was investigated by Montecinos et al. [206] for alloys that are initially single-phase alloys and undergo SIM transformation during tensile testing prior to the onset of plastic deformation. They reported that trigger stress follows the modified Hall-Petch equation. Sadeghpour et al. [105] studied the influence of the grain size on the SIM, and concluded that volume fraction of SIM increases with increasing grain sizes from 150 μm to 250 μm, but further increases in the grain size up to 500 μm lead to a decrease in the volume fraction of SIM.

Equation 2.4 is also applicable when dominant deformation mechanism is mechanical twinning in β-Ti alloys [164, 207]. It is well known that the activation of twinning largely depends on the β grain size [207]. Mechanical twinning was facilitated in coarse grains in copper, titanium alloys, magnesium alloys and twin-induced plasticity steels [208-211]. When dominant deformation mechanism transfers from mechanical twinning to dislocation slip, the Hall-Petch slope, *k*, is generally increased [212-214], which indicates the varying grain size has larger influence on the trigger stress to activate twinning than that to dislocation slip. Yu et al. [215] found that accumulated intersections of dislocations facilated the growth of twins, and claimed that large grain size enhanced twinning activity. Marcinkowski et al. [216] explained that the increased Hall-Petch slope to activate mechanical twinning is associated with both higher stress required to nucleate twins and unfavourable orientations. Barnett et al. [217] considered the higher Hall-Petch slope to activate twinning was induced by a greater twin number density required for yielding in the materials with smaller-sized grains. More twin nucleation can lead to an increasing applied stress.

Twin nucleation also depends on the stress concentrations around grain boundaries [218, 219]. In many cases, twins formed from a grain boundary [218, 220, 221], which indicates that the density of twin nucleation is related to the grain size and grain boundary area. Increasing grain size increases twin density in polycrystalline alloys [217] due to the increased grain boundary area associated with increasing grain size. In addition, Grain size limits the growth of individual twins, i.e., only shorter twins can be generated in small grains. Thus, volume fraction of twins per grain is increased with increasing grain size [222], in view of the increase in the average number of twins and volume fraction of individual twins. Therefore, large grain sizes are favourable for higher twin volume fractions.

2.2.4.5. Twinning-induced plasticity and Transformation-induced plasticity

A strategy to obtain a combination of superior ductility and strength through transformation-induced plasticity (TRIP) and twinning-induced plasticity (TWIP) was reported in metastable β-Ti alloys [223]. As mentioned above, several deformation-induced phase transformations, ω phase, α″ phase, and mechanical twinning can be activated at varying external stress [5, 224-226], and the mechanical behaviours of β-Ti alloys are dependent on the activated deformation mode [131]. SIM α″ transformation induced plasticity in β-titanium alloys is a good candidate for achieving favourable balance between strength and ductility similar to that in TRIP steels. TWIP β-Ti alloys have also received attention due to high ductility and strain hardening rate in these alloys in association with $\{332\}\langle 113\rangle$ twinning [42, 227]. Min et al. and Hanada et al. suggest that mechanical twinning simultaneously improves the strength and ductility of β-Ti alloys due to dynamic grain refinement [228, 229]. Weiss et al. reported an optimisation of mechanical properties in a β-Ti alloy. They investigated the β phase stability through change their composition, and found that critical resolved shear stress (CRSS) for mechanical twinning and Ms temperature were influenced by the stability of β phase [35, 142, 230]. Marteleur et al. [187] reported a large uniform elongation with both TRIP and TWIP behaviours in a Ti-12Mo alloy. Sun et al. [35] also reported that the combined effects of phase transformation and mechanical twinning, $\{332\}\langle 113\rangle$ and $\{112\}\langle 111\rangle$, result in a high rate of strain hardening in a metastable β Ti-Mo alloy. TRIP and TWIP mechanisms can be activated simultaneously in some specifically designed metastable β-Ti alloys exhibiting superior elasticity, high strain-hardening behaviour and good mechanical strength [32, 38, 187, 224-226, 231].

Marteleur et al. designed an approach with the intention to activate TRIP and TWIP simultaneously in a Ti-12Mo alloy with high strain hardening rate [187]. Experimental validation of this design showed the Ti-12Mo alloy exhibited a high strength, an large elongation and superior strain hardening rate [187, 191]. The values of strength and elongation were high for bcc alloys.

2.3. Deformation mechanism in Mg alloys

2.3.1. Twinning activity

Due to the characteristics of the hexagonal close packed (hcp) structure, the dislocation activity associated with basal or prismatic $\langle a\rangle$ slip and the number of slip systems are limited due to the high

threshold stresses for the dislocations [60]. In combination with the strong textures present in most rolled and extruded products, this results in poor tensile ductility, fracture toughness and formability of magnesium at room temperature and limits its potential applications due to a lack of dislocation-based mechanisms to accommodate strain in the $\langle c \rangle$ axis direction. Therefore, deformation twinning becomes an important mode of strain accommodation to satisfy the requirement for independent deformation systems in hcp metals during deformation at low and medium temperatures by providing additional independent deformation modes. Three types of twins are frequently reported in magnesium alloys, $\{10\bar{1}2\}\langle 10\bar{1}1\rangle$ extension twinning, $\{10\bar{1}1\}\langle 10\bar{1}2\rangle$ contraction twinning and $\{10\bar{1}2\}-\{10\bar{1}1\}$, $\{10\bar{1}1\}-\{10\bar{1}2\}$, $\{10\bar{1}3\}-\{10\bar{1}2\}$ double twinning. They have been reported to be of importance in relation to shear localisation and fracture. Twin variant selection depends on whether the accumulated local stresses reach a corresponding CRSS. A low CRSS (~2-4 MPa) required for nucleation and propagation of $\{10\bar{1}2\}\langle 10\bar{1}1\rangle$ extension twinning, facilitates the most commonly observed twinning mode [232]. A second twin type, $\{10\bar{1}1\}$ twins, can also form in the primary $\{10\bar{1}2\}$ twins, but are not typically formed until strain levels of greater than ~5% are reached [233].

2.3.1.1. $\{10\bar{1}2\}$ extension twins

Theoretically, $\{10\bar{1}2\}$ twinning can be activated on six variants of $\{10\bar{1}2\}$ twinning planes with a corresponding variant of $\langle 10\bar{1}1\rangle$: $(10\bar{1}2)[\bar{1}011]$, $(\bar{1}012)[10\bar{1}1]$, $(01\bar{1}2)[0\bar{1}11]$, $(0\bar{1}12)[01\bar{1}1]$, $(\bar{1}102)[1\bar{1}01]$ and $(1\bar{1}02)[\bar{1}101]$. This twinning mode induces an extension strain along the c-axis in the hcp crystal lattice (so called extension twinning as it results in an elongation of the unit cell along the c-axis direction) and a contraction strain along the $\langle \alpha \rangle$ axis. These are activated during the deformation of randomly textured materials or when uniaxial tension is applied along the c-axis of materials [234].

According to the nature of $\{10\bar{1}2\}$ twins, they conform to the external stress conditions. For example, when extruded Mg alloys are compressed along the extrusion direction, $\{10\bar{1}2\}$ twinning occurs and becomes a major deformation mechanism because the samples are compressed in the $\langle \alpha \rangle$ direction. In contrast, when the samples are deformed in tension along the extrusion direction, $\{10\bar{1}2\}$ twinning is not expected to occur. However, $\{10\bar{1}2\}$ twins were also formed and induced a strain whose direction opposed that of the external stress in the study of Koike et al [235]. They reported a relation between the tendency for basal dislocation slip and the tendency for odd $\{10\bar{1}2\}$ twinning. This relation is thought to be due to the anisotropy and inhomogeneity of dislocation plasticity among

neighbouring grains. If basal slip occurs easily in one grain but not in the surrounding grains, negatively strained $\{10\bar{1}2\}$ twinning would occur in order to reduce the incompatibility of plastic strain caused by the basal slip.

Apart from coordinating plastic deformation, $\{10\bar{1}2\}$ twinning can lead to significant microstructural changes. The operation of twinning during deformation also has a strong effect on the flow stress and on texture evolution, as a result of the lattice reorientation that accompanies twinning [164]. The characteristics of $\{10\bar{1}2\}$ twinning reported in the literature were demonstrated below [234, 236]:

(i) Reorientation of ~86 °is caused by the $\{10\bar{1}2\}$ twining and influences following twinning activities and dislocation slip;

(ii) Grains can be subdivided by well-developed $\{10\bar{1}2\}$ twinning, which results in a mechanism similar with grain refinement.

(iii) A small amount of pre-straining was reported to facilitated $\{10\bar{1}2\}$ twinning in the Mg alloys [72, 236].

The orientation of grains is associated with texture in materials, and the refinement of grains generally significantly enhance the mechanical properties. Therefore, appropriate twinning activity in magnesium alloys can improve the mechanical properties.

2.3.1.2. Contraction twins

When the c axes of Mg alloys are placed in compression, $\langle c+a \rangle$ slip on the $\{11\bar{2}\bar{2}\}$ plane was observed. More frequently, the activation of contraction twinning has been reported. These deformation modes allow for limited plasticity because it turns out that contractions along the c axis are the least ductile. Mg alloys exhibiting this type of deformation are of commercial interest. Texture evolution during cross-sectional reductions involve contraction along the c-axis and this is relevant to sheet and tube products [237].

Contraction along the c-axis of the hcp lattice structure can activate different variants of contraction twins. Twins were observed to be complex doubly twinned structures that exhibit high local shear strains. There has been some debate over the sequence of twinning and the twinning modes involved in this mechanism [75], but the following are in agreement with observation in single crystals:

- $\{10\bar{1}1\}$ or $\{10\bar{1}3\}$ are the two frequent observed planes, where primary twins generated.
- Twins with habit planes near $\{30\bar{3}4\}$ frequently form.

$\{10\bar{1}1\}-\{10\bar{1}2\}$ or $\{10\bar{1}3\}-\{10\bar{1}2\}$ double twins were frequently followed the activation of contraction twins in Mg alloys [75, 238]. In addition, in the case of secondary twinning, a preferential alignment of the basal planes for slip is produced.

The primary $\{10\bar{1}1\}$ and $\{10\bar{1}3\}$ twins have characterised misorientation angles and corresponding axis directions of 56.2 °$\langle 1\bar{2}10\rangle$ and 64.0 °$\langle 1\bar{2}10\rangle$, respectively. Barnett et al. and Cizek et al. obtained four distinct misorientation relations [239, 240]. The misorientation angle for the $\{10\bar{1}1\}-\{10\bar{1}2\}$ double twinning are 37.5 °$\langle 1\bar{2}10\rangle$, 30.1 °$\langle 1\bar{2}10\rangle$, 66.5 °$\langle 5\bar{9}43\rangle$ and 69.9 °$\langle 2\bar{4}21\rangle$ [239], respectively. The corresponding misorientations for the $\{10\bar{1}3\}-\{10\bar{1}2\}$ double twinning are 22.3 °$\langle 1\bar{2}10\rangle$, 29.7 °$\langle 1\bar{2}10\rangle$, 63.6 °$\langle 3\bar{9}62\rangle$ and 66.3 °$\langle 3\bar{7}41\rangle$ [240].

2.3.2. Identification method

2.3.2.1. Orientation

An understanding of twinning activity related to grain orientation for any given deformation mode is an important part of the development of a study on plasticity behaviour. In general, two approaches can be used to obtain such information. In one approach, crystal plasticity parameters are adjusted to match the predicted and observed texture evolution [241-243]. In the other approach, the microstructure for slip or twinning deformation modes, is analysed on an individual grain-by-grain basis [244-246]. For the second approach it is necessary to know the orientation of each examined grain prior to deformation. The situation is simplified for Mg alloys because extensive twinning occurs at low strains, where the plastic rotations in each grain induced by the slip are observed as small misorientations. Therefore, this approach for determining the initial grain orientation is sufficient to collect useful data for analysing the specific twinning activity.

For each $\{10\bar{1}2\}$ and $\{10\bar{1}1\}$ twinning system, six variants are potentially activated depending on the orientation of parent grains. Thus, The combination of selected variants for each twinning mode leads to a large number of twinning modes in double twin results in a large number of possible final twinned orientations [239]. Therefore, study on the relationships between orientation of parent grains and different twinning modes is important for understanding of twinning activity in Mg alloys.

2.3.2.2. Schmid factor

Schmid factor is applicable to analyse twinning nucleation. The CRSS for a given twinning mode is equal to the applied external stress multiplied by the Schmid factor as defined in Equation 2.3. Therefore, Twin variant selection in Mg alloys has been frequently evaluated in uniaxial deformation using the SF. The theoretical twin variant with the maximum SF value is predicted to be generated in the grain during deformation. Experiments have been performed on specific twin variants by use of a SF parameter. These investigations have shown that most twin variant selections correspond well with the SF values. For example, an investigation of the effect of loading method on variant selection of extension twinning was performed by Hong et al. [237]. Their results showed that for both loading modes the observed twin variants could be explained using the SF parameter. The grain orientation dependence of twinning within individual grains has also been discussed by several authors in terms of the SF.

However, multiple twin variants are usually activated in one grain due to the plastic deformation being affected by several internal or external factors. For example, when the external loading is parallel to the c-axis of a magnesium single crystal, all possible theoretical variants $\{10\bar{1}2\}$ extension twinning have have similar values of SF [178, 236], indicating that six variants could be simultaneously generated based on the Schmid's law. When compressive stress applied in the rolling direction of Mg plates, the $\{10\bar{1}2\}$ twin variant pair with the maximum SF is generated at the early stage of deformation. With further strain, the new variants with lower SF can also be activated as long as the local stress reach the CRSS value [247].

2.3.2.3. Non-Schmid twins

The selection of twin variant is a complex process and is affected by several factors apart from the SF, such as strain accommodation between grains, strain path and strain parameter. The first twins activated during tension or compression loading of single crystals or polycrystals are mostly primary variants with the highest SF as shown in previous studies [178, 236, 247, 248]. Significant deviations from this have been reported, both for $\{10\bar{1}1\}$ compression twinning and more recently for $\{10\bar{1}2\}$ primary and secondary twinning in Mg alloys [249].

Luo et al. found that some initial twins did not comply with the Schmid's law in AZ31 Mg alloy under specific loading conditions due to the local-stress fluctuations near grain boundaries [247]. The

deviation angles ranging from 30 °to 40 °were the threshold transferred from $\{10\bar{1}2\}$ twin variants to the non-Schmid behaviour [178, 236]. Niezgoda et al. [250] observed that although nucleation of extension twin variants could be predicted using the SF parameter, the growth of extension twin variants was more dependent on strain accommodation to deformation in adjacent grains. Jiang et al. [251] reported that two twin variants were observed in one grain, many twins corresponded to variants with the 3rd or lower ranked SF values. Barnett et al. [239] concluded that this was due to non-Schmid behaviour. Koike et al. [252] also observed non-Schmid $\{10\bar{1}2\}$ twinning during tensile deformation of Mg alloy sheets, and ascribed this behaviour to local accommodation of strains caused by basal dislocation slip.

In terms of studies concerning double twins [253-256], the double twins reported in the literature generally do not have the largest value of the six potential SFs, even negative values of twin variants were selected in some reports. Barnett et al. [239] studied the so-called non-Schmid double twins through a series of tensile and compressive tests on rolled and extruded magnesium alloy. They explained this type of double twins using a theory concerning the capacity to accommodate strains, which indicated that secondary twins have to select the closest variant to the primary twins where they generated. Cizek et al. focused on the local strain accommodation associated with the deformation caused by shear stress or twinning activity [253]. Ando et al. [255] performed tensile experiments on AZ31 alloy for studying twinning activity, and reported that non-Schmid double twinning were activated by required local strain accommodation transferred from primary twins to secondary twins.

The efficiency of twin transfer through grain boundaries can be defined by a strain compatibility factor, where ψ is the angle between the twinning plane normal of the two neighbouring grains, and κ is the angle between twinning shear directions of the two neighbouring grains [239].

$$m_0 = \cos\psi \times \cos\kappa \qquad \text{Equation 2.5}$$

The m_0 between neighbouring twins can be calculated using orientation data from EBSD. A larger strain compatibility factor m_0 indicates that it is easier for a given twin to transfer its shear strain to the neighbouring area facilitating nucleation of another twin. It has been reported that the m_0 is a characteristic feature of non-Schmid twins, especially for $\{10\bar{1}2\}$ secondary twins, where the twinning variant selection is determined by the requirement for local accommodation.

2.3.3. Relations of twinning and mechanical properties

2.3.3.1. Why do twins affect mechanical properties

Twin variant selection and multiple twin variants have a significant effect on the microstructural evolution and mechanical properties of Mg alloys. The nucleation of multiple twin variants change the internal stress state within a grain. Wang et al reported that twin-twin boundaries with misorientation relationships of 60°⟨$10\bar{1}0$⟩ and 60.4°⟨$8\bar{1}\bar{7}0$⟩, which are generated by the interaction between varying $\{10\bar{1}2\}$ variants, can retard the growth of twins and promote twinning nucleation [257, 258]. In addition, multiple twinning modes influence both the texture evolution during deformation and microstructural subdivision due to the intersection of different twin variants.

When Mg alloys are deformed in a direction favourable for $\{10\bar{1}2\}$ twinning, the yield strength is much lower than that in other deformation directions [57]. The $\{10\bar{1}2\}$ twinning will rotate the lattice by 86.3°, which means that the texture will be influenced greatly by the generation of $\{10\bar{1}2\}$ twinning [57, 259]. So, the texture and the mechanical properties of Mg alloys can be tailored and optimised by controlling twinning activity. Hong et al. changed the texture of Mg alloys through a small amount of pre-twinning strain in their experiments [236]. According to the literature, 7-9% pre-twinning strain can lead to significant texture reorientation [66, 236]. because of the morphological characteristic associated with the lenticular shape of the twins, $\{10\bar{1}2\}$ twins were observed to developed to be lenticular shape in parent grains. So this type of twins can cause an analogous grain refinement phenomenon by subdividing grains to strengthen in specific directions [77, 260].

For twinned structures, both matrix texture and twin texture have to be studied as described in the literature [77]. The twin texture plays an important role in the subsequent deformation characteristics by the volume fraction and orientation. As mentioned, $\{10\bar{1}2\}$ twinning is most frequently observed deformation mechanisms in most Mg alloys, and it is reported that the strain hardening behaviour and texture evolution are closely related to the $\{10\bar{1}2\}$ twinning activity [72, 78]. Park et al. [261] conducted experiments with respect to the deformation behaviour of Mg alloy using pre-strain $\{10\bar{1}2\}$ twins. They found that twinning activity was strongly influence by the calculated SF values and grain sizes in samples. A strengthening behaviour associated with the $\{10\bar{1}2\}$ twins was observed in their experiments and it was attributed to the pre-twinned structure. Therefore, $\{10\bar{1}2\}$ twinned structures are desirable for a so-called pre-twinning strengthening.

Yoo [54] reported that hcp metals that display profuse twinning possess higher ductility. A favourable effect of $\{10\bar{1}2\}$ twinning in Mg alloys can be observed in the single crystal stress-strain curves of Fig. 2.7. The crystal, in which extension occurred in the direction parallel to the c-axis, transformed completely to the twinning orientation. During twinning the stress remained relatively steady, but the stress increased rapidly to failure once the twinning was complete. The twinned lattice possesses a similar orientation to that for the c-axis compression sample. The failure strain in this case appears to be extended due to strain similar in magnitude to the resolved twinning strain [74].

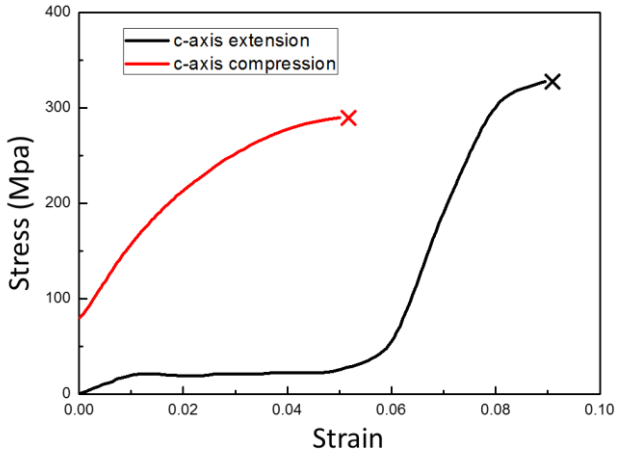

Fig. 2.7. Influence of crystal orientation on the stress strain curve obtained in channel die compression. The c-axis extension sample displays profuse $\{10\bar{1}2\}$ twinning. [74]

2.3.3.2. Strengthening of twinning in Mg alloys

There are several methods to strengthen Mg alloys in the literature, such as age hardening, texture hardening, solid-solution hardening, refinement hardening and dislocation hardening. $\{10\bar{1}2\}$ twinning may interfere with the apparent strain hardening behaviour according to the study of Barnett [75]. This is a general phenomenon observed in deformed Mg alloys undergoing twinning [262]. It was reported that the effect of $\{10\bar{1}2\}$ twinning on the apparent strain hardening behaviour can also enhance uniform elongation in Mg alloys [75].

A small pre-strain can induce profuse twins in Mg alloys. The texture evolution caused by the pre-twinning strongly influence yield strength. The formation of the lamellae shape of twins significantly enhances yield strength for deformation along the unfavourable directions. In the study of Song et al., the increments were 34 MPa and 49 MPa for tension and compression, respectively [263]. It has been

reported in the literature that with an increase in rolling reduction from 1.5% to 3.6% on Mg plates, the yield strength increased gradually with the increasing deformation, which indicates the formation of twins with the change of texture can increase the yield strength [264]. Larger deformations on Mg plates was also reported in the literature [258], the result showed the growth of pre-existing twins instead of the nucleation of new twins during deformation. Other similar results were also reported in the literature [236, 258].

The yield strength of twinned Mg alloys is considered to depend on the amount of twin lamellae [260], and it was reported that grain refinement can improve the yield asymmetry of magnesium alloys. As mentioned above, pre-existing twins can cause almost complete reorientation of grains and analogous refinement strengthening by subdividing grains, because twin boundaries are considered as a significant factor to increase the strength of polycrystalline metals [111].

For hcp alloys, the common strengthening method is texture hardening due to the strong plastic anisotropy. $\{10\bar{1}2\}$ twinning lead to a complete change of texture due to lattice rotation by ~86 °. Xin et al. performed a pre-strain experiment on Mg plates, the c-axis of parent grains and twins rotated to be perpendicular to the strain direction [63]. The result showed that pre-strain along the transverse direction changed the dominant deformation mechanism for the pre-twinned Mg alloy sheets along the unfavourable directions for $\{10\bar{1}2\}$ twinning [77].

Hong et al. performed a compression test on Mg alloy plates. They suggested that with a horizontal shift the compressive curves were coincident. Knezevic et al. and Wang et al. reported that the texture hardening plays the most important role in enhance strain hardening in Mg alloy. They explained that the reorientation caused by $\{10\bar{1}2\}$ twinning generally increase the resistance to deform. The texture hardening is much more effective than the refinement strengthening caused by the twin boundaries in their experiments [78, 265]. The texture hardening strongly depends on the number of grains with unfavourable direction to deform. Therefore, yield strength of Mg alloys can be increased by the texture hardening mechanism by pre-twinning.

Depending on the above discussion, pre-existing twins can be utilised to strengthening Mg alloys by the texture hardening and refinement hardening mechanisms. The yield strength can only enhance pre-twinning along certain crystallographic directions. Hence, the stress state should be taken into account when this strengthening method is used.

2.3.3.3. Texture of Mg alloys

$\{10\bar{1}2\}$ twinning is possible on six $\{10\bar{1}2\}$ twin planes with a specific direction of $\langle 10\bar{1}1\rangle$ with respect to shear stress. The six equivalent twin variants were listed in Table 2.3 [266]. The orientation of twins can be defined by the selected twin variants. The variant selection of twins can be predicted by the Schmid factor as mentioned in the last section. For deformed Mg alloys with c-axis parallel to the strain direction, multiple twins are favourable to be activated with morphologies of intersection and lamellae. When the deformation direction is perpendicular to the c-axis, only one twin variant is favourable to be activated. In this case, twin lamellae generally presents parallel geometry [236].

Table 2.3. Various $\{10\bar{1}2\}$ twin variants in magnesium alloy. [266]

	V1	V2	V3	V4	V5	V6
Twin variants	$(\bar{1}102)[1\bar{1}01]$	$(1\bar{1}02)[\bar{1}101]$	$(\bar{1}012)[10\bar{1}1]$	$(10\bar{1}2)[\bar{1}011]$	$(0\bar{1}12)[01\bar{1}1]$	$(01\bar{1}2)[0\bar{1}11]$

In terms of industrialisation and mass production, the rolling of tubes can generate profuse twins in Mg alloys due to the tri-axial strain paths. Thus, the rolling process of tubes is usually strictly controlled. The two main parameters during cold rolling, ε and Q, are as defined below [267], where, A_0 and A_1 are the initial and final cross-sectional area; t_0 and t_1 are the initial and final wall thickness; D_0 and D_1 are the initial and final outside diameter.

$$\varepsilon = \frac{A_0 - A_1}{A_0} = \frac{t_0 \times (D_0 - t_0) - t_1 \times (D_1 - t_1)}{t_0 \times (D_0 - t_0)} \; ; \qquad \text{Equation 2.6}$$

$$Q = \frac{((t_o - t_1)/t_0)}{((D_0 - D_1)/D_0)} = \frac{(t_0 - t_1) \times D_0}{(D_0 - D_1) \times t_0} \qquad \text{Equation 2.7}$$

The ε is defined as the amount of deformation on the cross section of the tubes and is an indicator of the change of cross-sectional size. The Q is exclusive to tubes as compared with parameters used to describe the rolling of sheets. As Q increases, the ratio of wall-thickness to perimeter decreases and the tubes become thinner. Therefore, the parameter Q indicates the change in cross-sectional shape. No elongation occurs as Q changes. The selection of twin variants can be controlled by changing the ε and Q in each rolling step, thereby importing desirable mechanical properties to the final fine tube products.

The twinned samples obtained by rolling or extruding have a large anisotropy [268], but rolled tubes are produced by multiple processes with varying ε and Q, resulting in decreasing anisotropy. Therefore, designing texture via pre-twinning is not an effective way to control the plastic anisotropy of cold rolled Mg alloys.

2.3.3.4. Twinning effect on fatigue behaviour

Reed-Hill et al. reported that various twins, $\{30\bar{3}4\}$, $\{11\bar{2}4\}$, $\{10\bar{1}4\}$ and $\{10\bar{1}5\}$, were associated with fracture planes [269]. $\{11\bar{2}4\}$ and $\{10\bar{1}3\}$ twins have been reported to act as crack initiation sites [238]. The $\{10\bar{1}1\}-\{10\bar{1}2\}$ double twin has also been proposed to be related to failure by providing fracture initiation sites [270]. According to the fracture model in their report, small voids form along $\{10\bar{1}1\}-\{10\bar{1}2\}$ double twin interfaces and grow to become microcracks as the stress increases. Fracture then occurs along the weakened twin interface. It has been suggested by Barnett et al. that the formation of double twins in Mg alloys can cause shear failure in early stage because of the combination of formation of localised void and strain softening effects [75]. Hartt et al. studied single crystals in order to explain flow localisation and failure resulting from contraction twins. They concluded that the preferential alignment of basal planes in the interior of certain twins resulted in softening, rapid unloading, high strains and internal ductile failure [271]. Ando et al. studied sharp surface steps that led to crack formation. TEM of a substructure of more than 30 surface steps indicated that all these steps accompanied $\{10\bar{1}1\}-\{10\bar{1}2\}$ double twins [272].

The K_{IC} values determined from fatigue pre-cracked fracture specimens have generally been in the range 15 to 25 MPa $m^{1/2}$ [273]. For a rolled Mg alloy having near basal texture (grain size of $\sim$ 65 μm), K_{IC} value varied from 17.6 to 20.7 MPa $m^{1/2}$ depending on whether the crack line is aligned [273]. Somekawa also studied the grain size dependence of K_{IC}, where K_{IC} increased from 12.7 MPa $m^{1/2}$ to 17.8 MPa $m^{1/2}$ by reducing the grain size from 55 μm to 1 μm [273-275]. This was rationalised on the basis of decreased tendency for twinning with reductions in the grain size [207].

Somekawa et al. investigated fracture toughness of AZ31 Mg alloys [276]. A detailed microstructural examination suggested that crack propagation occurs along the boundary between the extension twins and the matrix, resulting in brittle fracture. More recently, higher value of K_{IC} were reported for a fine-grained Mg-Zn binary alloy with grain size of 1-3 μm [277]. This was attributed to suppression of extension twins and occurrence of sub-grain structures.

For deformed Mg alloys, the twinned region may be favourable for detwinning when the release of external stress, although lattice has been rotated by the twinning activity [57, 278]. Fatigue behaviour of deformed Mg alloys is associated with the alternative effects of twinning and detwinning during each deformation cycle [279]. In some reports, detwinning resulted in reduced yield stress in Mg alloys. However, for the uniaxial loading with relative large strain, detwinning is exhausted, while twinning is activated with the increasing strain, which contributes to the increase of flow stress [65].

Alternation of twinning–detwinning in deformed Mg alloy strongly influence the fatigue behaviour. Therefore, studies have been performed on pre-twinning in order to optimise the characteristics of twinning-detwinning effects. Hong et al. [258] modified the alternative effects of twinning and detwinning through pre-twinning in rolled AZ31 alloy. They found that the fatigue properties was improved by the modification in their experiments. The pre-existing twins facilitated the detwinning activity under tensile stress. However, in other cases, pre-twinning was reported to cause a decrease in fatigue properties when unfavourable direction were applied. Park et al. reported that the pre-existing $\{10\bar{1}2\}$ twins formed during pre-straining along a given direction of rolled AZ31 Mg alloy plates increased the tensile stress along the direction, thereby deteriorating the fatigue resistance [279].

There is some controversy surrounding the nucleation of twins around notches. Kaushik et al. [280] performed fracture tests on notched Mg specimens corresponding to three lattice orientations. The results indicated the occurrence of profuse tensile twinning in all three orientations. However, the pattern of twin development differs for the three orientations. Twins spread out from the notch root in two orientations. In comparison, they initially form near the specimen edge ahead of the notch root and extend toward it with increasing loading in the other orientation. A small region around the notch root is free of twins. They concluded that tensile twins impart toughening through dissipation. However, Somekawa et al. [276, 277] argued that these twins are detrimental because crack propagation occurs along their boundaries which are inherently brittle.

Chapter 3 The Papers

3.1 Overview of the Papers

Metallic fine tubes are used widely to fabricate biomedical stents. The current work was carried out in order to develop a systematic understanding of mechanical properties and microstructural evolution during processing of metallic fine tubes. In the last decade, a variety of metastable β titanium alloys have been developed as candidates for biomedical applications due to their excellent combination of biocompatibility and mechanical properties. Magnesium alloys are another promising material for the biomedical application of fine tubes. Biodegradable stents have been attracting extensive attention recently. It has been reported that magnesium alloys exhibit biodegradability after implantation into the human body. Therefore, a metastable β titanium alloy, Ti-25Nb-3Mo-3Zr-2Sn and a magnesium alloy Mg-3Al-1Zn were selected in the current work for the study of metallic fine tubes.

Little literature is available reporting on cold rolling of metallic fine tubes. The mechanical properties and microstructure in the processing of metallic fine tubes exhibit different variation with that in deformation of bulk materials or rolling of plate due to differing stress state in the processing of tubes in comparison with those of uniaxial stress and plane stress states, which was illustrated in Paper 4. The development of texture from cold rolling of fine tubes has not been reported, particularly the combination of varying mechanical mechanisms, the formation and morphology of their products, etc. On the other hand, deformation mechanisms in the processing of metallic fine tubes may be altered via changing processing parameters, which further contributes to modified mechanical properties. Therefore, understanding the deformation mechanisms including martensitic transformations and twinning were an important focus of the current work.

The as-received tubes of Mg-3Al-1Zn with an outside diameter of 7.7mm and a thickness of 0.87mm were received in the extruded condition and annealing was performed to remove deformation structures. The Mg-3Al-1Zn samples used in this work were collected after the cold rolling process. Tensile samples were obtained based on AS 1391-2007, which was detailed in Paper 1. The Ti-25Nb-3Mo-3Zr-2Sn tubes were cold rolled and annealed in multiple steps to reduce them from an outside diameter of 8mm to 3mm. Ti-25Nb-3Mo-3Zr-2Sn fine tubes in both cold rolled and annealed conditions were studied. The details of processing parameters were present in Paper 2.

The evolution of mechanical properties and microstructure of Mg-3Al-1Zn fine tubes were assessed with respect to the processing parameters, ε the ratio in cross-sectional reduction and Q the ratio of wall-thickness to diameter reduction, in Paper 1. Cold rolled tubes were subjected to a ε of up to

19.7%, and were further processed at various Q from 0 to 2.24 with a constant ε of 19.7%. The results show that the cold-rolled tubes exhibited a rise in ultimate tensile strength, yield strength and a reduction in elongation with increasing ε. The ultimate tensile strength and yield strength increased with increasing ε, while it decreased with an increase in Q from 0 to 2.24. Elongation in both cases decreased with an increase in ε and Q.

Mechanical twinning was observed in the cold rolled tubes. $\{10\bar{1}2\}$ extension twins increased with increasing ε until they were almost saturated when ε was above 16.5%. Then contraction/double twins and secondary $\{10\bar{1}2\}$ twins propagated dramatically at high-levels (≥16.5%) of ε and in the case of increasing Q.

Paper 1 revealed that extension twins played an important role in determining the evolution of mechanical behaviour in the case of increasing ε, whilst contraction/double twins and secondary extension twins had a large effect on mechanical behaviour in the case of varying Q. The ultimate tensile strength, yield strength and elongation exhibited the same tendency due to the formation of $\{10\bar{1}1\}$ - $\{10\bar{1}2\}$ double twins. The $\{10\bar{1}2\}$ extension twins were the dominant deformation mechanism and overshadowed that of contraction and double twinning in the case of varying ε. Texture hardening and $\{10\bar{1}2\}$ extension twinning are the two dominant effects on the mechanical properties in the case of increasing ε. Contraction and double twinning played a dominant role in determining the mechanical behaviour in the case of varying Q. The results in Paper 1 indicated that the proportions and types of twins play a major role in determining the mechanical behaviour of Mg-3Al-1Zn tubes, which needs to be further studied.

Paper 2 and Paper 3 studied the effects of cold rolling and annealing on the mechanical properties of biomedical Ti-25Nb-3Mo-3Zr-2Sn fine tubes, which were cold rolled from an outside diameter of 8mm to 3mm. The processing Ti-25Nb-3Mo-3Zr-2Sn tubes with outside diameter of 8mm to 5.6mm and wall thicknesses of 1mm to 0.7mm were investigated in Paper 2. The evolution of microstructure was also studied in order to investigate the mechanical properties and their impact on the processing of the tubes. In these 2 papers, effects of annealing and cold rolling were studied separately.

The annealed fine tubes with single β phase microstructures exhibited double yielding phenomenon during tensile testing. Strain hardening rate - strain (θ-ε) curves were presented and 3 stages of strain hardening rate were proposed in Paper 2. The onset of the martensitic phase transformation was observed to occur after the lowest point of strain hardening. Cold rolling of annealed tubes facilitated

the formation of the stress induced martensitic α″ phase. Therefore, the rate of strain hardening and the modulus of the tubes are related to the stress induced transformation of the β phase to the α″ phase. It was also demonstrated that the stress induced α″ slightly improved the yield strength of the tubes at low levels of strain.

Grain growth were observed when strain reached 51% under both annealing and cold rolling conditions, which diminished the mechanical properties. The yield strength was enhanced at low levels of ε. However, it was substantially reduced when ε was 51% possibly due to the growth of β grain size. Ductility was also decreased at an ε of 51%, which also may be related to the increased proportion of low-angle grain boundaries in the annealed condition. The tubes in the cold rolled condition had original stress induced martensitic α″ phase. The fraction of martensitic α″ phase increased with increasing ε. The yield strength and Young's modulus reduced due to an increased proportion of martensitic α″ phase in the cold rolled tubes.

The mechanical properties and deformation mechanisms varied with further reductions in diameter of Ti-25Nb-3Mo-3Zr-2Sn fine tubes. Tubes with outside diameter from 5mm to 3mm were investigated in Paper 3. The modulus increased with decreased diameter for both cold rolled and annealed tubes. Annealed tubes exhibited superior strain hardening rate and ductility in comparison with cold rolled tubes. Stress induced martensitic transformation and mechanical twinning were investigated in this Paper. The deformation induced products were identified as {332}⟨113⟩ mechanical twins, primary and secondary stress induced α″ phase. Effects of twinning induced plasticity and transformation induced plasticity were active during processing of the Ti-25Nb-3Mo-3Zr-2Sn fine tubes, contributing to excellent tensile ductility in conjunction with high levels of strain hardening rate for the annealed fine tubes. For the tubes in annealed conditions, yielding occurred when the stress reached the threshold to activate both twinning and stress induced martensitic transformations. High strain hardening rates were associated with the increasing volume fraction of mechanical twins and the martensitic α″ phase.

Cold rolling facilitated the transformation from β to the α″ phase and mechanical twinning as described in Paper 2. However, they were only activated at specific levels of tensile strain for annealed tubes. Twins developed with increasing levels of strain, and secondary martensitic transformation occurred within twinned β regions.

The textures of β and the α″ phase were also studied in Paper 3. The varying moduli were related to the evolution of β and α″ phase textures. β grains experienced rotations from (100) and (110) to (211) on the observation plane parallel to the rolling direction with reductions in the outside diameter. The β texture evolution resulted in an increased modulus with reductions in the tube diameters. The evolution of α″ phase texture was related to the transformation from the β to α″ phase and their resultant orientation relationship. The development of the α″ phase texture and its increased volume fraction have an opposing effect to that of β phase texture, which limits increases in the modulus with reductions in the diameters of the tubes.

In summary, Paper 2 and Paper 3 established a systematic understanding of the processing of β titanium fine tubes through the investigation of the evolution of mechanical properties and deformation mechanisms. Ultimate strength, yield strength, ductility, modulus and strain hardening rate were analysed via characterising the martensitic α″ phase, mechanical twins and texture during the processing.

Because the proportions and types of twins play a dominant role in determining the mechanical properties of Mg-3Al-1Zn tubes as concluded in Paper 1, identification of twins formed during cold rolling of magnesium fine tubes was investigated in order to figure out detailed deformation mechanisms during cold rolling of Mg-3Al-1Zn tubes. As described in Paper 1, three twinning modes, extension $\{10\bar{1}2\}$ twins, contraction $\{10\bar{1}1\}$ twins and double twins, were detected. Extension $\{10\bar{1}2\}$ twins were most frequently observed in the cold rolled samples due to their relatively low critical resolved shear stresses. Approximate 60% of the grains examined contained $\{10\bar{1}2\}$ twins, even though many of them had orientations which were predicted to be unfavourable for the activation of $\{10\bar{1}2\}$ twins. When Extension $\{10\bar{1}2\}$ twinning and contraction $\{10\bar{1}1\}$ twinning had close and high Schmid factor values, the former was activated, whereas $\{10\bar{1}1\}$ twinning was activated when it had a high Schmid factor exclusively. The complex twinning activity in the cold rolled tubes resulted from the large proportion of grains with their c-axes 30 °-60 °to the radial direction.

A modified Schmid factor for tube rolling was proposed in Paper 4 and was shown to be a pertinent parameter to predict the active twinning modes in the cold rolled Mg-3Al-1Zn tubes. Most of the $\{10\bar{1}1\}$ twins and some of the $\{10\bar{1}2\}$ twins obey the Schmid law exhibiting the highest or second highest Schmid factor values. Twins with low Schmid factors were activated in the cold rolling of AZ31 tubes due to the influence of strain accommodation. Strain transferred among twins contributes to non-Schmid behaviour in the cold rolled tubes. As a result, non-Schmid twins were frequently

observed with most of them exhibiting favourable strain accommodation with respect to their strain compatibility factor. Secondary $\{10\bar{1}1\}$ twins can be activated at the intersection of primary $\{10\bar{1}2\}$ twins due to transfer of shear strain from one twin to the adjoining twin. Therefore, the twinning mode in processing of magnesium fine tubes could be determined via both the modified Schmid factor and a strain compatibility factor for non-Schmid twins.

PAPER 1

The cold-rolling behaviour of AZ31 tubes for fabrication of biodegradable stents

Yaowu Zhang, Damon Kent, Gui Wang, David StJohn and Matthew Dargusch

Journal of the Mechanical Behavior of Biomedical Materials
2014, Volume 39, Pages 292-303

Abstract

Mg alloys are receiving considerable attention for biomedical stents due to their combination of good mechanical properties and high biodegradability. Cold rolling is necessary to process Mg alloy tubes before final drawing and fabrication of the magnesium stents. In this paper, cold-rolled tubes were subjected to a cross-sectional reduction rate (ε) of up to 19.7%, and were further processed at various ratios of wall-thickness to diameter reduction (Q) from 0 to 2.24 with a constant ε of 19.7%. The results show that the cold-rolled tubes exhibited a rise in ultimate tensile strength (UTS), yield strength (YS), and a reduction in elongation as ε increased from 5.5% to 19.7%. UTS, YS and elongation decreased when Q was increased from 0 to 2.24. Mechanical twinning was observed and analysed. Extension twins increased with increasing ε and were almost saturated at an ε of 16.5%. Extension twins play an important role in determining the evolution of mechanical behaviour in the case of increasing ε, whilst contraction/double twins and secondary extension twins have a large effect on mechanical behaviour in the case of varying Q. The results indicate that the proportions and types of twins play a major role in determining the mechanical behaviour of the AZ31 tubes.

1. Introduction

Biodegradable magnesium stents are capable of providing good mechanical properties and can achieve properties similar to conventional stents. However, biodegradable magnesium stents are able to temporarily open the blood vessels until they remodel and then can be absorbed into the body reducing the likelihood of long-term complications or risks [24, 25]. Several magnesium alloys, such as AE21 (2 wt.% Al and 1wt.% rare earth elements) and WE43 (4 wt.% Y and 3 wt.% rare earth elements), have been investigated in recent years [26]. Also, another alloy, Mg-Li-Zn, has been patented for use in biodegradable implants [1]. Although there is still discussion on the addition of aluminium to bio-materials [27, 28], Mg-Al-Zn alloys are widely used for research on the processing of biomedical Mg alloys as they are commonly available commercial alloys [29, 30]. AZ31 was used in this paper to investigate the cold-rolling behaviour of magnesium tubes.

The hexagonal close-packed (HCP) structure of magnesium alloys is associated with poor formability and restricts plastic deformation at room temperature [49, 50]. Manufacture of Mg alloy tubes traditionally requires processing at elevated temperatures. However this is not suitable for fabrication of small-dimension magnesium tubes, because grain growth at elevated temperatures negatively

impacts the mechanical properties and cannot be improved during consequent drawing processes [51, 52]. Therefore, cold rolling is a necessary process during the manufacture of the small-dimension magnesium tubes [53]. The two main parameters during cold rolling, ε and Q, are as defined below [267]:

$$\varepsilon = \frac{A_0 - A_1}{A_0} = \frac{t_0 \times (D_0 - t_0) - t_1 \times (D_1 - t_1)}{t_0 \times (D_0 - t_0)} \; ; \quad (1)$$

$$Q = \frac{((t_o - t_1)/t_0)}{((D_0 - D_1)/D_0)} = \frac{(t_0 - t_1) \times D_0}{(D_0 - D_1) \times t_0}. \quad (2)$$

Where, A_0 and A_1 are the initial and final cross-sectional area; t_0 and t_1 are the initial and final wall thickness; D_0 and D_1 are the initial and final outside diameter (OD). ε is defined as the amount of deformation on the cross section of the tubes and is an indicator of the change of cross-sectional size. Q is exclusive to tubes as compared with parameters used to describe the rolling of sheets. As Q increases, the ratio of wall-thickness to perimeter decreases and the tubes become thinner. Q, therefore, indicates the change in cross-sectional shape. No elongation occurs as Q changes. In the present paper, either ε or Q was held constant while the other parameter was changed during cold rolling in order to investigate their effects on the mechanical properties.

It is well known that in order to understand the deformation behaviour of Mg alloys during cold rolling two types of deformation modes, slip and twinning, need to be considered [53, 72]. Strain along the c-axis can be accommodated by <c + a> slip and twinning. However, Mg alloys exhibit a strong preference for mechanical twinning because the twinning has a lower threshold stress than <c + a> slip [1-4][139]. Therefore, twinning plays a vital role during deformation [70]. It is well known that there are typically two types of deformation twins which form in Mg; one type are $\{10\bar{1}2\}$ extension twins and the other are $\{10\bar{1}1\}$ contraction twins [54]. Extension twins are formed when there is an extension strain component parallel to the c-axis which is generated at the onset of plastic deformation and contributes to strain [55-57]. Contraction twins are generated when there is a contraction strain component parallel to the c-axis at larger levels of deformation in order to relax the stress concentration [58, 59]. As well as the two types of primary twins, secondary twinning, called double twins, can be activated within the reoriented primary twins. The extension and contraction twins are associated with the mechanical anisotropy of Mg alloys [55-57]. Deformation twinning may contribute to a radical reorientation of the volume fraction of the grains that have twinned, which leads to texture modification. Conversely, during cold-rolling the activation of extension and

contraction twins during plastic deformation greatly depends on the texture [67-69]. Twinning activity can be investigated in order to explain the evolution of mechanical behaviour of Mg tubes during cold-rolling. Liu et al. [70, 71] studied the relationship between texture and deformation mode and concluded that the shape of the flow curve was determined by the type of twinning that occurs and by when the twins were activated. Variations in the strain hardening behaviour can be attributed to the influence of mechanical twinning. Knezevic et al. [78] reported that mechanical twins in AZ31 affected strain hardening and the main contribution to hardening comes from texture hardening. Rohatgi et al. [79] considered that the reason that twinning retards the decrease in strain hardening rate lies in the effective grain refinement that results from twinning. However., Barnett [73] provided another explanation; that reorientation of the c-axes by almost 90 ° has a more significant effect on the strain hardening produced by twinning with c-axis extension. Jiang, et al. [72] conducted a study to determine the twinning modes and texture development under different strain paths. Their view was in accordance with that of Barnett that the effect of mechanical twinning and corresponding texture development on the flow stress is more significant than the effects of grain size. Thus, twinning development has been investigated in the present paper in order to explore the underlying mechanism of how the two cold-rolling parameters, ε and Q, act in determining mechanical properties of the AZ31 Mg tubes.

The cold rolling behaviour of Mg alloys has been investigated in recent years [50, 80]. However, most studies have focused on magnesium sheets. Little research has been conducted on the fabrication of magnesium tubes, especially for mini-tubes. In this paper, the mechanical properties of magnesium mini-tubes was examined, and twinning activity was investigated in regards to the morphology and orientation of twins formed during cold rolling in order to develop an understanding of the cold-rolling behaviour of Mg alloy mini-tubes.

2. Experimental Methods

AZ31 alloy ingot was cast with a diameter of 350mm. Surface oxides were removed by turning. It was then heated to 400 ℃ and extruded with an extrusion ratio of 42:1. The final extruded tubes had outside diameter of 7.9mm and wall thickness of 0.9mm. The chemical composition of the final extruded tubes, determined by the wet analysis method, is shown in Table 1. A mill with 3 rollers (LD-8) was used to cold roll the extruded AZ31 tubes into a series of final dimensions as shown in Table 2.

The effect of the two cold rolling parameters, ε and Q, has been investigated with ε held constant at approximately 19%, while the value of Q was varied from 0 to 2.24. Similarly, ε was increased from 5.5% to 19.7% while Q was held constant at 1.37. Note that the E4/Q3 group was prepared as the benchmark condition, which was cold-rolled with an ε of 19.7% and a Q of 1.37.

Table.1 Chemical composition of the AZ31B tubes (*wt. %*).

Mg	**Al**	**Zn**	**Mn**	**Cu**	**Fe**	**Ni**
Balance	2.70	0.71	0.20	0.008	0.007	0.001

Table. 2 Sample groups and processing parameters ε and Q used in investigation.

Sample	**E1**	**E2**	**E3**	**E4/Q3**	**Q1**	**Q2**	**E4/Q3**	**Q4**
Outside Diameter (mm)	7.71	7.51	7.32	7.19	6.57	6.91	7.19	7.41
Wall thickness (mm)	0.87	0.84	0.81	0.79	0.90	0.84	0.79	0.77
ε	5.5%	11.1 %	16.3 %	19.7 %	Approximately 19%			
Q	1.37				0	0.53	1.37	2.24

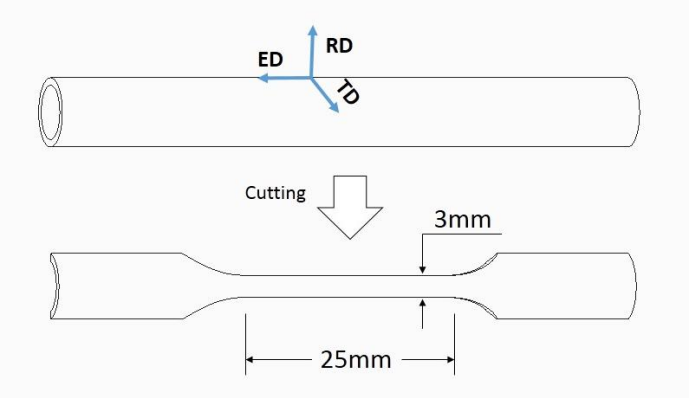

Fig.1 Schematic diagram relating the elongation direction (ED), tangential direction (TD) and radial direction (RD) to the sample orientation.

Uniaxial tensile tests were performed on all of the cold-rolled Mg tubes. Tensile specimens with nominal gauge dimensions of 25mm (length) × 3mm (width) were taken from the tubes with their axis aligned along the Elongation direction (ED) by wire-electrode cutting (Fig. 1). In order to avoid the influence of minor notches on the machining surfaces, polishing was conducted before the tensile

tests. To ensure repeatability of the results, three tensile specimens were tested for each set of conditions and the average value was then used in the results. Tensile tests were conducted on an Instron-4505 universal testing machine. A contact extensometer was used to measure the strain. As the mechanical behaviour of cold rolling and the corresponding twinning activity were of interest, tests were conducted at ambient temperatures and at a loading rate of 0.001 s^{-1}.

The surfaces examined by SEM were perpendicular to the tangential direction (TD) and polished using 6 µm, 3 µm, 1 µm diamond paste and 0.02 µm colloidal silica. Sample were then etched in a solution of 5g picric acid, 5ml acetic acid, 80ml ethanol and 10ml water for 20 s to 30 s. The microstructure was observed using a JEOL JSM-6460 scanning electron microscope. The statistical results of average grain size were obtained by the average grain intercept method using SEM images based on ASTM standard E112-13 [281]. For the EBSD samples, mechanical polishing was followed by a final 2-4 s etch using a solution of 5ml nitric acid, 5ml hydrofluoric acid and 90ml distilled water to improve the quality of the electron backscatter diffraction patterns (EBSP). The EBSD data were collected using an EBSD camera attached to a JEOL JSM-7001F Scanning Electron Microscope at a voltage of 25 kV. The pole figures (PFs) were obtained from post treatments using the HKL® Channel 5 software.

3. Results

3.1 Mechanical behaviour

The true stress-true strain curves for specimens processed with ε from 5.5% to 19.7% with a constant Q of 1.37 are presented in Fig. 2 (a). The nominal true stress was calculated based on the applied load and the strain, assuming constant volume and uniform deformation. As seen in Fig. 2 (a), all the true stress-true strain curves have a power-law type strain hardening region. With the increase of ε, the flow curves exhibit a distinct yield point increasing from 211MPa (ε of 5.5%) to 316MPa (ε of 19.7%). The rate of strain hardening decreased with the increase of ε. When the ε was 5.5% and 11.1%, obvious strain hardening occurs following yield. In comparison, when ε was increased to 16.5% and 19.7%, post-UTS regions were found to be relatively short and indicated no obvious strain hardening. Thus, the strain hardening behaviour tends to decrease with an increase in ε. As shown in Fig. 2 (b), the increase in ε results in a decrease in elongation and an increase in the ultimate tensile strength (UTS) and yield strength (YS), which indicates fairly conventional evolution of the UTS, YS and elongation during cold working.

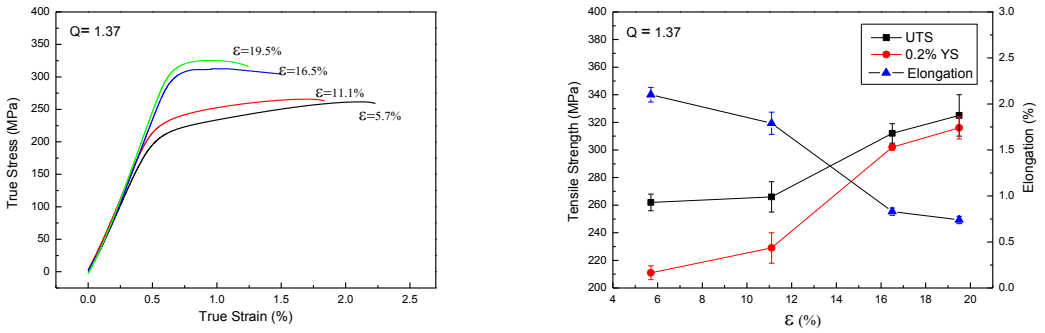

Fig. 2 (a) True stress-true strain plots for varying ε; (b) Evolution of mechanical properties with ε (Standard error bars)

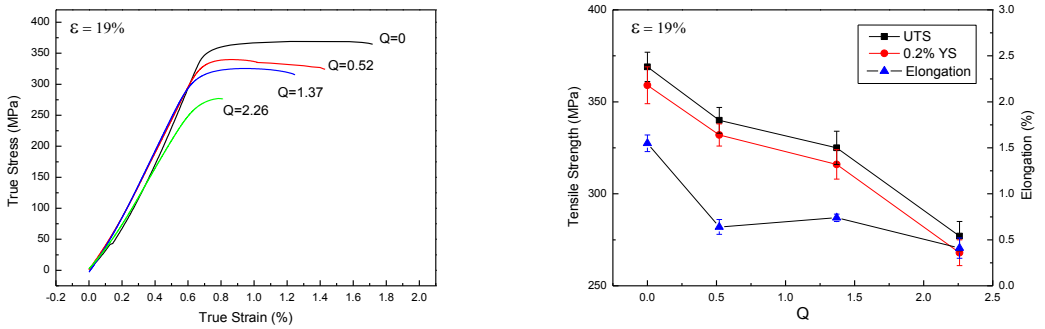

Fig. 3 (a) True stress-true strain behaviour with varying Q; (b) Evolution of mechanical properties with Q (Standard error bars)

The true stress-true strain curves for specimens processed with Q from 0 to 2.24 and a constant ε of 19% (Fig. 3 (a)) show that yielding of the four flow curves occurred at a similar true strain of around 0.7%. The rate of flow hardening had a propensity to decrease with an increase of Q from 0 to 1.37, as did the UTS, which dropped from 369MPa to 277MPa. The UTS and YS declined with an increase in Q as shown in Fig. 3 (a). Elongation decreased from 1.55% to 0.41% showing the same trend as that of UTS and YS. This indicates that both the strength and elongation are superior in this group of specimens when the Q is at its lowest values. This does not fit the conventional relationship in that the elongation would typically be expected to increase in conjunction with reductions in the strength.

In view of the fact that the E4/Q3 group had the highest UTS and YS in the case of increasing ε, further increases in the UTS and YS (increased by 13.5%) were achieved when Q was reduced. On the other hand, elongation doubled as Q decreased from 0.53 to 0, while it remained at the same level when Q was more than 0.53. Therefore, lower Q values are beneficial to both strength and ductility.

3.2 Evolution of the microstructure

The distribution of texture within extruded AZ31 tubes and rolled AZ31 sheets has been widely reported in previous literature [53, 282, 283]. The grain orientations within the extruded AZ31 tubes were divided into two groups; one with their c-axis approximately parallel to the RD, called the RD component, and the other with their c-axis parallel to the TD are called the TD component [139]. As ε was introduced during cold-rolling, the ED component was activated due to the resolved stress in this direction (Fig. 4). It is analogous to the transverse direction in the deformation of sheets. Therefore, texture in the ED will be considered in the following analysis. According to previous literature, the morphology of well-developed $\{10\bar{1}2\}$ extension twins, are irregular, chunky and coarse [139], which is quite unlike that of $\{10\bar{1}1\}$ contraction twins and double twins which are typically thin, straight and long [252, 284]. Contraction twins which form in magnesium alloys frequently appear as the $\{10\bar{1}1\}$ - $\{10\bar{1}2\}$ double twinned structure, and they have similar morphologies and effects on the mechanical behaviour [285]. For a given imposed displacement along the planes of maximum shear stress, extension twins only produce small amounts of shear per unit volume and therefore a relatively large volume fraction of extension twins is required to accommodate the strain. Conversely, contraction twins produce large amounts of shear per unit volume and therefore much smaller volume fractions are produced. This explanation was originally proposed for Zr [28] and Jiang et al. [139] further applied that explanation to magnesium alloys. Because there are substantial differences in the morphology of the twins, it is possible to distinguish the different types of mechanical twins from the microstructure.

Fig. 5 (a) - (c) illustrates the microstructures corresponding to increasing ε with a constant *Q* of 1.37. All the optical micrographs presented here are perpendicular to the TD. It shows almost equiaxed grains for the four sets of conditions. This was consistent with the report published by Ion and co-workers [286]: the grain size was homogeneous for AZ31 specimens deformed at strains of up to 25%. Twinning was observed to occur even during the initial stages at an ε of 5.5%. Twins can be also observed within grains for all specimens. Table 3 shows the statistical results for the average grain size obtained by the average grain intercept method based on ASTM Standard E112-13 [281] using Image J software on SEM images. The average grain sizes do not experience a substantial change. For this reason the grain size is not considered to be a factor in further analysis relating to the mechanical behaviours.

Table. 3. Statistical grain sizes with Q of 1.37

	ε of 5.5%	ε of 11.1%	ε of 16.5%	ε of 19.7%
Grain sizes	17.64 μm	17.51 μm	17.81 μm	18.17 μm

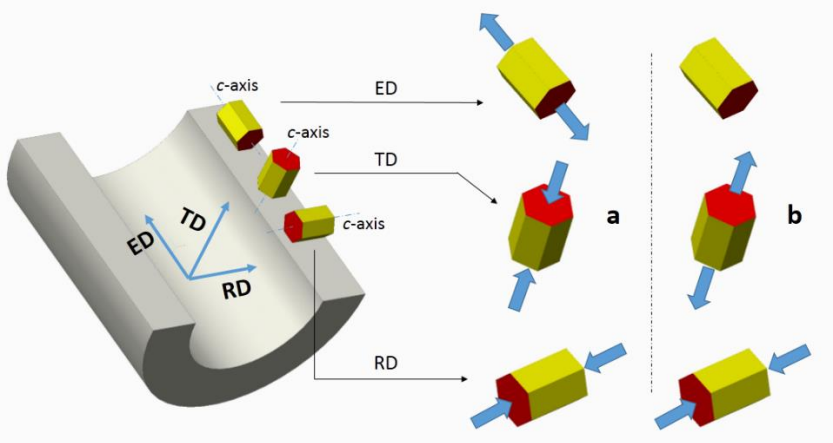

Fig. 4. Schematic diagram relating the orientaion of c-axes and resolved stresses on crystals with HCP structure in different directions. (a) resolved stresses as ε increases; (b) resolved stresses as Q increases

All of the samples in the present paper are considered to have grains which were reoriented by twinning activities, because a small amount of strain (~3%) on tubes induces deformation twins [75, 284, 287]. Valle et al. [288] reported that the volume fraction of twins increased with increase in strain from 5% to 15%, which is in accordance with Fig. 5 (a) - (c). The fraction volume of twins increased dramatically with an increase in ε, which indicates that a large amount of twins were activated during cold rolling. Fig. 5 (c) shows almost all grains contained deformation twins at an ε of 19.7%. It is noted that some of the twins within a particular grain were essentially parallel (see white arrows in Fig. 5 (c)). These twins were $\{10\bar{1}1\}$ contraction twins or double twins. The morphology of the extension twins had a tendency to be thick. The characteristic lenticular morphology (see black arrows in Fig.5 (a)) was also observed, as reported by Ion et al. [286]. Sideways growth of the twins occurred with increasing ε. In Fig.5 (b) and (c) some of the extension twins have grown and developed into a thick rodlike morphology.

Fig. 5 (d) - (f) shows the evolution of microstructure of AZ31 specimens as Q increased from 0 to 2.37 with a constant ε of approximately 19%. Equiaxed grains remained without DRX. Grain sizes, therefore, remained constant while Q increased. In comparison with Fig. 5 (c), the volume fraction of twins remained at the condition of almost saturation. However, the proportion of contraction and double twins increased with an increase in Q (see blue arrows in Fig. 5 (e) and (f)).

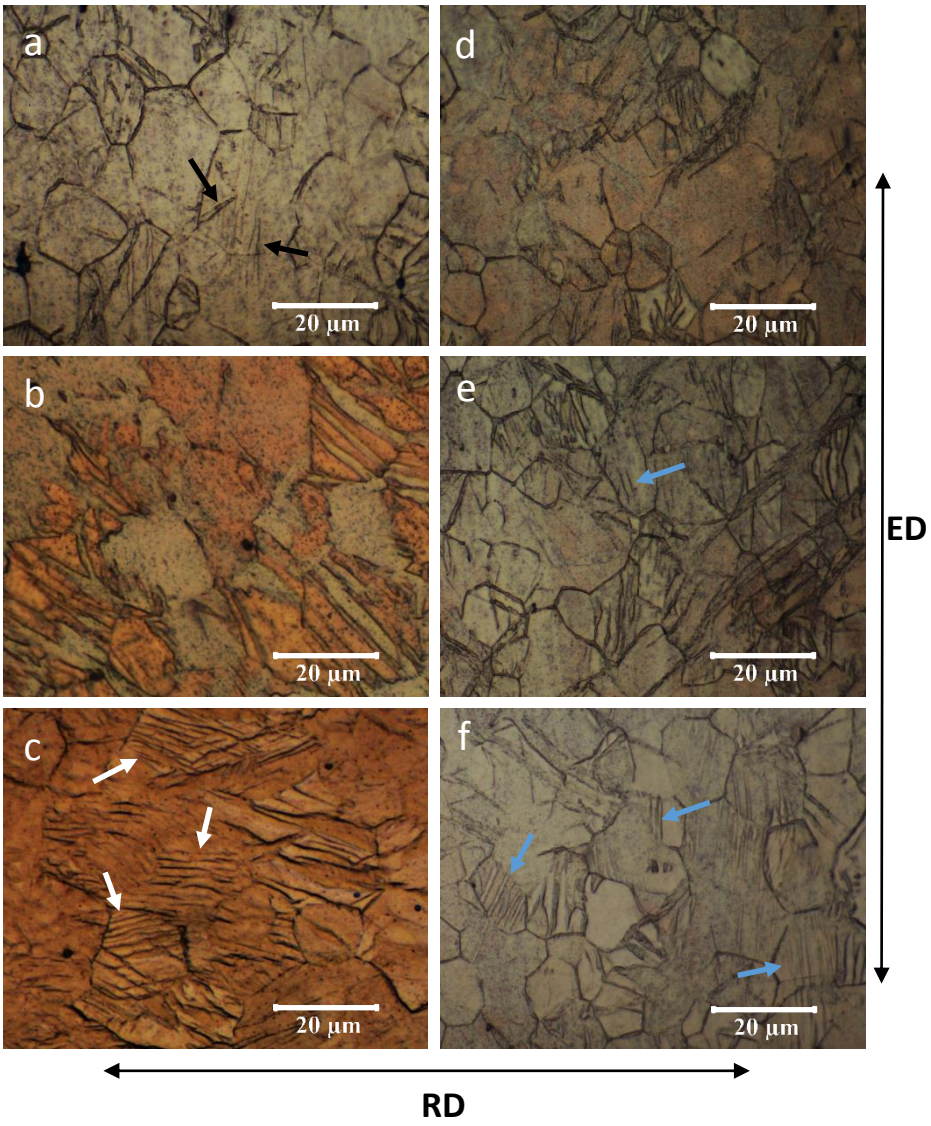

Fig. 5. Microstructures of cold-rolled AZ31 tubes:(a) ε: 5.5%, Q: 1.37 (b) ε: 16.5%, Q: 1.37 (c) ε: 19.7%, Q: 1.37 (d)ε: 19.7%, Q: 0, (e) ε: 19.7%, Q: 0.53, (f) ε: 19.7%, Q: 2.24

It is noticed that there are two types of grains with different contrast, light-coloured and dark-coloured (Fig. 5 (a) - (c)). The basal plane of a certain grain is parallel to the observation surface, grains are light-coloured, whilst grains perpendicular to the observation surface appears to be dark-coloured [284]. Therefore, grains in the TD orientation should be light-coloured, and dark-coloured grains are considered to be in the RD or ED. In Fig. 5 (c), the fraction of twins appears to be low because many of the grains have been entirely consumed by well-developed extension twinning. The intersection of twins can occasionally be observed for high levels of ε (Fig. 5 (e) and (f)).

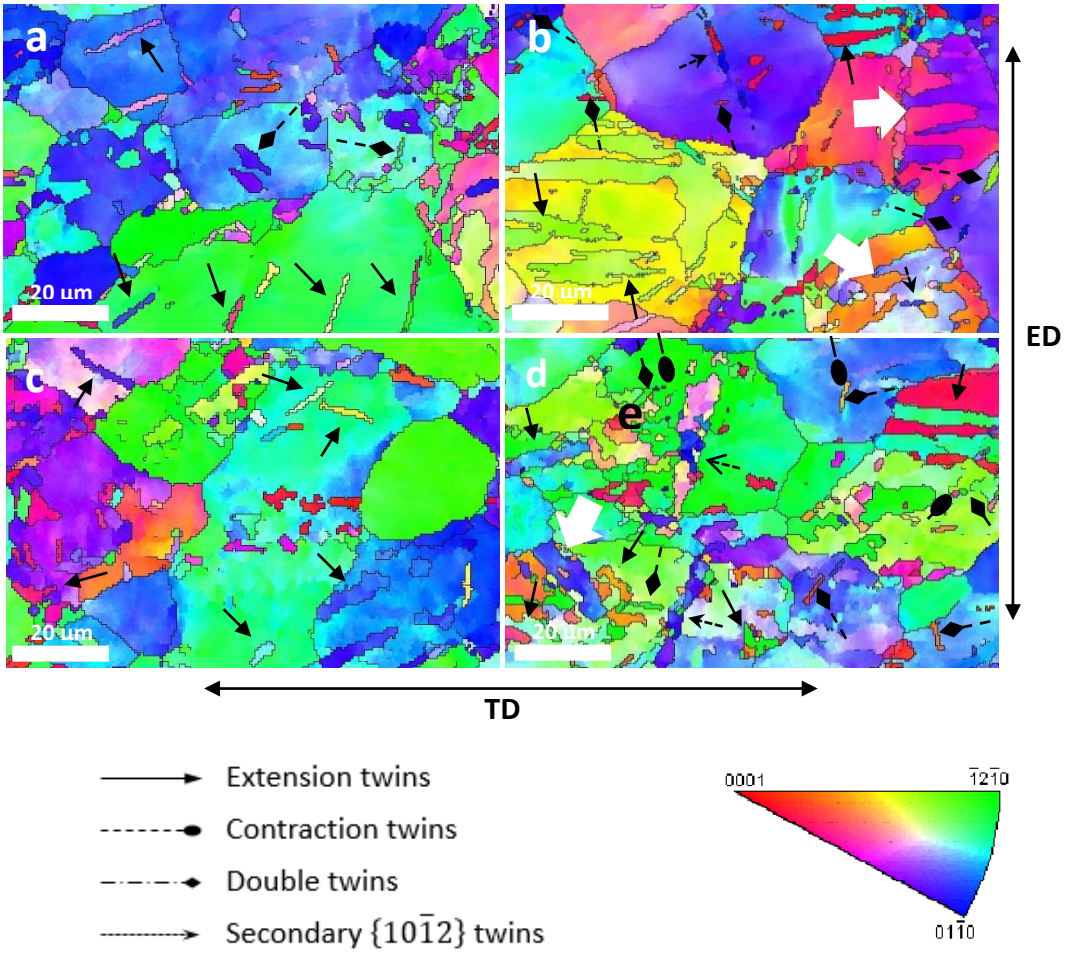

Fig. 6. Inverse pole figure maps obtained by EBSD serial image analyses showing extension twins, contraction twins and double twins in AZ31 magnesium tubes deformed at different ε and Q. (a) ε: 5.5%, Q: 1.37; (b) ε: 19.7%, Q: 1.37; (c) ε: 19.7%, Q: 0; (d) ε: 19.7%, Q: 2.24 The IPF maps correspond to the orientation with respect to the map key in (e).

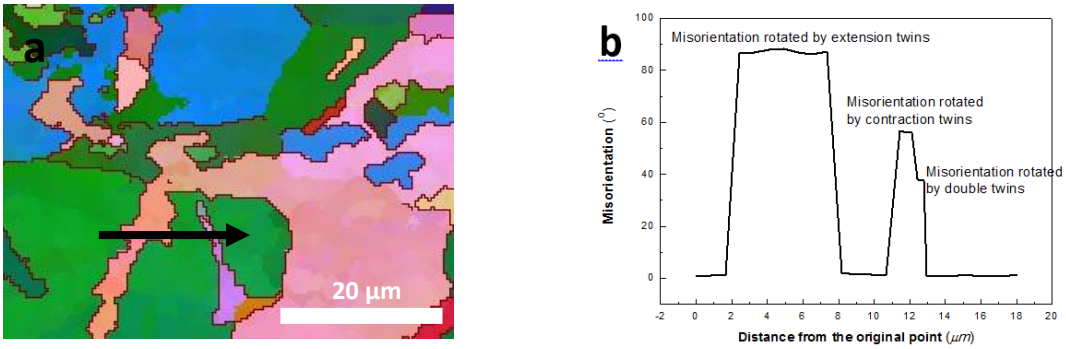

Fig. 7. Schematic diagram for identifying different types of twins by characteristic reorientation angles. (a) Inverse pole figure of the sample with ε of 19.7% and Q of 2.24, reorientation angles were detected along with the black arrow. (b) Misorientation angles for specific twins, extension twins (87 ° ±3 °), contraction twins (56 ° ±3 °) and double twins (37 ° ±3 °) were detected, respectively

In order to obtain the orientation of grains and identify the twinning, EBSD serial analyses was performed (Fig. 6). The data around twins had low indexing rate due to the lattice distortion of

magnesium under cold rolling conditions. However, the type of twins can be identified by their characteristic reorientation angles (87 °, 56 °and 38 ° for extension, contraction and double twins, respectively) [289]. The observed surface is perpendicular to RD. Therefore, <0001> in Fig. 6 is parallel to RD. Fig. 7 is a schematic showing how to identify the different types of twins were identified. Extension twins were observed in most grains, whilst contraction and double twins can only be identified in grains with their c-axis not aligned along the <0001> direction. Fig. 6 (a) and (b) are from N08 and N03, where ε was increased from 5.5% to 19.7% with a Q of 1.37. The volume fraction of extension twins increased dramatically. Fig. 6 (c) and (d) are from N02 and N07, where Q was increased from 0 to 2.24 with a constant ε of 19%. Contraction and double twins were not observed in Fig. 6 (c), but they were generated with increasing Q (corresponding arrows in Fig. 6 (d)). Double twins were observed within the contraction twins. This phenomenon is consistent with previous reports [139, 286]. In Fig. 6 (b) (c) and (d), the ε was approximately 19%, some of grains had almost half of their area occupied by well-developed extension twins (see white arrows in Fig. 6), and the intersection of twins can be observed for high levels of ε.

4. Discussion

4.1 Twinning development during cold-rolling

During cold rolling, <c + a> slip was suppressed, while twinning was generally favoured. Therefore, twinning played an important role during fabrication of the Mg tubes. Texture development and reorientations of grains are inevitable during deformation of the AZ31 tubes and both extension and contraction twinning may be activated simultaneously [290, 291]. The *c*-axis of the grains tends to rotate into alignment with the deformation direction [292, 293]. In the case of increasing ε, there was compressive stress on the RD and TD components (Fig. 4), while extension twins were observed in reoriented grains with their c-axis parallel to the ED due to elongation in this direction (see blue arrows in Fig. 6 (b)). Jiang et al. [139] reported that twinning activities were active in the RD component and TD component for extruded tubes. However, extension twinning that occurred in the ED component was observed during cold rolling for the present paper (Fig. 6). Thus, there were grains which were reoriented to the ED component during the cold-rolling of AZ31 tubes.

Contraction twinning remained inactive during the early stages of straining until the local stress reaches the critical resolved shear stress value for contraction [284]. Therefore, although both the RD component and TD component favour contraction twinning, contraction twins were not observed at

an ε of 5.5% (Fig. 6 (a)). In comparison, extension twinning occurred in the ED component more readily than contraction twinning. The extension twins contribute a majority of twins in the case of increasing ε, even at the highest ε of 19.7%. However, it is observed that contraction twins or double twins also formed for the higher levels of ε (Fig. 6 (c)). Fig. 8 shows pole figures for E1 and E4/Q3, where the ε was increased from 5.5% to 19.7%. Both exhibit a strong overall texture, but the basal planes for those parallel to the ED was enhanced with the increasing ε, caused by tensile stress on the ED and compressive stress on the RD and TD.

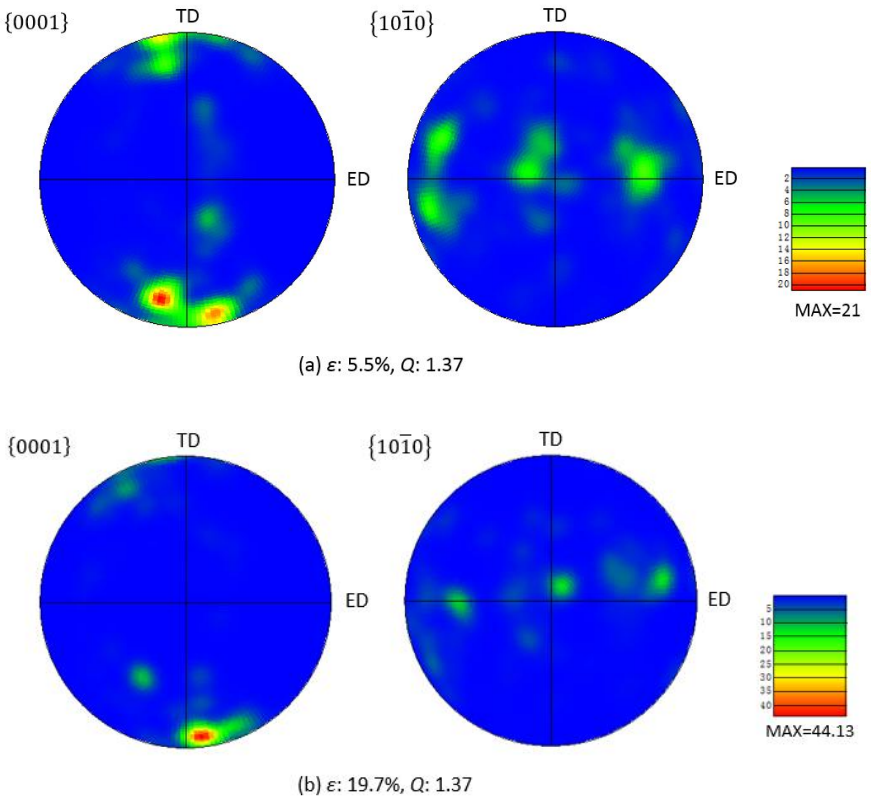

Fig. 8. Texture development during rolling of AZ31 tubes with the increasing Q. Recalculated {0001} and $\{10\bar{1}0\}$ pole figures (a) ε: 5.5%, Q: 1.37 (b) ε: 19.7%, Q: 1.37

As Q was increased, tensile stress and compressive stress was applied on the TD and RD components, respectively (Fig. 4). In comparison with the case of varying ε, no resolved stress was applied along ED. Mechanical twinning in the ED component could not be activated. Extension twins were broadly distributed in all samples of Q groups, which resulted from the high-level ε of 19.7%. However, limited extension twins propagated in the TD. Referring to the Schmid Factor (SF) criterion, only those twin variants above a threshold value of SF can form during deformation [294, 295]. The resolved stress in the case of those samples with varying Q is similar to the condition of tests conducted by Godet et al. [178], where contraction twins were shown to have a higher SF than that

of extension twins. Therefore, contraction twins developed rapidly with an increase in *Q*. Much more contraction twins formed than extension twins as shown in Fig. 6 (d). As mentioned above, texture intensity near the TD component became lower for the higher level of ε. This may also contribute to the suppression of extension twinning in the case of varying *Q* (ε remained at approximately 19%) due to the lack of an appropriate component for twinning. Jiang et al. [139] analysed a similar condition, and concluded that the RD component was rotated more readily towards ED than towards the TD component using the SF criterion, which is consistent with the above result.

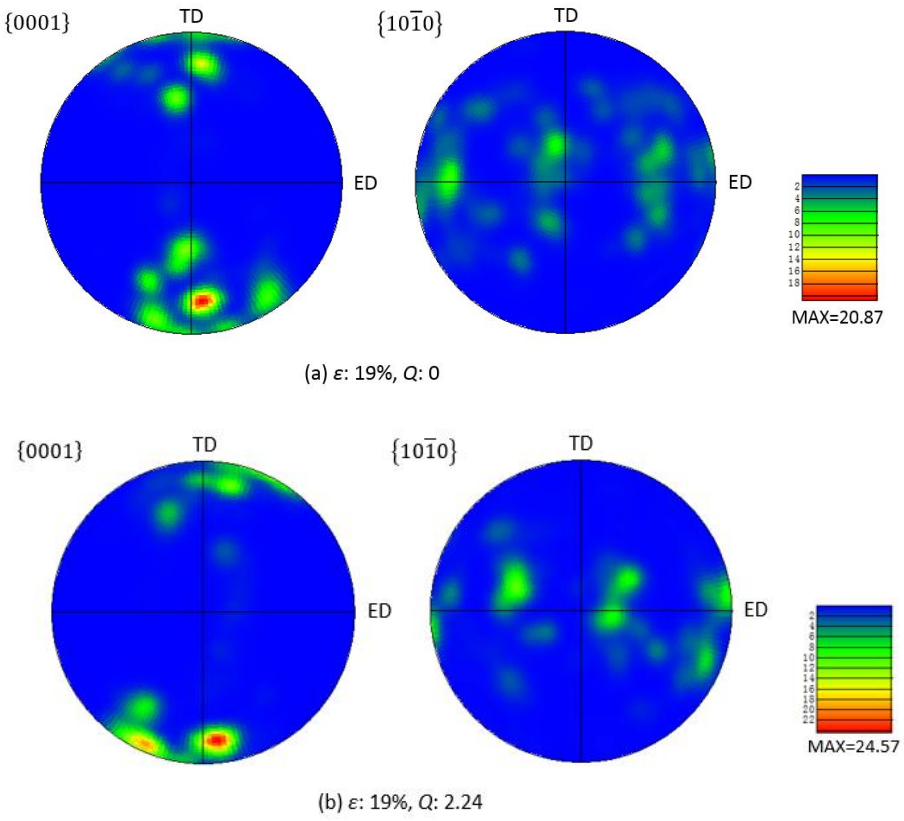

Fig. 9. Texture development during rolling of AZ31 tubes with the increasing Q. Recalculated $\{0001\}$ and $\{10\bar{1}0\}$ pole figures (a) ε: 19%, *Q*: 0 (b) ε: 19%, *Q*: 2.24

4.2 Influence of twinning on mechanical behaviour

The influence of twinning on the mechanical behaviour of Mg alloys has been demonstrated in many studies [53, 259, 296, 297]. The twin boundaries formed in grains can act as barriers to dislocation motion, as do grain boundaries, which can lead to an increase in the work-hardening rate. In contrast, the twin boundaries accommodate strain along the *c*-axis, which can release the effect of work hardening. Therefore, the lattice rotation introduced by twinning can enhance or reduce the rate of

work hardening depending on the type of twinning. $\{10\bar{1}1\}$ contraction twinning reorients the basal planes by 56 ° and has an effect favourable for basal glide. Double twinning has the same effect as $\{10\bar{1}1\}$ twinning, which rotates the orientation of basal planes by 38 ° [72]. $\{10\bar{1}2\}$ extension twinning reorients the basal planes by 86 °[53].

In the case of increasing ε, extension twins were generated favourably in the ED direction, and most of the twins in Fig. 6 were identified to be extension ones. Barnett et al. [259] pointed out that the 86 ° reorientation induced by $\{10\bar{1}2\}$ extension twinning has a strong influence on improving strength. Oppedal et al. [296] reported that extension twinning induces dislocation transformation in the reoriented matrix, as twinning shear extracts from the parent dislocation and releases a transmuted dislocation in the twin [11, 23]. The increase in strength may also contribute to texture hardening which is verified by Oppedal et al. [296]. Texture hardening took place with increasing ε due to deformation in ED and reorientation of TD component grains. Therefore, the UTS at an ε of 19.7% increased by 33% over that at an ε of 5.5%. Therefore, the combined effect of texture hardening and extension twinning leads to an increase of the UTS and YS in the case of increasing ε.

$\{10\bar{1}1\}$-$\{10\bar{1}2\}$ double twinning is frequently formed within $\{10\bar{1}1\}$ contraction twins, and has a similar effect on softening to contraction twins [240, 293]. However, this type of structure is considered to lead to rapid flow localisation and failure [240] due to the combined effects of strain softening and localised void formation [75]. In both cases of increasing ε and increasing Q, the elongations declined. For the case of increasing ε, texture hardening and extension twinning may be factors which lead to the drop in elongation, so the effect of double twins on elongation could not be ascertained. But with increasing Q, elongation experienced a decreasing trend similar to UTS and YS, which is not consistent with typical mechanical behaviours. In consideration of the absence of texture hardening and the unchanged amount of extension twins, the effect of double twins may contribute to this seemingly abnormal tendency. Fig. 9 shows pole figures of the grain orientations for N02 and N07 (Q increased from 0 to 2.24). The texture was not enhanced along any particular direction.

The apparent fraction of twins in samples with high ε levels seemed lower because most of the grains have been almost entirely consumed and reoriented by twinning. These conditions favour the activation of secondary $\{10\bar{1}2\}$ twinning for all with increasing Q [240]. In the case of increasing ε, secondary $\{10\bar{1}2\}$ twinning was observed in the sample with ε of 19.7% (Fig. 6 (b) & (d)). The frequency of the secondary twin boundaries increases continuously with strain. More and more secondary twinning can be activated within primary $\{10\bar{1}2\}$ twins. Unlike most of the primary $\{10\bar{1}2\}$

twins, these secondary $\{10\bar{1}2\}$ twins were shorter and denser [72, 240]. That is because secondary twins have a high rate of lateral growth, and then consume significant lengths of the primary twins. The secondary $\{10\bar{1}2\}$ twins were observed in the samples processed at a *Q* of 2.24 (arrows in Fig. 6 (d)). As mentioned earlier, twin boundaries can have the effect of blocking dislocation motion. The primary $\{10\bar{1}2\}$ twins provide additional barriers to the secondary $\{10\bar{1}2\}$ twin systems. Hence, the formation of primary and secondary $\{10\bar{1}2\}$ twins contribute to hardening. However, Jiang et al. [72] reported a decrease in the strain hardening rate when primary and secondary $\{10\bar{1}2\}$ twin systems interacted, which is also observed in the results of this investigation. The reason for this behaviour is unclear and requires further research.

Texture in the ED did not change with varying *Q*. As deformation took place in the TD and RD, the UTS and YS exhibited a rapid drop with increasing *Q*, which suggests that the change of texture in TD and RD does not play as important a role as that in the case of varying ε. However, the formation of $\{10\bar{1}1\}$ contraction twinning had a significant influence on the flow stress. Its effect was reported to be similar to that of <c + a> slip [32]. It is observed that $\{10\bar{1}1\}$ contraction twinning and double twinning can be activated in the RD (Fig. 4), and they increased linearly with the increase of *Q*. Decreasing strain hardening resulted from the formation of contraction and double twins due to the reduction of the strain hardening index, *n* [298]. Extension twinning may also be activated in the TD. However, as mentioned earlier, many of the grains have been almost completely consumed and reoriented by twinning at an ε of 19.7%, so extension twinning was suppressed even when *Q* is 0. The amount of primary $\{10\bar{1}2\}$ twins rarely increased because they were almost saturated, while the shorter and denser secondary $\{10\bar{1}2\}$ twins are introduced. The twins lost their effectiveness as barriers to dislocation motion. This contributes to the decrease in strain hardening rate observed in Fig. 3 with increasing *Q*. Therefore, in the case of increasing *Q*, primary $\{10\bar{1}2\}$ extension twinning has no influence on the mechanical behaviour, while the combined effects of $\{10\bar{1}1\}$ twinning/double twinning and secondary $\{10\bar{1}2\}$ twinning play a dominant role.

5. Conclusion

The effect of cold rolling on the mechanical behaviour of AZ31 Mg alloy tubes was investigated through an analysis of mechanical properties and the evolution of twinning under different processing parameters. The properties were assessed with respect to the tube rolling parameters; ε the ratio in cross-sectional reduction and Q the ratio of wall-thickness to diameter reduction.

1. For the AZ31 tubes, the UTS and YS increased with increasing ε, while it dropped with an increase in Q. Elongation in both cases decreased with an increase in ε and Q. The UTS/YS and elongation show the same tendency due to the formation of $\{10\bar{1}1\}$-$\{10\bar{1}2\}$ double twins.
2. $\{10\bar{1}2\}$ extension twins increased with increasing ε until they are almost saturated when ε is above 16.5%. Then contraction/double twins and secondary $\{10\bar{1}2\}$ twins propagated dramatically at high-levels ($\geq$16.5%) of ε and in the case of increasing Q.
3. The $\{10\bar{1}2\}$ extension twins were the dominant deformation mechanism and overshadowed that of contraction and double twinning in the case of varying ε. Texture hardening and $\{10\bar{1}2\}$ extension twinning are the two dominant effects on the mechanical properties in the case of increasing ε. Contraction and double twinning played a dominant role in determining the mechanical behaviour in the case of varying Q.

PAPER 2

Evolution of the microstructure and mechanical properties during fabrication of mini-tubes from a biomedical β titanium alloy

Yaowu Zhang, Damon Kent, Gui Wang, David StJohn and Matthew Dargusch

Journal of the Mechanical Behavior of Biomedical Materials
2015, Volume 42, Pages 207-218

Abstract

The processing of Ti-25Nb-3Mo-3Zr-2Sn tubes with outside diameters of 5.6mm-8.0mm and wall-thicknesses of 0.7mm-1.0 mm were investigated in order to study the evolution of microstructure and mechanical properties and their impact on the processing of the tubes. The annealed small tubes with single β phase microstructures exhibit double yielding during tensile tests. The onset of martensitic phase transformation was observed to occur after the lowest point of the strain hardening. Cold rolling also activates the formation of the stress induced martensitic α″ phase. Its volume fraction increased with increasing ε. The rate of strain hardening and the modulus of the tubes are related to the stress induced transformation of the β phase to the α″ phase. The stress induced α″ slightly improves the yield strength of the tubes at low levels of strain. However, larger strains result in grain growth during annealing, which diminishes the mechanical properties.

1. Introduction

Metastable β Titanium alloys are receiving extensive attention for a wide range of biomedical applications because of their excellent toughness, corrosion resistance and biocompatibility [299]. Ti-V-based alloys [300], Ti-Mo based alloys [7] and Ti-Nb-based alloys [9-12] β-Ti alloys have been reported to display shape memory and superelastic behaviours [5]. They are favourable for the application of stents: the large elastic strains in β-Ti alloys reduce the risk of damage to the stent both during delivery into the body and operation [8]. The potential release of harmful V and Al ions from Ti alloys used for biomedical applications has been reported and research has attempted to overcome their long-term health risks [13, 14]. In regards to the biocompatibility of NiTi alloys for use in medical applications, the hypersensitivity caused by the release of Ni remains a concern [301-303]. Also, it has been reported that the rates of Ni release can significantly increase over time [304, 305]. Thus, considerable research has focused on new metastable β titanium alloys for biomedical applications which do not contain Ni, V and other toxic elements [9, 11, 15, 16]. Ti-Nb-Sn, Ti-Nb-Al, Ti-Nb-Mo and Ti-Nb-O alloys exhibit good shape memory and superelasticity. The Ti-Nb-based alloys are promising candidates for manufacturing biomedical stents. They have dominant β phase, whilst other phases are reported to form during deformation and heat treatments. Due to their metastable β phase structure, other phases which may form in these alloys include α, ω and α″ phases [17-19]. A metastable β Ti alloy, Ti-25Nb-3Mo-3Zr-2Sn (wt%), was developed by Yu et al. [20] and has been researched as a promising material for biomedical applications [12, 18, 19, 21-23]. The Ti–

25Nb–3Zr–3Mo–2Sn alloy has low modulus, high strength and exhibits considerable plasticity and pseudoelastic character. The alloying elements Zr and Sn have similar abilities to enhance strength and improve the plasticity of the β Ti alloys [20, 97]. Binary Ti-Nb alloys with stable β phase structures exhibit undesirably high elastic moduli. Replacing some of the Nb with Zr reduces the elastic moduli to lower levels, but the Zr does not significantly affect the stability of the β phase. Additionally, the stabilising effect of Zr is much weaker than that of Sn in the Ti-Nb-Zr-Sn system [39]. The addition of Sn to the Ti–25Nb–3Zr–3Mo–2Sn alloy improves the stability of β phase. In this work, the fabrication of fine Ti-25Nb-3Zr-3Mo-2Sn tubes was investigated with a view to their use in the fabrication of biomedical stents.

The metastable β alloy can deform by plastic slip, formation of stress induced martensite (SIM), deformation twinning, or any combination of these processes. [31-34]. When subjected to an external load, the formation of SIM in metastable β-Ti alloys depends on factors, such as chemical composition, strain rate, extent of deformation and grain size. It is well known that the α″ martensitic transformation can be easily triggered by external stresses because the martensitic start temperature is below room temperature for many of the metastable β titanium alloys [306-308]. The β phase stability is controlled by the levels of alloying elements. The elements Nb, Mo and Sn are β phase stabilisers which have a high degree of solubility in the β phase and lower the β transus temperature. For binary Ti-Nb alloys, the least amount of Nb necessary in order to stabilise the β phase is 24 at% (38 wt%) [39]. The use of Mo and Sn makes it possible to stabilise the β phase in the Ti-25Nb-3Mo-3Zr-2Sn alloy despite its reduced levels of Nb. As Ti-25Nb-3mo-3Zr-2Sn is a metastable β titanium alloy, athermal martensitic α″ may form by quenching and stress-induced martensite α″ by cold working. A portion of SIM formed by cold rolling reverts to the β phase when the external stress is unloaded, while the remainder can readily decompose into the β phase by annealing. The SIM transformation can strongly influence the mechanical behaviours of the metastable β-Ti alloys both during processing and service. Neelakantan et al. [40] concluded that SIM effects can be tailored to achieve improvements in the mechanical properties and performance of the metastable β-Ti alloys. If the stress required to trigger the SIM transformation is lower than the stress for dislocation slip of the β phase, the β-Ti alloy often exhibits a characteristic strain plateau with double yielding phenomena (Fig. 3 (b)) in the tensile stress-strain curve [309], whilst the shape of the stress-strain curve will not be effected when the triggering stress for the martensitic transformation is close to or higher than the stress for slip.

Typically, in the fabrication of mini-tubes from titanium alloys, cycles of cold rolling and annealing are conducted to form the fine tubes which are then cold drawn. In the present study, the cold rolling and annealing behaviours of Ti-25Nb-3Mo-3Zr-2Sn tubes were investigated for the fabrication of β-Ti biomedical stents. The Ti-25Nb-3Mo-3Zr-2Sn alloy has a low β phase stability and is readily transformed into a partially reversible, stress induced martensitic α'' phase [12, 142]. Tensile tests have been used to evaluate the evolution of the mechanical properties during fabrication of the β-Ti mini-tubes. The relationship between the evolution of microstructure and mechanical properties during the processing of the tubes was investigated.

2. Experimental Methods

As-rolled Ti-25Nb-3Mo-3Zr-2Sn tubes were received with an outside diameter (OD) of 8.0 mm and a wall thickness (WT) of 1.0 mm. A mill (LD-8) with 3 rollers (mandrel bar inside) was used to keep the tubes in an intact round geometry down to a diameter of 3mm. Cold drawing without any internal support was used to further reduce the diameters of the tubes. Annealing was conducted at 1023K for 30 minutes under vacuum between each cold rolling pass in order to release residual stress. The processing of tubes was shown in Fig. 1. Final dimensions of the cold rolled and annealed tubes are shown in Table 1. The tubes in the order of processing are N1, N1A, N2, N2A, N3, N3A, N4, N4A ('A' means annealed tubes). During the fabrication of tubes, the parameter ε used to measure the deformation is defined as below [267]:

$$\varepsilon = \frac{A_0 - A_1}{A_0} = \frac{t_0 \times (D_0 - t_0) - t_1 \times (D_1 - t_1)}{t_0 \times (D_0 - t_0)} \; ; \qquad (1)$$

Uniaxial tensile tests were conducted for all of the cold rolled and annealed samples. Samples for tensile testing were cut by wire-electrode cutting machining from the tubes with their axis aligned with the axial direction (Fig. 2). Specimens with a nominal 3.0 mm width and a gauge length of 25 mm were used. Polishing was conducted before the tensile tests in order to avoid the influence of minor notches on the machined surfaces. Tensile testing was conducted using an Instron universal tensile testing machine (Instron 4505) with an initial stain rate of 0.001 s^{-1} at room temperature. A minimum of 3 tensile tests was conducted for each group to ensure the repeatability of results. A contact extensometer was used to record strain from the gauge length of the specimens. Samples for microstructural observation and X-ray diffraction (XRD) were wet ground with waterproof silicon

carbide papers to 4000 grit, polished with OPS colloidal silica solution and ultrasonically cleaned. Then etching was conducted with Kroll's reagent for 20 seconds for SEM observation. For the Electron Backscatter Diffraction (EBSD) specimens, mechanical polishing was followed by chemical polishing with a solution of ethanol (90 ml), nitric acid (5 ml) and hydrofluoric acid (5ml) for 2-4 seconds. SEM was conducted on JEOL JSM 6610 and JEOL JSM 6460 instruments. In order to identify the phase composition, XRD spectra were obtained on a D8 Advance X-Ray Diffractometer operated at 40 KV and 30 mA, equipped with a graphite mono-chromator, a Ni-filtered Cu Kα (λ=1.5406nm) source and a scintillation counter. The EBSD investigations were carried out using a FEI field-emission gun scanning electron microscope (JEOL JSM 7001) at 25kV. All images in this paper are presented with the tensile direction and rolling direction parallel to the horizontal direction.

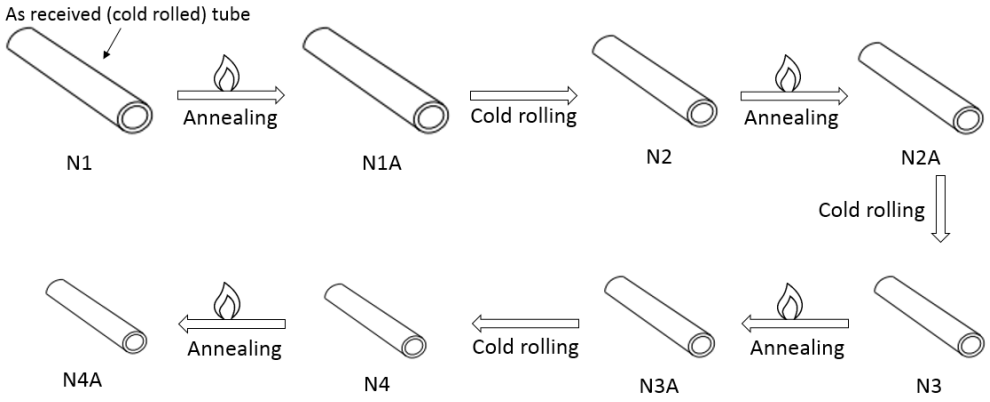

Fig. 1. Schematic diagram for the processing of Ti-25Nb-3Mo-3Zr-2Sn tubes

Table.1. Sample groups and ε for β-Ti tubes used in investigation.

Samples	**N1**	**N1A**	**N2**	**N2A**	**N3**	**N3A**	**N4**	**N4A**
Outside Diameter (mm)	8.0	8.0	6.9	6.9	6.1	6.1	5.6	5.6
Wall Thickness (mm)	1	1	0.85	0.85	0.7	0.7	0.7	0.7
ε	N/A	N/A	26.5%	26.5%	46%	46%	51%	51%

3. Results

3.1 Tensile tests

A series of tensile stress-strain curves for cold rolled and annealed samples are shown in Fig. 3 (a) and (b). A comparison of mechanical properties is plotted in Fig. 3 (c) and (d). The cold rolled tubes with a ε of 26.5% have an ultimate tensile strength (UTS) of 974 MPa, a yield strength (YS) of around 912 MPa and ductility of 6%. In comparison with the as-received tubes (N1), the YS shows a slight reduction while the UTS was increased slightly due to the substantial improvement of ductility and post-yield strain hardening. The ductility was increased by approximately 25% (Fig. 3 (c)). The further increase of ε to 51% resulted in reductions of the UTS, YS and ductility to 714 MPa, 642 MPa and 14.3%, respectively (Fig. 3 (c) (d)). The annealed tubes showed significant enhancements in the ductility with an approximate 4-fold increase in comparison with the cold rolled samples (Fig. 3 (d)), whilst the UTS and YS of the annealed tubes decreased. In particular the YS experienced a sharp drop to around a half of the cold rolled strength. In comparison with the reducing tendency of the YS in the cold rolled tubes, the annealed tubes show an increase in the YS for low levels of ε (<46%). The annealed tensile samples exhibit "double yielding" characterised by the presence of a stress-plateau in the stress-strain curve. Double yielding in the β-Ti alloys is reported to be associated with the stress-induced α″ martensitic transformation [306, 310]. It can occur if the triggering stress for the stress-induced α″ phase is lower than the yield point for slip of the β phase [311]. In comparison with the cold rolled tubes, a higher post-yield strain hardening rate was observed for the annealed tubes.

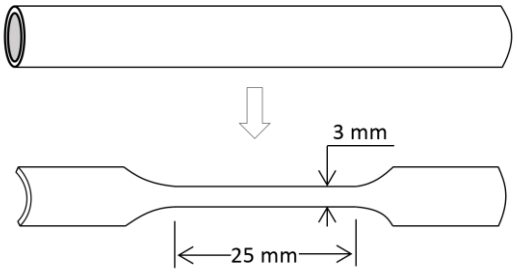

Fig.2 Schematic diagram of the tube and the tensile sample.

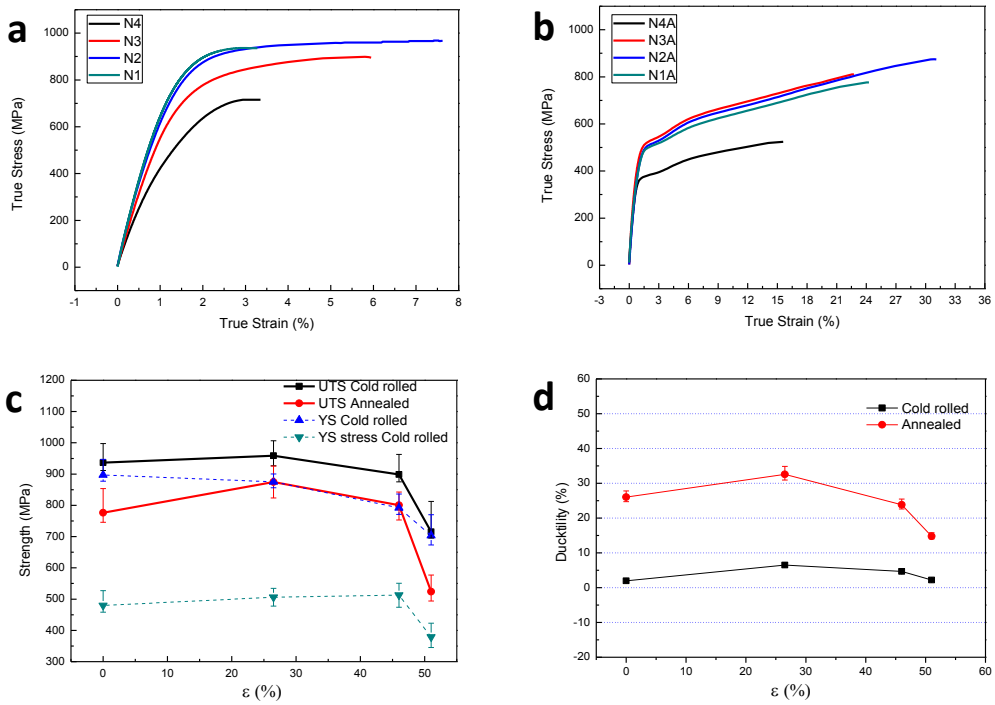

Fig. 3. (a). Tensile stress-strain curves for Ti-25Nb-3Zr-3Mo-3Sn tubes before annealing; (b). Tensile stress-strain curves for Ti-25Nb-3Zr-3Mo-3Sn tubes after annealing; (c) Comparison of the tensile strengths; (d) Comparison of the elongation

3.2 Microstructures and phase transformation

Fig. 4 shows the microstructures of the cold-rolled and annealed Ti-25Nb-3Zr-3Mo-3Sn alloy tubes. In Fig. 4 (a), the as-received samples are composed of equiaxed grains with acicular features. Peaks associated with β phase and martensitic α″ phase are observed. Body-centred cubic (bcc) β phase was identified as the dominant phase, while the diffraction peaks can be observed at 58.3 °and 72.5 °from (200)α″ and (220)α″, respectively. Because the β transus temperature is around 710 ℃ to 720 ℃ [20], after annealing at 750 ℃ for 30 min the tubes have a fully β phase structure as the dissolution of orthorhombic α″ phase (Fig. 4 (b) (d) (f)). The four characteristic peaks of the β phase were identified in the XRD spectrum for the annealed samples (Fig. 5 (b)). The widths of diffraction peaks for the annealed tubes was narrowed, which is due to the release of residual stress and lattice distortion and the dissolution of martensitic α″ phase. Cai et al. [312] conducted experiments on the reverse transformations in a metastable β-Ti alloy and observed that the reverse transformation of α″ to β and α to β took place simultaneously when the temperature was above 900K. Thus, a single β phase is predicted to form for the annealed tubes in this work, which is consistent with the results of the XRD analysis. In Fig. 4 (c), the martensitic phase transformation occurred substantially, when the β-Ti tubes were cold rolled with a ε of 26.5% from the annealed condition. Characteristic peaks from the β phase and the SIM α″ phase are identified for the cold rolled tubes in the XRD spectrum (blue trace

in Fig. 5 (a)). The relative peaks of the $200_{\alpha''}$ peak and $220_{\alpha''}$ peak indicate that the cold rolling resulted in martensitic phase transformation which is also evident from the microstructures shown in Fig. 4 (c) (e) and (g).

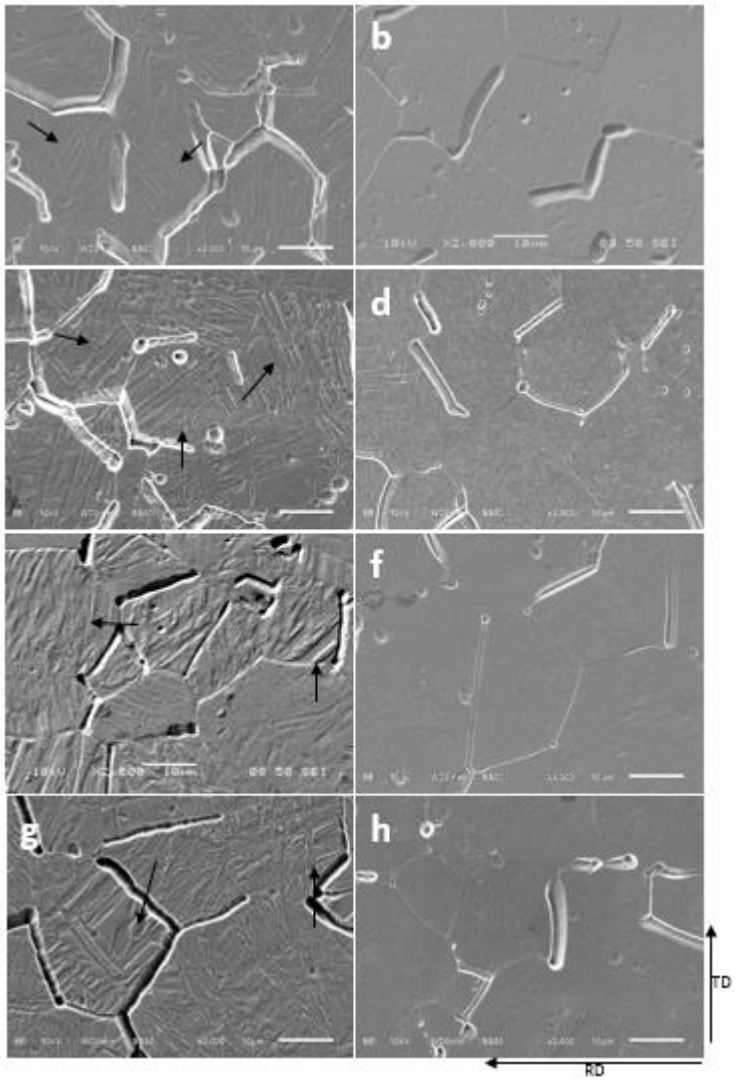

Fig. 4. SEM microstructures,
(a) As-received samples from N1; (b) Annealed samples from N1A; (c) Cold rolled samples from N2; (d) Annealed samples from N2A; (e) Cold rolled samples from N3 (f) Annealed samples from N3A (e) Cold rolled samples from N4; (f) Annealed samples from N4A.

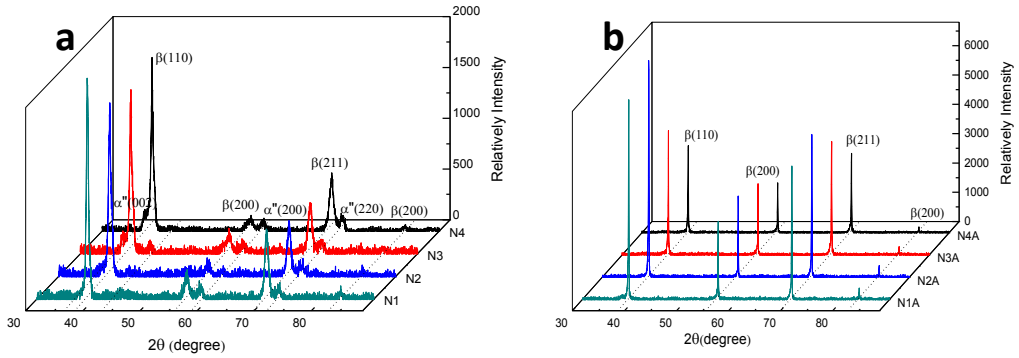

Fig. 5. XRD profiles of Ti-25Nb-3Zr-3Mo-2Sn alloys at various deformation reductions and annealing conditions, (a) Cold rolled tubes; (b) Annealed tubes

4. Discussion

The results shown in Fig. 3 (a) (c) indicate that strength decreases with increasing strain (ε of 0 → ε of 51%) for the cold rolled tubes. It had been reported that the α″ phase can lead to reduced yield strength, ultimate tensile strength and Young's modulus [20, 251, 313, 314]. The low value of e/a and Bo in Ti-25Nb-3Mo-3Zr-2Sn indicates that martensitic α″ is expected to be formed easily under external stress. XRD profiles identified that the cold rolled samples were composed of the β and α″ phases. The SEM images (Fig. 4) show that the SIM α″ phase exists in all of the cold rolled samples. The formation of the stress-induced martensitic α″ phase is responsible for tensile behaviour characterised by decreasing yield strength and Young's modulus, which corresponds to the volume fraction of SIM α″ formed during cold rolling [107, 251]. Fig. 6 shows the relative intensities of the XRD peaks with varying strains. The relative intensity of $I_{\alpha''(220)}/I_{\beta(110)}$ and $I_{\alpha''(200)}/I_{\beta(110)}$ increases with increasing strains. In combination with the results of the tensile tests in Fig. 3 (a), the proportion of martensitic α″ in the cold rolled β-Ti tubes is closely related to the yield strength and Young's moduli of the tubes, as reported in the previous studies [20, 315, 316]. Akanuma et al. reported that SIM transformation in a near β-Ti alloy (Ti1023) negatively affects the yield strength and ductility [315]. Similar phenomena were also reported by Yu et al. for solution treated and rolled Ti-25Nb-3Mo-3Zr-2Sn rods [20]. Also, it is reported that the size of the α″ martensite plate is related to the internal elastic energy in the β phase and the internal frictional resistance between the β and α″ phases influences the yield strength [312].

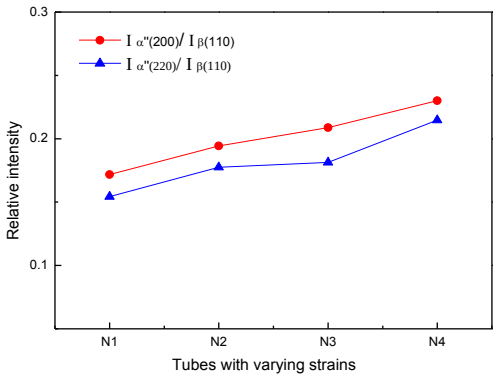

Fig. 6. Relative intensities of XRD peaks in the tubes with varying strains

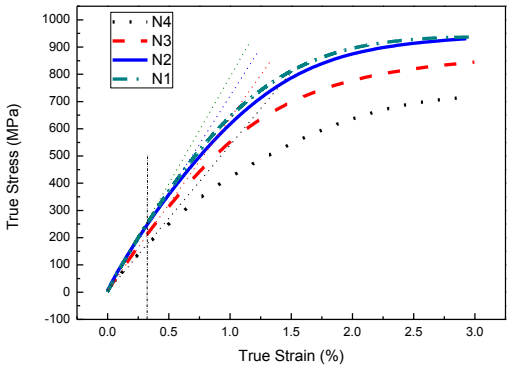

Fig. 7. Magnified incipient tensile curves of cold rolled tubes and tangent Young's modulus in dotted straight lines

The initial portion of the stress-strain curve shown in Fig. 3 (a) is redrawn for strains ranging from 0 to 3% in Fig. 7. Young's modulus can be measured from a dotted straight line drawn along the stress-strain curve at an initial stage of deformation. The measured Young's modulus may be slightly altered by the strain range employed. Because the linearity of the line in Fig. 7 appears to be satisfied at strains ranging from 0 to 0.3%. The tangent modulus at strains ranging from 0% to 0.3% was regarded as the Young's modulus and listed in table 2. The Young's modulus in the cold rolled tubes decreases with the increasing strains. Hanada et al. reported that the Young's modulus was reduced by inducing the martensitic transformation. In contrast, the Young's modulus remained unchanged for annealed tubes (Fig. 3 (b)). The annealed tubes have a Young's modulus ranging from 91.89 GPa to 97.14 GPa. The following explanation has been added to the discussion section. β Ti alloys exhibit elastic anisotropy. The Young's moduli along <110> and <111> are larger than <100> [107]. The Fig. 12 (a)(b)(c) is the inverse pole figure corresponding to the orientation with respect to the EBSD data. The orientation of most grains is in the shaded (101) plane shown in Fig. 8. Therefore, the tensile direction is along <111> or <110> as they are parallel to the observation plane. This is the likely reason for the annealed tubes having a higher modulus than in previous reports.

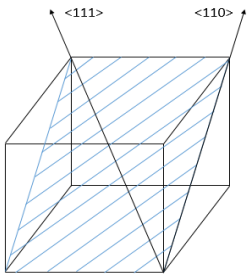

Fig. 8. Schematic diagram of main grain orientation and tensile direction

Table. 2 Tangent Young's modulus for the cold rolled and annealed tubes

	N1	N2	N3	N4	N1A	N2A	N3A	N4A
Tangent Young's modulus (GPa)	89.79	83.12	75.14	53.17	97.14	95.33	91.89	96.31

During the tensile tests, double yielding occurs in the annealed samples as shown in Fig. 9, which is a well-known phenomenon associated with the stress-induced martensitic transformation in single β phase titanium alloys [317]. It is noted that the double yielding effect observed previously does not occur for the cold rolled samples. This is possibly due to the well-developed martensite, which hinders the nucleation of new martensitic plates during tensile tests. The strain hardening rate-strain (θ-ε) curve pertaining to the σ-ε curve for the annealed tubes is presented as Fig. 10 in order to investigate the strain hardening rate associated with the double yielding. The strain hardening rate was typically divided into three stages; a sharply dropping stage (stage I),an increasing stage (stage II) and a steady declination stage (stage III) [72]. At the first yielding point, the strain hardening rate exhibits a sharp decrease. A conventional transition between the elastic and plastic regimes occurs in stage I [35]. Between the double yielding points, stage II exhibits a large increase in the strain-hardening rate from the elastic limit to a strain of approximately 2.7%. Sun et al. [187] reported that two major deformation modes occur in the stage II, martensitic phase transformation and mechanical twinning, and interacted continuously throughout the plastic deformation.

In order to investigate the SIM transformation during tensile tests of the annealed tubes, samples from N4A were subjected to interrupted tensile testing up to true strains of 1.2%, 2.4% and 3.5%, respectively. The strain values were selected on the basis of the different regions of the strain hardening rate – true strain curve in Fig. 10. 1.2% is for the fast decreasing part of stage I, 2.4% is for the slow decreasing part of stage I, 3.5% is for the stage II. XRD spectra from these samples are shown in Fig. 11. The α″ phase was induced within β grains and its amount increased during tensile tests. It was identified by XRD as a phenomenon of grain refinement, which broadened the peaks in Fig. 11. The increased residual stress also broadened the characteristic peaks. The explanation has been added in the discussion. The martensitic phase transformation did not occur in the stage I, which is consistent with the above analysis. Also, the tangent Young's modulus of the annealed tubes all fell within a narrow range, indicating that no SIM transformation occurred in the elastic stage of the tensile curves. In stage II, peaks associated with the orthorhombic α″ phase were identified (Fig. 11). SIM transformation can be readily triggered in titanium alloys with low β phase stability. The "double yielding" phenomena and related strain plateau correspond to the critical stress to induce α″ martensitic transformation from the parent β phase. Previous reports have demonstrated that the

reversible β to α″ transformation is related to pseudoelastic behaviour in the biomedical β-phase titanium alloys [5, 318]. Also, the low β phase stability is related to the low Young's modulus observed in these alloys as well as their propensity to exhibit SIM transformation during deformation [107, 319]. β-Ti alloys exhibiting the "double yielding" phenomena may possess low fatigue strengths, which is disadvantageous for the stent applications. Cold-processing can increase the critical stress to induce martensitic transformation and improve their fatigue strengths [318]. Hanada et al. [107] investigated double yielding occurring in Ti-33.6Nb-4Sn rods, the double yielding was observed for hot-forged and quenched samples, but it was not present for rolled samples. They reported that the stress-induced martensite α″ formed during stage II remained after unloading of the tensile stress even though the applied stress was removed before the second yield.

The SIM transformation plays an important role in the tensile properties of the annealed Ti-25Nb-3Mo-3Zr-2Sn tubes. The XRD spectra in Fig. 11 indicates that a great deal of martensitic α″ phase was produced during the tensile tests on the annealed β-Ti tubes. The acicular martensite adopts a distorted hexagonal structure, which has an orthorhombic unit cell [300]. Given the fewer slip systems in the orthorhombic structure than in the bcc crystal of the β phase, the α" phase may be less able to accommodate plastic deformation than the β matrix [309]. Thus, greater stress is required as the strain proceeds. At the beginning of formation of the martensitic α″ phase, the nucleation of α″ is free to extend the full length of the β grains. These initial formed martensitic plates have fairly mobile interfaces and can easily revert to the β phase on unloading [50, 107]. So they have acicular morphology and are almost parallel with each other. As the strain increases, the martensitic phase becomes unrecoverable when unloading, and new martensite was formed with intersectional morphologies [33]. Most SIM plates developed to extend across the full width of the β grains and intersect each other. The strain hardening rate of the annealed tubes following the SIM transformation was higher than those of the cold rolled ones. This is possibly caused by the SIMs formed in the annealed tubes during tensile tests, being different to the well-developed SIMs formed during cold rolling, in consideration of the softening effects of the latter. It is reported that the phenomenon of no obvious strain hardening can be attributed to the saturation and well-developed boundaries between SIMs and the β-matrix [17]. Thus, the yield strength increased for the annealed tubes N1A, N2A and N3A with increasing strain as shown in Fig. 9.

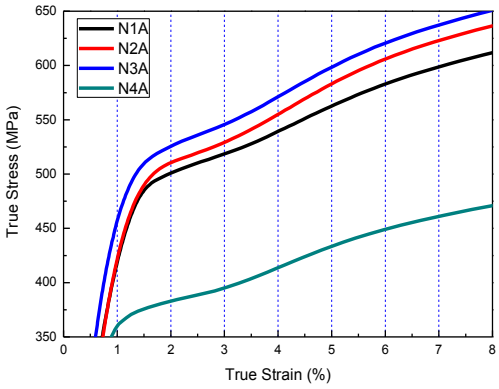

Fig. 9. True stress-true strain curves for the annealed tube samples

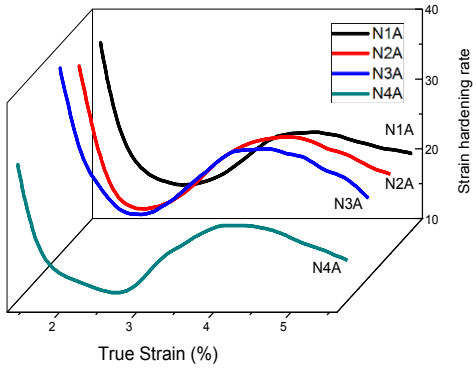

Fig. 10. The strain hardening rate – true strain curve, (a) N4A; (b) N3A; (c) N2A; (d) N1A

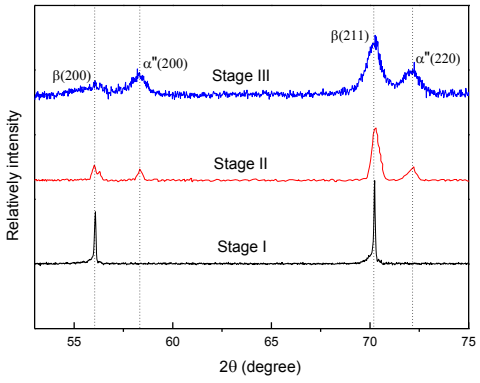

Fig. 11 Comparison of XRD spectrum at different stages of strain hardening

When the ε was 51% (N4A group), the strain hardening rate had a remarkable change in stage I (Fig. 10), where the decreasing rate was slowed down at around the first yielding point. It shows that the strain hardening rate begins to slow down at a strain of around 1.6%, when the martensitic phase transformation is predicted to occur according to the XRD spectra on samples from the interrupted tensile tests. Thus, the SIM transformation altered the strain hardening rate and the triggering stress for the SIM transformation was reduced dramatically when ε reached 51%. In combination with Fig. 3 (b) (d), the unique four-stage shape for group N4A is also related to the reduction in strength. Jiang et al. [72] reported a similar four stage strain hardening rate around double yielding. They concluded that the presence of the second stage is attributed to the combined action of both twinning and dislocations. In this stage, the flow stress began to increase, but the work hardening rate continues to decrease. The phenomenon of enhanced strain hardening occurring in association with twinning has also been observed by Salem et al. [320]. They concluded that the strain hardening rate in titanium alloys was related to deformation twinning, which is the inhibition of non-coplanar slip by dislocation pile-up and storage at the twin-matrix boundaries.

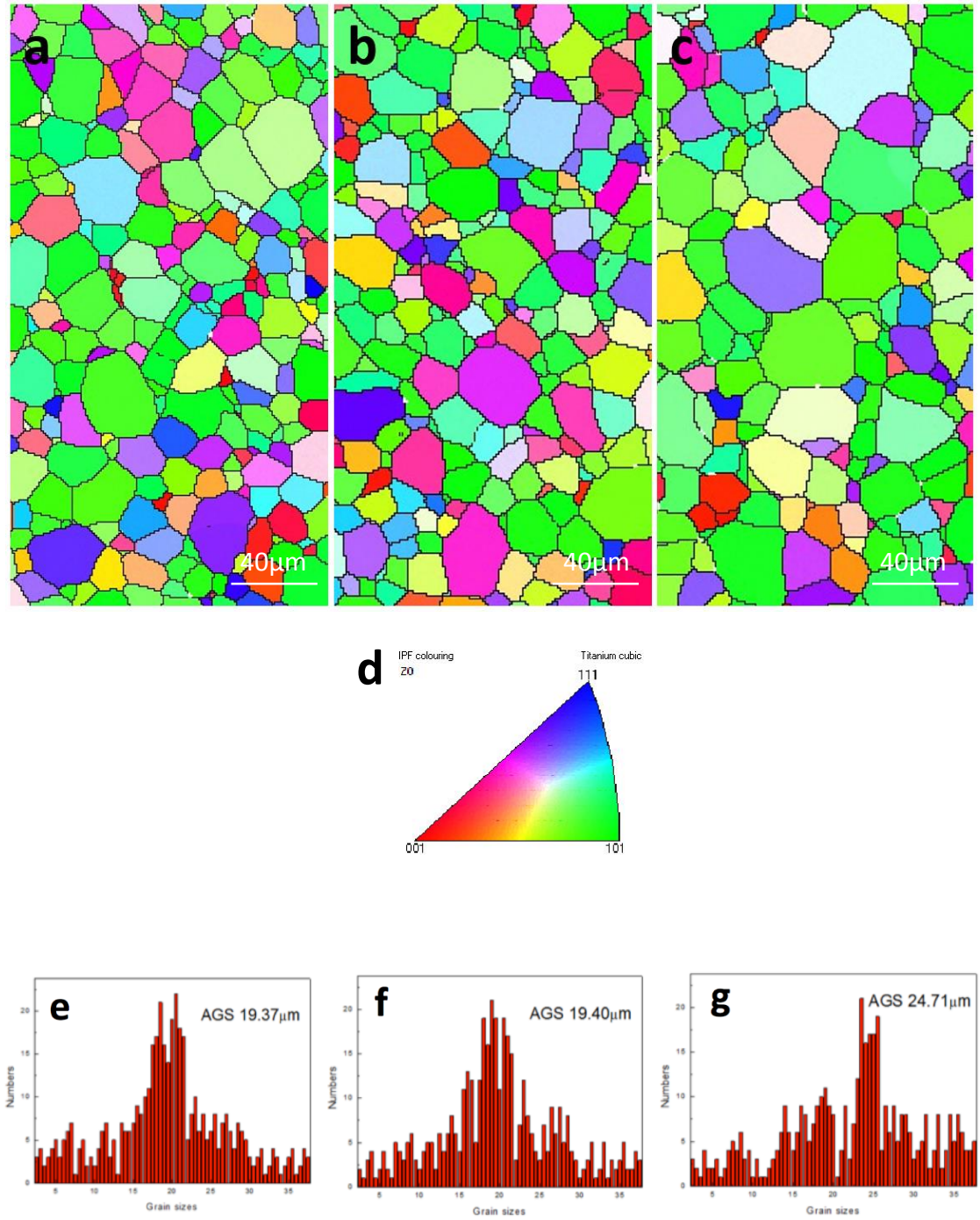

Fig. 12. IPFs from annealed tubes and statistics of grain sizes. (a) N1A (ε of 0), (b) N2A (ε of 26.5%), (c) N4A (ε of 51%), (d) IPF coluring for (a)(b)(c), (e) statistics of grain sizes of N1A, (f) statistics of grain sizes of N2A, (g) statistics of grain sizes of N4A

However, the remarkable reduction of yield strength in the tubes with the strain of 51% cannot be explained by the above. The value of yield strength can be influenced by several factors, the internal

elastic energy stored in the matrix, the reverse formation of SIM α″, the grain sizes and the fraction of low-angle grain boundaries (LAG) and high-angle grain boundaries (HAG).

Fig. 12 are inverse pole figures (IPFs) of the annealed tubes, which shows single β grains without any twins and SIM α″ phase. No obvious difference was observed in the textures for samples with varying strains. However, the grain size in N4A (strain of 51%) was increased by 27.6% in comparison with the N1A group. The interfacial area between β and α″ becomes smaller when the grain size increases [120]. The internal frictional resistance decreases correspondingly with the increasing grain size. Therefore, the yield strength of the N4A tubes was substantially reduced in comparison with other groups due to an increased grain size.

The formation of high angle grain boundaries in the β titanium tubes is primarily related to the complex stress state and dislocation configurations induced by martensitic transformation [321]. The fraction of high-angle grain boundaries (HAG), which was defined as the length of boundaries with misorientation angles above 10 ° over the length of all grain boundaries, was plotted in Fig.13. The fractions of grains with high-angle boundaries in all annealed tubes exceeds 90%. Accordingly, the proportion of low-angle grain boundaries (LAG) remained low for low levels of strains (<46%), whereas the tubes with a strain of 51% show an almost doubling in the proportion of LAG up to 8.77%. It is known that the combined effects of grain boundaries and voids leads to soft vulnerable zones which deform preferentially during the tensile tests, and the high stress concentrations and high local strains at boundary triple points and voids results in separation of the β grains [322, 323]. This is probably because the LAG at triple points will bear a larger load than HAG [324]. LAG are not as effective in interfering with the slip process as the high angle grain boundaries. The energy required to propagate micro-cracks increases dramatically when they interact with HAG, so the development of micro-cracking is inhibited. Therefore, the dramatic reduction in the yield strength of β-Ti tubes with a strain of 51% was partially attributed to the doubling in the proportion of LAG.

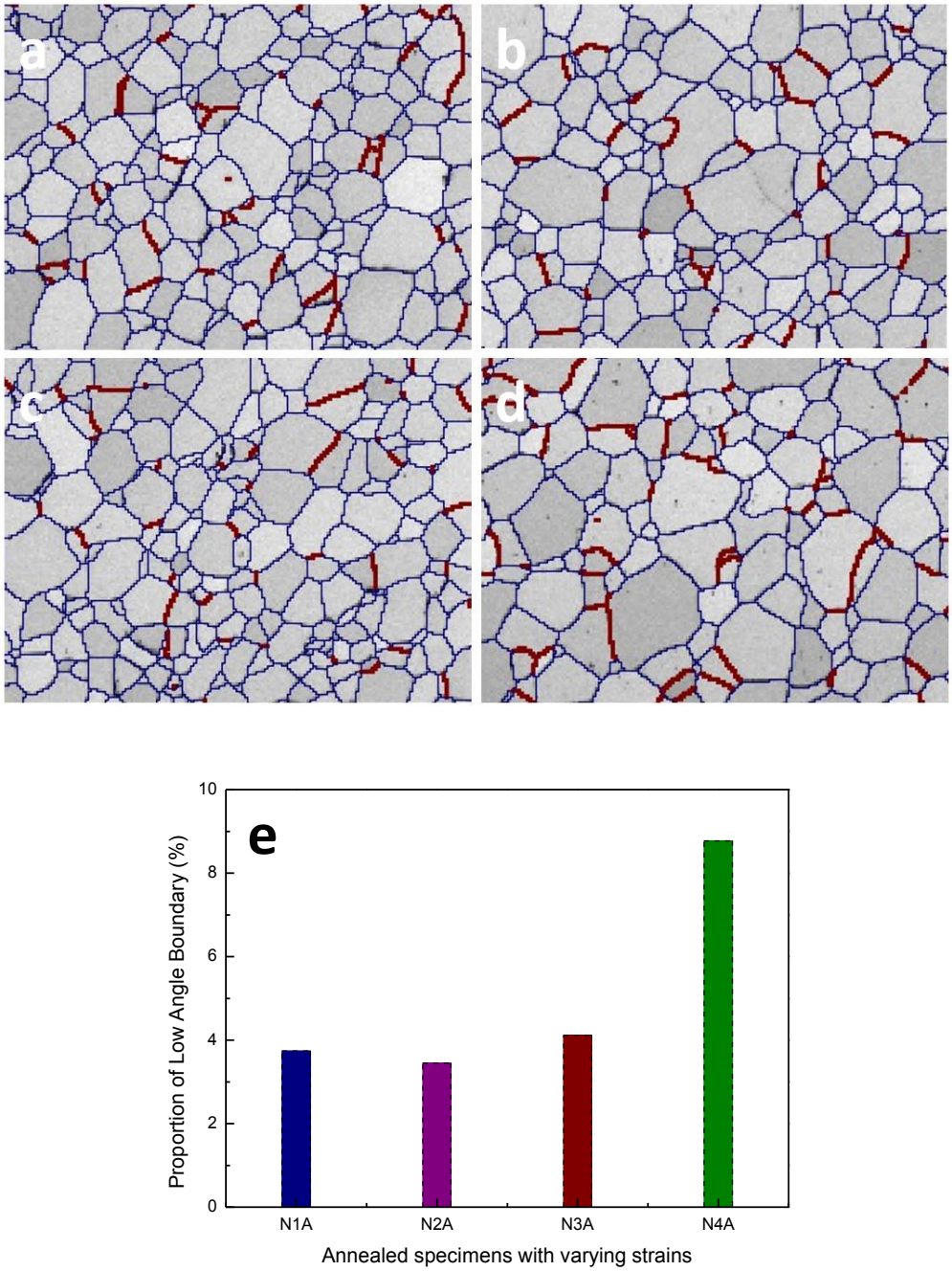

Fig. 13. High-angle grain boundaries and low-angle grain boundaries in annealed tubes from EBSD data (a) N1A, (b) N2A, (c) N3A, (d) N4A, (e) statistics of low-angle grain boundaries in annealed tubes

5. Conclusions

In this study the effects of cold rolling and annealing on the mechanical properties of biomedical Ti-25Nb-3Zr-3Mo-2Sn small tubes were investigated. The main results are summarized as follows:

- For annealed tubes, double yielding occurs during tensile tests. The onset of martensitic phase transformation occurs after the lowest point of strain hardening. The SIM α″ phase was formed and increased the strain hardening rate. The yield strength was enhanced at low levels of ε (<46%). However, it was substantially reduced when ε reached 51%. This is possibly because of the growth of the β grain size. The decrease of ductility at a ε of 51% may be related to the increased proportion of low-angle grain boundaries in the annealed tubes.
- Cold rolled tubes were composed of the β phase and SIM α″. The fraction of SIM α″ phase increased with increasing ε during cold rolling. The yield strength and tangent Young's modulus reduced with increases in the proportion of the martensitic α″ phase.

PAPER 3

An investigation of the mechanical behaviour of fine tubes fabricated from a Ti–25Nb–3Mo–3Zr–2Sn alloy

Yaowu Zhang, Damon Kent, Gui Wang, David StJohn and Matthew Dargusch

Materials and Design
2015, Volume 85, Pages 256-265

Abstract

This study investigates the mechanical properties and the deformation mechanisms active in Ti-25Nb-3Mo-3Zr-2Sn fine tubes. Ti-25Nb-3Mo-3Zr-2Sn alloy is a recently developed metastable β titanium alloy intended for biomedical applications. Tensile tests were carried out on the fine tubes. The modulus of the Ti-25Nb-3Mo-3Zr-2Sn fine tubes increased with reductions in the diameter for tubes in the cold rolled and annealed conditions. In comparison with cold rolled tubes, the annealed tubes exhibit increased strain hardening behaviour and superior ductility. Mechanical twins, stress-induced martensitic transformation and the textures of the β and α″ phases were investigated. The results show that the fine tubes exhibit different moduli which are related to the evolution of β and α″ phase textures during processing. Cold rolling facilitates the transformation from β to the α″ phase and mechanical $\{332\}\langle 113\rangle$ twinning. For the annealed tubes, mechanical twinning as well as primary and secondary martensitic transformations were activated at specific levels of tensile strain. Twins developed with increasing levels of strain, and secondary martensitic transformations occurred within the twinned β regions. Annealed fine tubes exhibit multistage strain hardening behaviour and superior ductility due to the synergetic effects of twinning induced plasticity and transformation induced plasticity during tensile deformation.

1. Introduction

Metallic materials are used widely for biomedical implants in applications such as, stents, artificial hip joints and dental prostheses [1, 2]. Materials to be used as implants in the human body typically require superior mechanical properties such as elasticity, corrosion resistance and high levels of ductility and strength [3, 4]. Titanium alloys meet all of these requirements and have good biomechanical and biochemical compatibilities and so are attractive materials for biomedical applications. Metastable β-Ti alloys have advantages over α and α+β alloys for biomedical applications due to their greater biocompatibility, lower modulus, high toughness and good mechanical processability, e.g., the superior elasticity effectively reduces the risk of damage to the stents as they are compressed during delivery into the body before being deployed in the target location [5, 6]. However, long-term health problems caused by the release of toxic ions from implanted titanium alloys has hindered their uptake. Research has been undertaken to overcome long-term health risks [13, 14], with studies on the development of new metastable β-Ti alloys with biocompatible and non-toxic compositions containing elements such as Nb, Mo, Zr and Sn [39, 325].

Any material intended for implants, such as stents, needs to be mechanically stable in biological environments for long periods, ideally for the lifetime of the patient. In order to fabricate mechanically suitable β-Ti fine tubes for stent applications, processing variables must be carefully controlled to obtain a suitable balance of mechanical properties such as strength and ductility. The mechanical properties of metastable β-Ti alloys are strongly influenced by the occurrence of several different deformation mechanisms [6], and studies dedicated to improving their mechanical properties have focussed on understanding and controlling these deformation mechanisms [6, 35]. The dominant deformation mechanism typically changes from stress induced martensite to mechanical twinning to slip with increasing levels of β phase stability [6]. The martensitic α″ transformation can be triggered by external stresses for alloys which have a martensitic start temperature below room temperature as is the case for many of the metastable β titanium alloys [17, 36, 37]. Twinning is a common deformation mechanism for materials which have low stacking fault energies and bcc structures [41]. In metastable β titanium alloys, $\{112\}\langle 111\rangle$ twinning has been widely observed, while $\{332\}\langle 113\rangle$ twinning has also been reported for some metastable β-Ti alloys [6, 45, 169].

A wide range of mechanical properties have been reported over the last decades due to the influence of different processing regimes and the large variety of compositions of the metastable β-Ti alloys. The stress and strain distributions during deformation vary between processing of bulk and sheet materials and fine tubes. Several gaps exist in the current literature in the understanding of the role played by deformation twinning and martensitic transformations on the mechanical properties exhibited in the processing of fine β-Ti tubes. A metastable β Ti alloy, Ti-25Nb-3Mo-3Zr-2Sn (wt.%), was developed by Yu et al. [20] and has been investigated as a promising material for biomedical applications [18, 20, 22, 23, 37, 326]. It has low modulus, high strength and exhibits considerable plasticity and superelastic character. Previously, the authors have reported on the evolution of mechanical properties during processing of Ti-25Nb-3Mo-3Zr-2Sn tubes with outside diameters >5 mm [37]. The tubes exhibit different deformation mechanisms and mechanical properties with reductions in the diameter. In the present work, tensile testing of fine tubes with diameters < 5mm was conducted to understand the evolution of Young's modulus, yield strength and strain hardening rates during processing to optimise their mechanical performance.

2. Method

2.1 Tensile tests to failure and interrupted tensile tests

The nominal composition of the alloy used in this investigation is Ti-25Nb-3Mo-3Zr-2Sn (wt.%). An ingot was melted three times in a vacuum arc remelting furnace using Ti-Nb master alloy, pure Ti, Mo, Sn and Zr as raw materials. The ingot was forged and hot extruded at 850 ℃ into pipes with a diameter of 32 mm and a wall thickness of 5 mm. During fabrication of the tubes, a strain parameter ε was used to measure the cross-sectional reductions, where $\varepsilon = \frac{A_0 - A_1}{A_0} = \frac{t_0 \times (D_0 - t_0) - t_1 \times (D_1 - t_1)}{t_0 \times (D_0 - t_0)}$. Multi-pass cold rolling with cross-sectional reductions of 25-30% followed byannealing at 1023K for 30 minutes was performed to alleviate residual stresses. The annealing was performed in tubular furnaces under vacuum (10^{-7} mbar) to prevent contamination and oxidation. 4 cycles of cold rolling and annealing were conducted to reduce the tubes from 5 mm in diameter to a final tube diameter of 3.2 mm. The samples in the present paper were obtained from different stages in the processing of the fine tubes in either the cold rolled or annealed condition. Dimensions of the samples are listed in Table 1 with the original order of processing being C1, A1, C2, A2, C3, A3, C4, A4 (Group 'C' for cold rolled samples, Group 'A' for annealed ones).

Table 1. Dimensions of Ti-25Nb-3Mo-3Zr-2Sn fine tubes used in the present investigation

Processing Order	**C1**	**A1**	**C2**	**A2**	**C3**	**A3**	**C4**	**A4**
Outside Diameters (mm)	5.0	5.0	4.5	4.5	4.0	4.0	3.5	3.5
Wall Thicknesses (mm)	0.5	0.5	0.4	0.4	0.3	0.3	0.25	0.25
Conditions	Cold rolled	Annealed	Cold rolled	Annealed	Cold rolled	Annealed	Cold rolled	Annealed

Wire-electrode cutting was used to prepare tensile samples from the fine tubes with their longitudinal directions parallel to the rolling direction of tubes. The cut surfaces were mechanically polished in order to limit the influence of minor notches. Fig. 1 shows the geometry of the fine tubes and the tensile specimens with nominal 2.5 mm widths and gauge lengths of 20 mm. Tensile tests were conducted to failure with an initial stain rate of 1.3×10^{-4} s^{-1} at room temperature (~23 ℃) using an Instron universal tensile testing machine (Instron 4505). A contact extensometer was used to record strains from the gauge length of the specimens. The reported tensile properties are the average of three individual experimental results in order to ensure the repeatability of results.

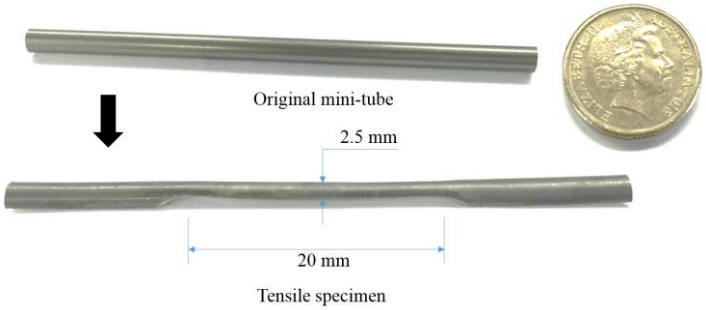

Fig. 1. Schematic diagram of the original fine tubes and the tensile specimens (OD of 4 mm).

Interrupted tensile tests were also conducted using the Instron 4505 tensile testing machine and the same parameters as those for the tensile tests to failure. A contact extensometer was used to measure strains during the interrupted tensile tests. Tubes with an OD of 4 mm were used for the interrupted tensile tests. The tests were interrupted when the calculated true strains reached 1.2%, 2.7% and 4.8%, which are related to the three different stages of strain hardening rate observed during the failure tensile tests. Samples from interrupted tensile tests were prepared for further microstructural analysis.

2.2 Microstructure observation

Microstructural characterisation was conducted using a combination of scanning electron microscopy (SEM), electron back-scatter diffraction (EBSD), transmission electron microscopy (TEM), and X-ray diffraction (XRD). All samples were prepared by wet grinding with waterproof silicon carbide papers to 4000 grit, polished with OPS colloidal silica solution and ultrasonically cleaned. Polished samples for SEM observation were etched by a solution of Kroll's reagent for 15-20 seconds. Samples for EBSD and XRD were prepared by chemical polishing with a solution of ethanol (90 ml), nitric acid (5 ml) and hydrofluoric acid (5ml) for 2-4 seconds following the mechanical polishing. Focused ion beam (FIB) sectioning was performed using a dual beam SEM/FIB FEI Quanta 3D FEG equipped with an injector needle capable of depositing Pt to protect the TEM foil from possible beam induced damage. Thin specimens with thicknesses of approximate 100 nm were prepared using the FIB. Observations were conducted on a JEM-2100 LaB_6 transmission electron microscope with an accelerating voltage of 200 kV. SEM was conducted on a JEOL JSM 7001 instruments at 20kV. XRD spectra were obtained using a D8 advance X-ray diffractometer equipped with a graphite mono-chromator, a Ni-filtered Cu Kα (λ=1.5406nm) source and a scintillation counter, operated at 40 KV and 30 mA with a scanning speed of 0.02 ° s^{-1}. EBSD scans were performed using a field-emission gun scanning electron microscope (JEOL JSM 7001) operated at 25kV with step sizes ranging from 0.2 μm to 0.3 μm.

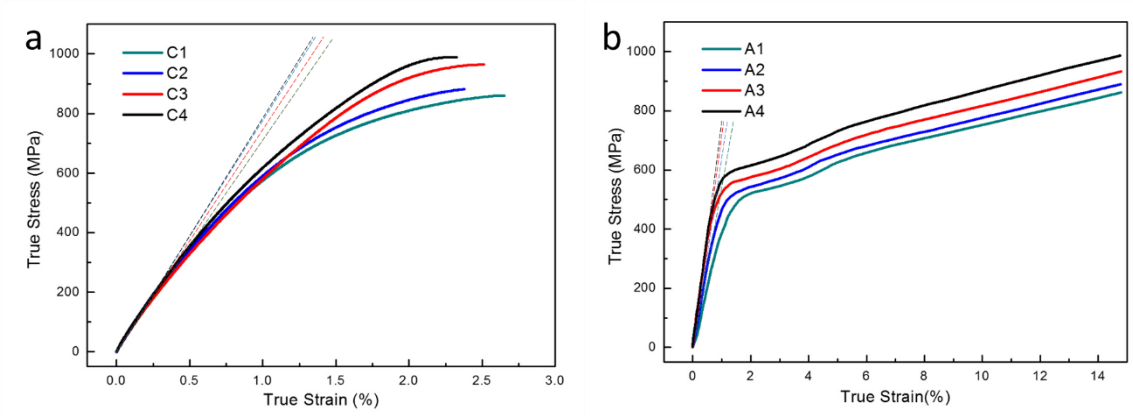

Fig. 2. True stress – true strain curves of Ti-25-3Mo-3Zr-2Sn fine tubes in uniaxial tensile tests. (a) Cold rolled tubes (b) Annealed tubes. (Dashed lines illustrate corresponding moduli.) (For interpretation of the references to colour in this figure, the reader is referred to the web version of this article.)

Table 2. Comparison between after fracture strain and nominal fracture strains

	C1	C2	C3	C4	A1	A2	A3	A4
Nominal fracture strain	0.014	0.014	0.011	0.009	0.225	0.218	0.241	0.204
After fracture strain	0.010	0.009	0.009	0.006	0.099	0.097	0.119	0.092
Recoverable strain	0.004	0.005	0.002	0.003	0.126	0.121	0.122	0.112

3. Results and discussion

True stress – true strain curves for the Ti-25Nb-3Mo-3Zr-2Sn fine tubes in the cold rolled and annealed conditions are shown in Fig. 2. The yield stress remained constant at approximately 540MPa for the cold rolled tubes, while it increased from 401 MPa to 518 MPa with reductions in the tube diameter in the annealed condition. Elongations of the fine tubes after annealing are above 20%, which is significantly greater than the cold rolled tubes which exhibited elongations of < 3%. Similar to the yield strength, the modulus of the cold rolled tubes remained approximately constant. In comparison, annealed tubes exhibited increased moduli with reductions in the tube diameter. The strain hardening exhibits characteristics of double yielding for the tubes in the annealed condition. Pseudo-elasticity may exist in some meta-stable β titanium alloys due to reversible martensitic phase transformations as has been observed for Ti-25Nb-3Mo-3Zr-2Sn alloy in a previous report [12]. The nominal fracture strains obtained from the tensile tests were compared with the after fracture strain to measure the degree of recoverable strain associated with the reversible martensitic transformation. The results of this analysis are shown in Table 2. The results demonstrate that a proportion of the

martensitic α″ phase formed during the tensile tests is reversible. For the cold rolled samples, the average recoverable strain was in the order of 0.002 to 0.005, while for the annealed samples it was approximate 0.12.

3.1 Elastic modulus and texture evolution in the fabrication of fine tubes

Materials for stent applications are typically required to undergo significant elastic deformation, so the modulus is an important mechanical property. It is defined as the slope of the linear elastic range before yielding. However, since the cold rolled tubes exhibit non-linear elastic behaviour, this definition is not suitable. In this circumstance, an incipient modulus can be adopted to characterise the elastic behaviour as represented by the dashed lines in Fig. 2 obtained from the slope of the tangent in the initial stages of loading. The incipient modulus was determined on the basis that for very low strains the deformation is primarily linear elastic strain. This approach was also adopted for previous studies on the deformation behaviours of low modulus β titanium alloys [32, 107, 327]. In the present paper, for the cold rolled tubes the incipient modulus was obtained from the slope of the tangent for the initial 0 to 0.5% strain, where the stress-strain curves are approximately linear. Young's modulus was used for the annealed tubes, as the elastic regions of the curves were linear. The lowest values of modulus for Ti-Nb based alloys are reported for compositions ranging between 15 and 42 wt.% Nb [32, 328]. Ozaki et al. [328] found that the modulus of Ti-35Nb alloys was approximately 70 GPa after solution heat treatments, which is similar to that of the annealed tubes with OD of 3.5 mm in the present work. A modulus as low as 55 GPa was obtained for the annealed tubes in the present work. In comparison, the modulus of the cold-rolled tubes measured from the true stress – true strain curves ranged from 71 GPa to 78 GPa. Fig. 3 shows the variation of modulus with deformation for the cold rolled and annealed conditions. The annealed tubes exhibit gradual increases in modulus with reductions in their diameters increasing from 55 GPa to 74.1 GPa, while the modulus showed smaller changes for the cold rolled tubes. Annealing after the cold rolling led to smaller decreases in the modulus with increasing levels of reduction in the diameters of the fine tubes.

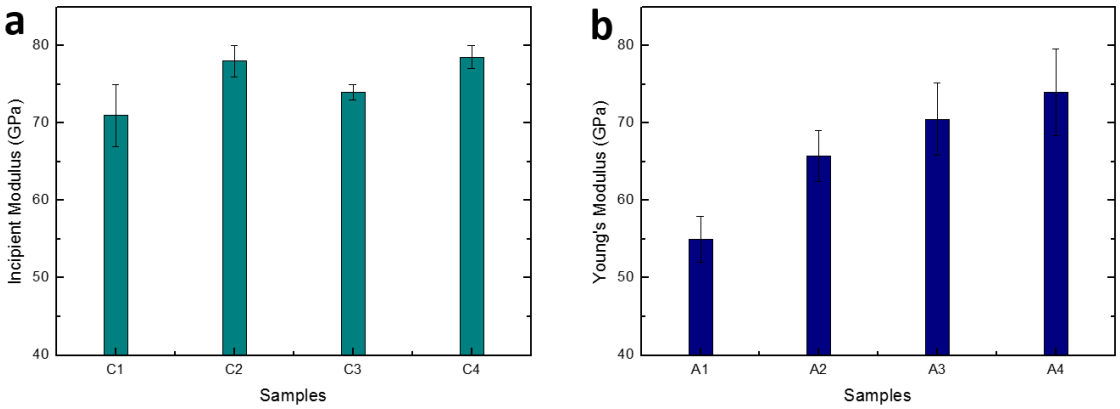

Fig. 3. Incipient moduli and Young's moduli variation with reducing diameter for the (a) cold rolled and (b) annealed conditions.

According to the authors' previous work on the Ti-25-3Mo-3Zr-2Sn alloy [37], martensite is readily generated within the β matrix during cold deformation. Fig. 4 shows normalised XRD profiles of the Ti-25Nb-3Mo-3Zr-2Sn fine tubes, which show characteristic diffraction peaks of the β and α″ phases. The cold rolled Ti-25Nb-3Mo-Zr-2Sn tubes experience a martensitic transformation from β to stress-induced martensitic α″ phase during processing. Fig. 4 (b) exhibits peaks of the β phase only, showing that annealing results in a reverse transformation from the α″ phase to the β phase. Images from the outer and inner regions of one of the fine tube (C3) are shown in Fig. 5 (a) and (b). According to theory, the microstructure of the tubes should vary over the cross section of the tubes due to the differing degrees of deformation. However, due to the thinness of the fine tubes walls and the effects of the internal mandrel used for the cold rolling, the deformation across the section of the tubes was approximately uniform. As a result, the grain sizes did not exhibit significant differences over the fine tube cross sections. In the following discussion, only microstructures obtained from the central regions of the tube cross-sections were used to understand the evolution of microstructure of the tubes in relation to their processing. Fig. 5 shows micrographs from the central regions of the Ti-25Nb-3Mo-3Zr-2Sn fine tubes composed of equiaxed grains with an average diameter of approximately 18.5 μm. The tubes in the cold rolled condition exhibit a high volume fraction of deformation induced products (Fig. 5 (c)), which were transformed to the β phase during annealing at temperatures above the β transus (Fig. 5 (d)).

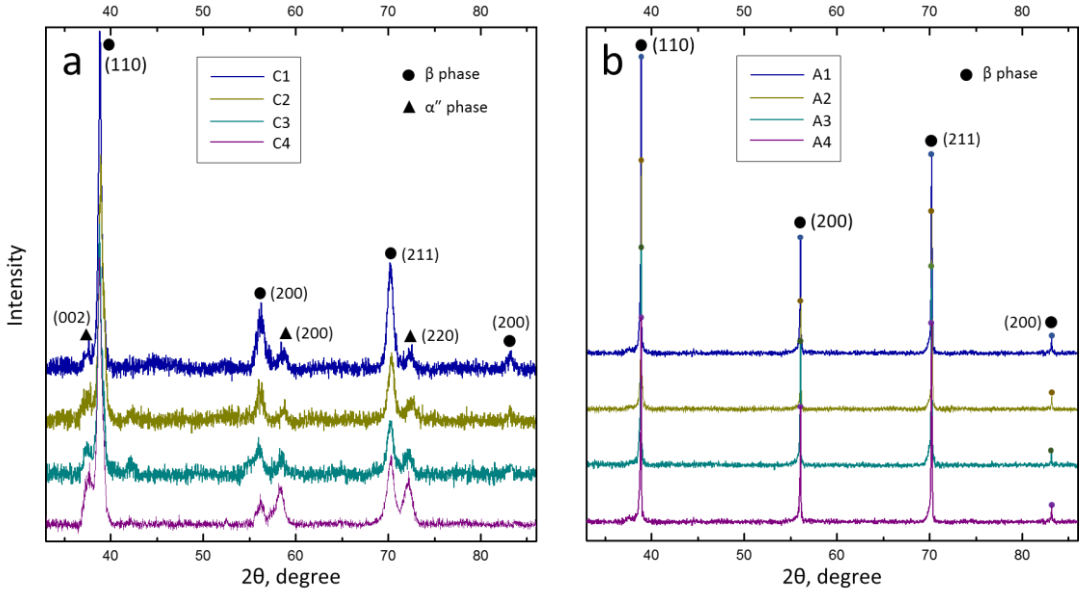

Fig. 4. Normalised XRD profiles of Ti-25Nb-3Mo-3Zr-2Sn tubes at various deformation reductions (a) cold rolled tubes (b) annealed tubes. (For interpretation of the references to colour in this figure, the reader is referred to the web version of this article.)

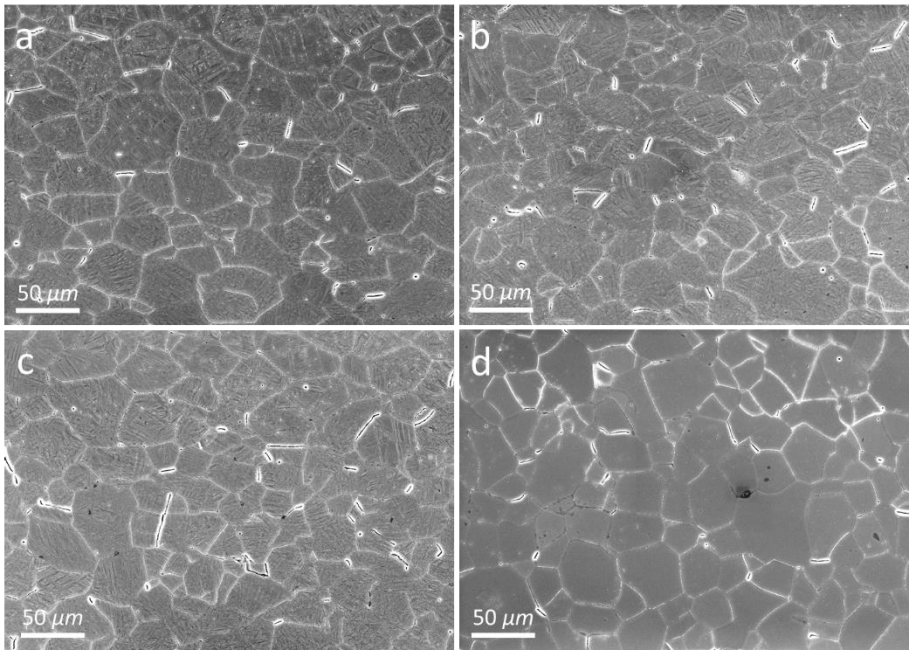

Fig. 5. Micrographs of Ti-25Nb-3Mo-3Zr-2Sn cold rolled tubes with an OD of 4 mm at (a) inner region (b) outer region (c) central region. (d) micrograph of the central region from an annealed tubes with an OD of 4 mm

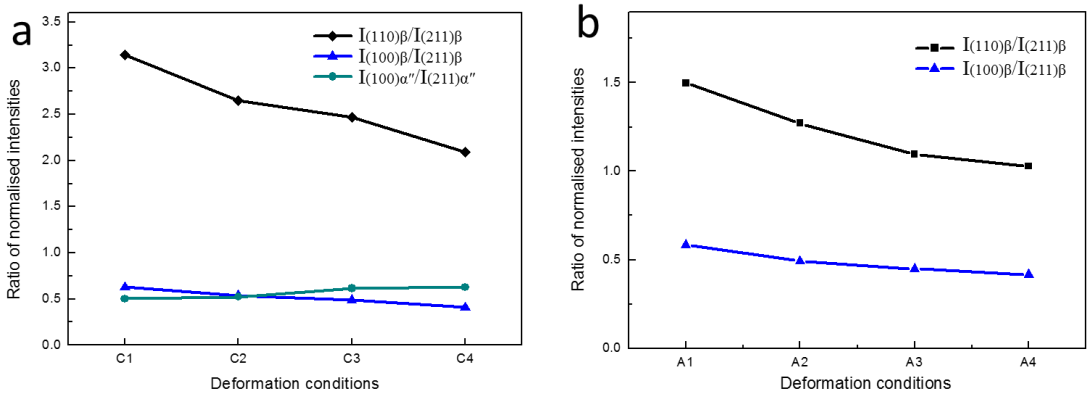

Fig. 6. Evolution of ratios of normalised XRD peak intensities for (a) cold rolled tubes and (b) annealed tubes.

Texture evolution and martensitic transformation, which have a critical influence on the modulus, occur with the reductions in the diameters of tubes. For β-Ti alloys, the modulus is anisotropic [329] and has a minimum value in a low index <100> direction, increasing as the direction is transferred to <110> and then to the <111> direction. The elastic deformation resistance is further increased when the strain path is along higher index directions [113, 196]. It is shown that the relative XRD peak intensities, $I_{(110)\beta}/I_{(211)\beta}$ and $I_{(100)\beta}/I_{(211)\beta}$, decrease simultaneously with reductions in the diameters of the annealed tubes as shown in Fig. 6 (b). Therefore, the increased resistance to elastic deformation along (211) β has a dominant effect on the modulus of the annealed tubes, as only β phase texture is developed. Matsumoto et al. [330] studied variation of modulus in the Ti-35Nb-4Sn (wt.%) alloy and suggested that varying modulus was also related to the martensitic texture developed due to the stress-induced martensitic phase transformation during plastic deformation. The modulus is decreased when the strain path is parallel to (220)α″, while an increase of the modulus may result from the development of texture other than (220)α″ [330]. The martensitic α″ identified in Fig. 4 (a) exhibits (100) and (110) textures in the cold rolled condition, as evidenced by the (200), (220) and (002) α″ phase peaks in XRD profiles taken from the plane parallel to the rolling direction of fine tubes. The result can be interpreted by the orientation relationship between the β and α″ phases. The orientation relationship proposed by previous reports [6, 9] are [100] α″//[100]β, [010] α″//[011] β and [011] α″//$[2\bar{1}1]$ β. In the present work, the (110) α″ texture was enhanced with decreasing OD of the fine tubes according to the increased ratio of the normalised intensities of the (220) α″ peak and the sum of (200) and (002) α″ ($I_{(220)\alpha''}/I_{(200)+(002)\alpha''}$) phase peaks as shown in Fig. 6 (a). Therefore, the evolution of α″ texture results in decreases in the modulus due to the relatively lower modulus of (110) α″ texture compared with (100) α″ texture. The effects of α″ may account for the smaller changes in the modulus for the cold rolled tubes in comparison with the annealed tubes which have a single β phase structure. The $I_{(110)\beta}/I_{(211)\beta}$ and $I_{(100)\beta}/I_{(211)\beta}$ intensities decreased simultaneously (Fig. 6), indicating

that the β phase with {110} and {100} planes parallel to the rolling direction were consumed by the β to α″ phase transformation with increasing deformation. The evolution of β textures in the annealed fine tubes is consistent with that of the cold rolled ones without regard to the influence of α″ texture.

Fig. 7 illustrates planes in the bcc β crystal and orthorhombic α″ crystal structures which were identified by XRD. When the planes favoured for elastic deformation are rotated to high index orientations, such as (211) β, the modulus is increased (as shown in Fig. 3) due to the higher elastic deformation resistance. However, the texture of the α″ phase has to be taken into account for the cold rolled fine tubes due to its relative high volume fraction. As shown in Fig. 7 (b) the α″ phase texture favoured (220) α″ with increasing deformation. The combined effects of α″ and β textures may account for the smaller changes in the modulus for the cold rolled tubes in comparison with the annealed ones, where only β phase texture was developed.

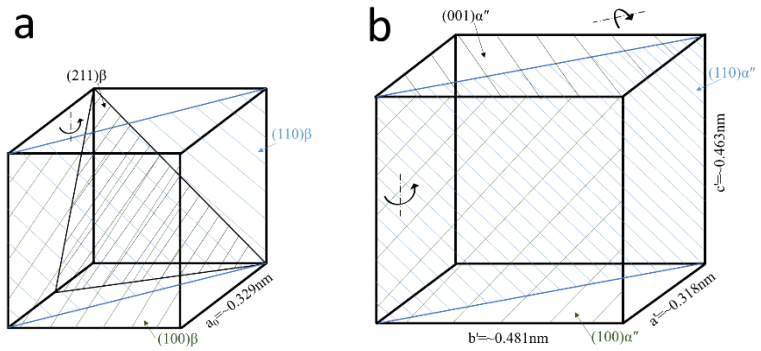

Fig. 7. Schematic diagrams of bcc β and orthorhombic α″ crystals and the planes identified by XRD (a) bcc β phase, a_0=0.329nm, in cold rolled Ti-25Nb-3Mo-3Zr-2Sn alloy (b) orthorhombic α″ phase, a'=0.318nm, b'=0.481nm, c'=0.463nm, based on Ti-24Nb (at.%).

The volume fraction of martensitic α″ phase exhibits an increase with the reductions in the diameters of cold rolled tubes according to the increased relative intensity $I_{\alpha''}/I_{\beta}$ as shown in Fig. 6 (a). In the authors' previous study [37], the increasing volume fraction of α″ phase resulted in a decrease in the modulus of the tubes. Yu et al. [20] also reported similar phenomena for solution treated and rolled Ti-25Nb-3Mo-3Zr-2Sn rods. In the view of the previous analysis on the textures, the changes of the modulus are proposed to result from both the changed volume fraction of martensitic α″ phase and the texture evolution. The effects of α″ textures and the increasing volume fraction of α″ phase account for the smaller changes in the modulus for the cold rolled tubes as compared to the annealed ones in which only β phase texture develops. However, the increased modulus with the reductions in the diameters of cold rolled tubes indicates (Fig. 3 (a)) that the β phase texture has a dominant influence on the modulus of the fine tubes due to its larger volume fraction.

3.2 Deformation mechanisms in the processing of Ti-25Nb-3Mo-3Zr-2Sn fine tubes

EBSD mapping was performed on the cold rolled and annealed tubes to investigate the active deformation mechanisms during processing. Fig. 8 shows inverse pole figures (IPF) for the β and α″ phases. When the fine tubes were cold rolled, the dislocation densities in the alloy increased dramatically. The lattice was distorted by the high density of dislocations. Therefore, index rates for EBSD maps from the cold rolled tubes were not as high as the annealed ones. Only portions of the twins and martensitic plates can be indexed in the microstructures of the cold rolled tubes. Other parts of the deformed area were left unidentified. Some of the unidentified areas were parallel to each other and most of them concentrated around twins or stress-induced martensitic boundaries. Transgranular deformation bands were evident in the deformed polycrystalline β matrix which are identified by white arrows. In the cold rolled condition, martensitic transformation and twinning are the dominant mechanisms. Both twins and stress-induced martensitic α″ phase were observed within the β matrix simultaneously. The twinning was identified as the {332}⟨113⟩ twinning system. The coincidence site lattice was determined to be Σ11 boundaries (a misorientation of 50.5 °around <110>) using the EBSD post-processing software, HKL Channel 5. Martensitic α″ phase could be formed as a primary product in the β matrix or within twinned β phase regions formed through a secondary mechanism, involving transformation of the β twins to the α″ phase. An interesting feature of the cold rolled microstructure is the presence of thick and distorted bands. The microstructure is complex in such severely deformed areas. The thick band indicated by red arrows is originally a primary twin and secondary α″ phase subsequently formed within the well-developed twin. Small segments of residual {332}⟨113⟩ mechanical twins (Fig. 8 (a)) and variants of needle-like stress-induced martensite (Fig. 8(b)) were observed in the band. The primary martensitic α″ phase is indicated by blue arrows in Fig. 8 (b). Thick twinning bands are partially or even fully occupied by secondary α″ phase laths. However, the volume fraction of twins is relatively high in the cold rolled Ti-25Nb-3Mo-3Zr-2Sn fine tubes in comparison with that of the martensite.

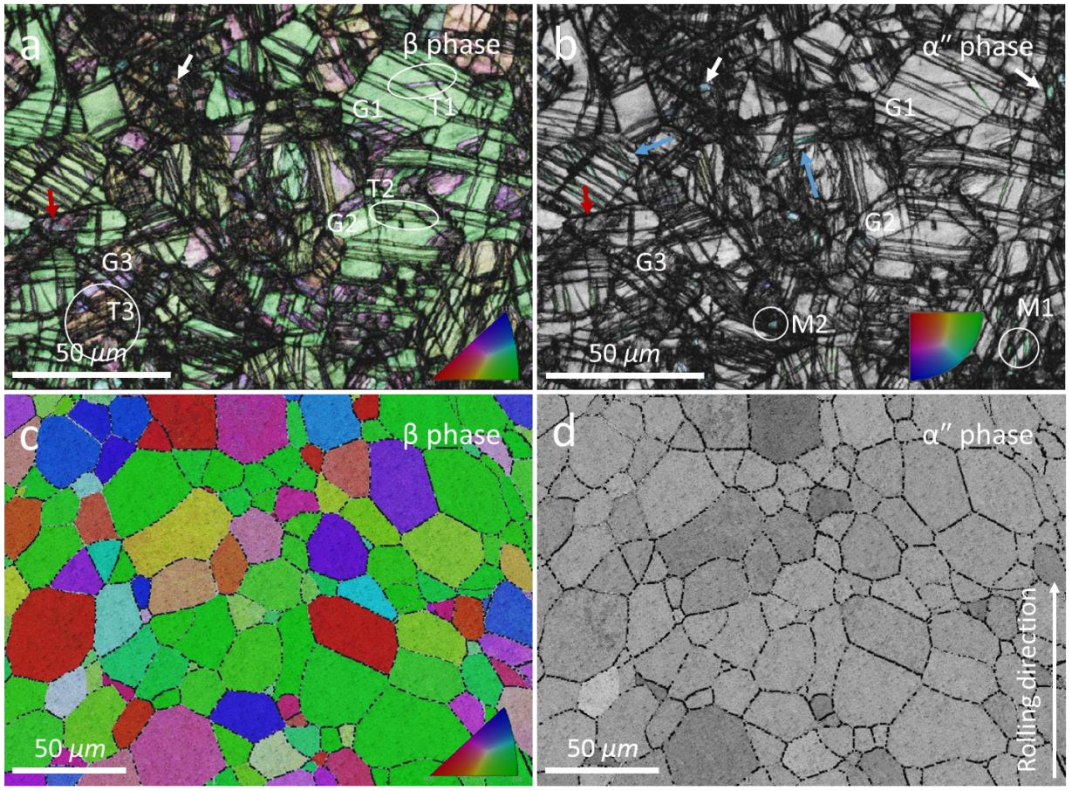

Fig. 8. EBSD inverse pole figure and band contrast maps of tubes with OD of 4mm, (a) and (b) are from cold rolled tubes, (c) and (d) are from annealed tubes. (a) Twins with different orientations within grains or cross grain boundaries (b) Parallel and thin α″ phase identified in β grains (c),(d) No twins nor α″ phase were detected in the annealed fine tubes. (For interpretation of the references to colour in this figure, the reader is referred to the web version of this article.)

Specific deformation mechanisms, involving stress-induced formation of the α″ phase or mechanical twinning with different crystallographic orientations, may be activated through the shear stress applied to the β matrix. As shown in Fig. 8 (a), twinned β zones were observed in almost all grains, while primary α″ phase was formed in a limited number of favoured grains. For example, a {332}⟨113⟩ twin T1 was observed in grain G1 without any secondary α″ phase in the interior. Primary martensitic α″ M1 and secondary martensitic α″ M2 had similar orientations, as shown in Fig. 8(b). For illustration, other grains are labelled as G2 and G3 with their twins, T2 and T3, respectively. Each grain was deformed by several twins of the same variant. T2 propagated through grain boundaries from G2 to a neighbouring grain while undergoing a small misorientation. It is very common to observe twins growing from a grain boundary, because the stress concentration at grain boundaries facilitates the growth of mechanical twins [218]. The width of T2 was measured to be approximately 0.8 μm, while some of other twins were well-developed, e.g. T3 occupies almost half of the initial grain. Several stress-induced martensite laths with parallel alignments can be formed in a single grain and propagate through the entire β grain.

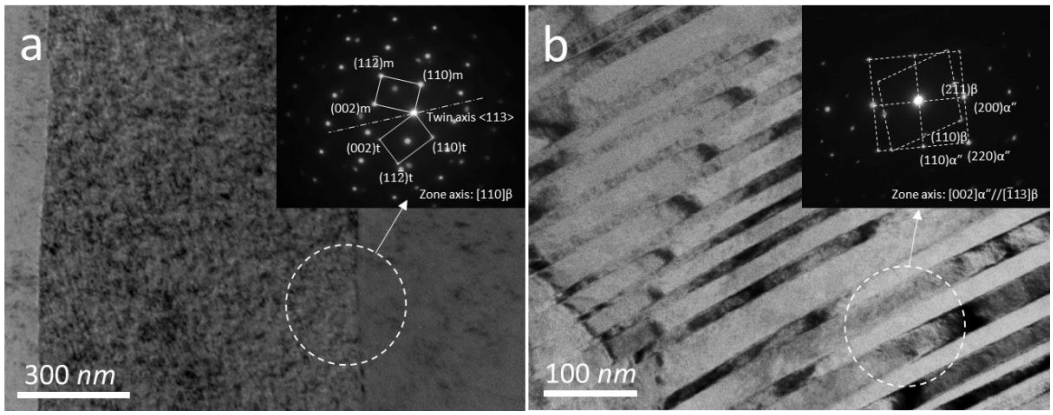

Fig. 9. TEM micrographs of deformation features in cold rolled Ti-25Nb-3Mo-3Zr-2Sn tubes with OD of 4 mm. (a) A {332}⟨113⟩ twin formed in the β matrix and the corresponding SAD pattern from the edge of the twin. (b) Parallel needle-like martensitic α″ phase and the corresponding SAD pattern showing the presence of the β and α″ phases.

TEM investigations were performed to identify micron-sized features within the cold rolled microstructures. Micrographs and corresponding selected area diffraction (SAD) patterns are shown in Fig. 9. Fig. 9 (a) shows a lath-like feature viewed along the [110] β zone axis, which is a {332}⟨113⟩ twin approximately 850 nm in width. No secondary martensite phase was observed within the interior or in neighbouring regions. The width is similar to that of T2 in the EBSD maps. Therefore, the relatively thin twins, e.g., T2 and the twin in Fig 9 (a), are considered to be nascent and under-developed. Parallel needle-like α″ phase was observed by TEM in Fig. 9 (b) with widths ranging from 11.5 nm to 32.5 nm. Previous reports observed {112}⟨111⟩ mechanical twins in an Ti-23Nb-0.7Ta-2Zr-1.2O (at.%) alloy [141, 331]. However, this twinning system is absent in the present alloy as the increased levels of Nb and other β stabilisers result in an increased stacking fault energy [170]. The {332}⟨113⟩ twinning system is preferred when the stability of the β phase is increased. Therefore, the {332}⟨113⟩ twinning system is dominant in the Ti-25Nb-3Mo-3Zr-2Sn alloy. No {112}⟨111⟩ twins were observed either by EBSD mapping or by TEM observation in the present work.

β-Ti alloys exhibit primary deformation mechanisms, such as stress-induced α″ phase and mechanical twinning, and secondary mechanisms within primary twins, such as the formation of secondary α″ phase laths. Sun et al. reported that an interconnected network of deformation mechanisms may create extra transgranular interfaces, significantly decreasing the mean free path for dislocation slip, described as a dynamic Hall-Petch effect [176]. Therefore, the collective effects of deformation mechanisms presumably contribute to the high work hardening rate and large plasticity of the Ti-

25Nb-3Mo-3Zr-2Sn alloy which exhibits both transformation induced plasticity (TRIP) and twinning induced plasticity (TWIP) simultaneously. In the present work, the activation of martensitic transformation and mechanical twinning are synergetic deformation mechanisms in the process of cold rolling, and both primary and secondary α″ phase were observed in confined regions. As a result, the deformation products, mechanical twins and primary α″ phase are almost saturated in the cold rolled fine tubes before tensile testing. The tensile stress-strain curves for the cold rolled fine tubes shown in Fig. 2 (a) exhibit non-linear elastic behaviour. It is reported that the combination of pre-existing martensite and deformation-induced transformation during tensile deformation contribute to this non-linear elastic behaviour [32]. In comparison, the annealed tubes had twin-free (Fig. 8 (c)) and martensite-free (Fig. 8 (d)) microstructures. Hence, during the tensile tests strain can be readily accommodated by TRIP and TWIP in regions with favourable grain orientations. Hanada et al. [107] reported that twinning and formation of martensitic α″ lead to low modulus and large elongations, while slip results in high yield strength and small elongations from their observations of a range of β-Ti alloys. This observation is supported by the decreased modulus and the much higher elongation observed for the annealed fine tubes (as shown in Fig 2). The mechanical response and active deformation mechanisms occurring at different levels of strain in the annealed tubes will be discussed in the following section.

3.3 Mechanical and Microstructural responses to strains in annealed Ti-25Nb-3Mo-3Zr-3Sn fine tubes

In comparison with the cold rolled tubes, the tensile curves for the annealed tubes exhibit normal linear elastic behaviour, double yielding and relatively high strain hardening rates in the absence of pre-existing martensitic α″ phase and twins. The strain hardening rate versus strain curve in Fig. 10 pertaining to the true stress – true strain curve for the annealed tubes reveals multiple modes of plasticity which are related to the different deformation mechanisms. Three distinct stages of strain hardening rate were detected and these are illustrated by dash-dotted lines.

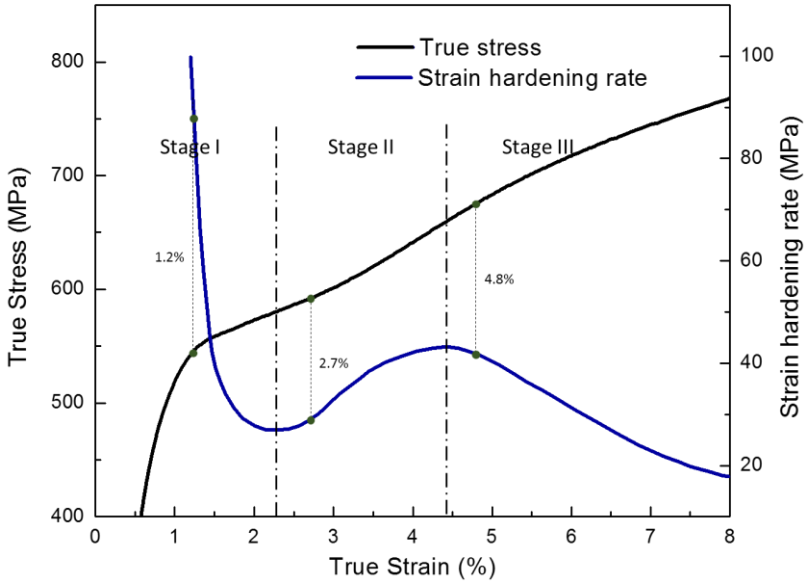

Fig. 10. True stress – true strain curve of annealed Ti-25Nb-3Mo-3Zr-2Sn fine tube with OD of 4 mm (black trace), and the corresponding strain-hardening rate to strain curve is plotted (blue trace). Three stages of strain hardening rate are illustrated by dash-dotted lines. Dotted lines at strains of 1.2%, 2.7% and 4.8% show the interruption points used in the interrupted tensile tests.

Stage I is normal elastic behaviour followed by a transition to plastic behaviour. A steep decrease occurred in the strain hardening rate when the strain was close to the first yield point. The strain hardening response increases during stage II and is associated with plastic deformation. After the increase, the strain-hardening rate decreases in Stage III. In order to understand deformation-induced transformation and twinning systems active at different stages of strain, the microstructural evolution was investigated by examining the deformed samples from the interrupted tensile tests at strains of 1.2%, 2.7% and 4.8%. Fig. 11 shows the micrographs with the vertical direction parallel to the radial direction of the tubes. The sample with 1.2% strain exhibited similar microstructures to that of the original annealed ones. However, a limited number of transgranular threads were observed. This suggests that a limited number of twins were activated by deformation prior to the formation of stress-induced α″ phase. The threads were observed in most grains and remained thin and parallel to each other with the increase in strain in stage II (Fig. 10 (b)). In this stage, the strain hardening rate increased and martensitic α″ phase was identified by XRD. The normalised diffraction intensities of the α″ phase continued to increase with increasing strain from stage II to stage III. The morphologies of the deformation-induced products exhibit increased widths and complex intersections as shown in the insert of Fig. 11 (c). Twin boundaries, grain boundaries and phase boundaries between β and α″ are difficult to distinguish.

EBSD mapping was performed in order to identify the deformation products. Fig. 12 (a) shows single β phase and the absence of mechanical twinning at a strain of 1.2%. At the onset of stage II with a strain of 2.7%, mechanical twins and stress induced α″ were observed in the EBSD maps. This finding is consistent with the observation in Fig. 11. The strain hardening rate is increased by the formation of mechanical twins and deformation-induced martensitic boundaries which provide barriers to slip [332]. Gray [333] analysed the relation between high strain hardening rates and mechanical twinning using a Hall-Petch type hardening mechanism, and suggested that the formation of mechanical twins increased the strain hardening rate. Salem et al. [334] established a correlation between the strain hardening rate and the Hall-Petch hardening mechanism. According to the previous reports, the increase in the twin volume fraction is associated with the increase of strain hardening rate in the early stages of deformation, whilst the strain hardening rate decreases after the twin volume fraction becomes saturated.

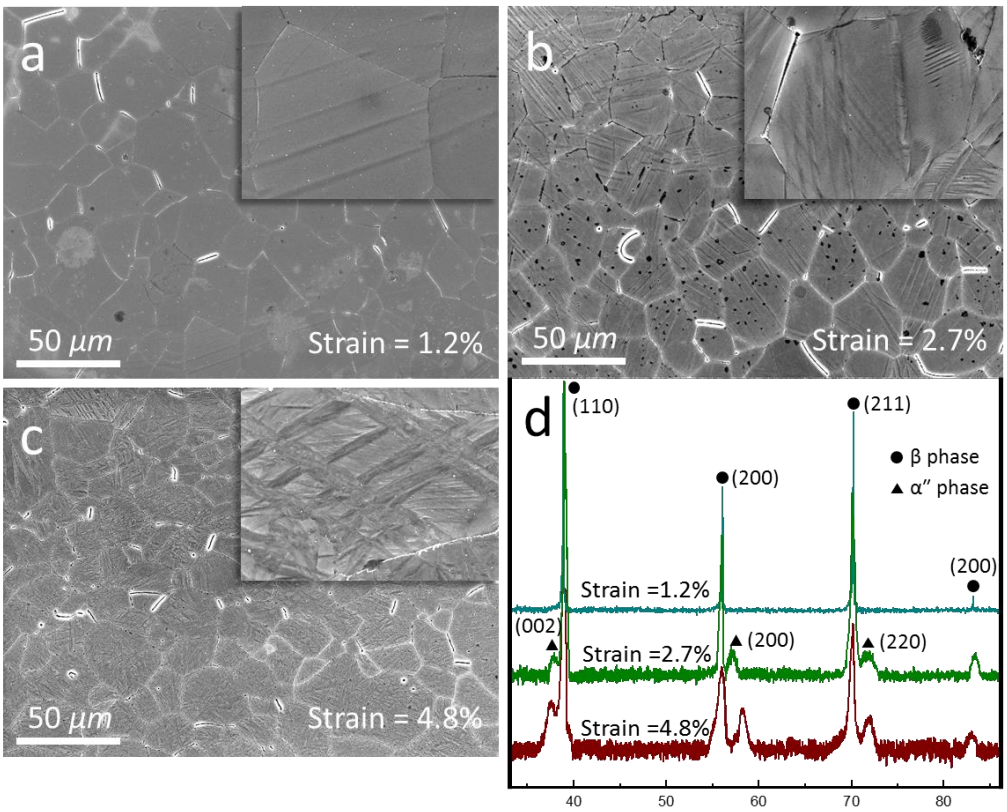

Fig. 11. Microstructural evolution in annealed fine tubes with OD of 4 mm and corresponding XRD spectra. (Inserts are enlarged features. Vertical direction is parallel to the radial direction of tubes.)

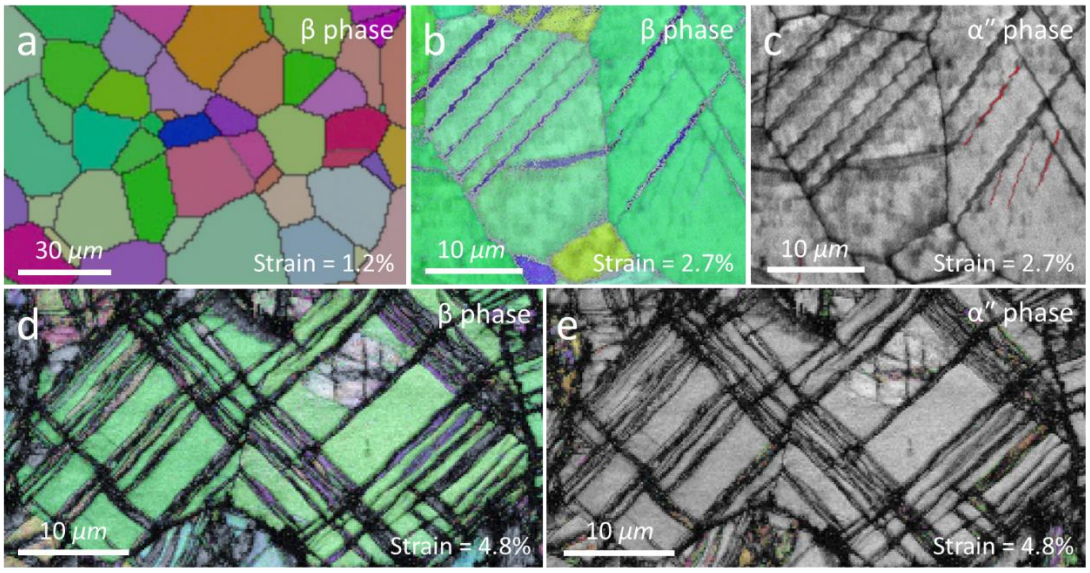

Fig. 12. Evolution of twinning and martensite identified by EBSD in annealed fine tubes with OD of 4 mm with the increase of strain during tensile deformation. (Vertical direction is parallel to the radial direction of tubes.) (For interpretation of the references to colour in this figure, the reader is referred to the web version of this article.)

Only the {332}⟨113⟩ twinning system was observed in EBSD maps, consistent with the observations of the cold roll tubes. Fig. 12 (b) and (d) indicate a significant increase in the volume fraction of twins from stage II to stage III, and the twin volume fraction approaches saturation in stage III. Well-developed thick twins were consumed by secondary α″ formation as shown in Fig. 12 (d) and (e). A similar situation was also observed by Song. et al. [335]. They investigated the volume fraction of twins in β-Ti alloys and reported that the volume fraction of twins hardly changes at high strain levels. The development of twins in β-Ti alloys involves nucleation of new twins and thickening of pre-existing twins. The twins tend to nucleate in grains with twinning planes close to the maximum local shear stress plane [336]. Therefore, it becomes difficult to nucleate twins when favourable grains with lower nucleation energy are depleted with increased levels of plastic deformation. Furthermore, the thickening of pre-existing twins is hindered due to the increasing boundary mismatch with increasing strains [337]. The falling strain hardening rate in Stage III is associated with the saturation of the twin volume fraction.

Stress induced α″ phase is preferentially activated in titanium alloys with low levels of β stabilising elements [6]. Martensitic α″ phase can be observed both in the β matrix and within well-developed twins with increases in the strain in the tensile tests. It is noted that some of secondary α″ laths were thicker than primary ones at the same strain as shown in Fig. 12 due to the lower resistance to broadening of the twins in favoured twinned β zones [320]. As a result of the formation of primary and secondary α″ phase, the volume fraction of α″ phase increases with strain. The volume fraction

of twins was much larger than that of the needle-like primary α″ phase. Twinning is the dominant deformation mechanism during deformation of the Ti-25Nb-3Mo-3Zr-2Sn fine tubes.

4. Conclusions

The modulus of Ti-25Nb-3Mo-3Zr-2Sn fine tubes was increased with reductions in their diameter for the cold rolled and annealed conditions. Annealed tubes exhibit greater strain hardening behaviour and superior ductility in comparison to cold rolled tubes. Stress induced martensitic transformation and mechanical twinning were activated during deformation of the Ti-25Nb-3Mo-3Zr-2Sn fine tubes. The deformation-induced products were identified as {332}⟨113⟩ mechanical twins, as well as primary and secondary stress-induced α″ phase. The synergetic deformation mechanisms contribute to the superior strain hardening rate and large ductility for the metastable β-Ti fine tubes in the annealed state.

1. β grains experience rotations from (100) and (110) to (211) on the observation plane parallel to the rolling direction with reductions in the outside diameter. The β texture evolution resulted in an increased modulus with reductions in the tube diameters. The evolution of α″ phase texture was related to the transformation from the β to α″ phase and their resultant orientation relationship. The development of the α″ phase texture and its increased volume fraction have an opposing effect to that of β phase texture, which limits increases in the modulus with reductions in the diameters of the tubes.
2. Transformation induced plasticity and twinning induced plasticity are active during processing of the Ti-25Nb-3Mo-3Zr-2Sn fine tubes and contribute to their mechanical behaviours.
3. For annealed tubes, yielding occurs when the stress reaches the threshold to activate both twinning and stress-induced martensitic transformation. High strain hardening rates are associated with increasing volume fractions of mechanical twins and the martensitic α″ phase. The synergetic effects of these deformation mechanisms impart excellent tensile ductility in conjunction with high levels of strain-hardening to the annealed Ti-25Nb-3Mo-3Zr-2Sn fine tubes.

PAPER 4

Identification and analysis of twinning activity in the cold rolling of Mg-Al-Zn alloy mini tube

Yaowu Zhang, Damon Kent, Gui Wang and Matthew Dargusch

Materials and Design

Abstract

During rolling, mini-tubes experience differing stress states to that of uniaxial deformation and sheet rolling. The twinning activity of cold rolled AZ31 magnesium alloy tubes with a processing strain of 15% has been investigated. Analysis of twinning modes was performed on the basis of orientation data from 417 grains analysed by electron backscatter diffraction. Extension $\{10\bar{1}2\}$ twins, contraction $\{10\bar{1}1\}$ twins and double twins were observed. Approximately 60% of the grains examined contained $\{10\bar{1}2\}$ twins, even though many of them had orientations which were predicted to be unfavourable for the activation of $\{10\bar{1}2\}$ twins. A modified Schmid factor was introduced to predict the twinning behaviour due to the specific stress state of the tube rolling. The twinning mode was analysed using both the modified Schmid factor and a strain compatibility factor for non-Schmid twins. It was found that ~72% of the grains have a modified Schmid factor larger than 0.3 and 41% have factors larger than 0.4 for $\{10\bar{1}2\}$ twins, whilst $\{10\bar{1}1\}$ twins have Schmid factor values larger than 0.4 in 62% of grains. The complex twinning activity in the cold rolled tube results from the large proportion of grains with their c-axes aligned 30 °-60 °to the radial direction. Strain transferred among twins contributes to non-Schmid behaviours in the cold rolled tubes. As a result, non-Schmid twins were frequently observed with most of them exhibiting favourable strain accommodation with respect to their strain compatibility factor.

1. Introduction

Mg alloys have attracted increasing attention due to their promise in applications for biodegradable stents formed from mini-tubes [1, 24]. The number of independent slip systems is limited in Mg alloys due to their hexagonal close packed structure especially at low temperatures. Due to the limited number of the slip systems and in order to meet the von Mises criterion, Mg alloys exhibit a strong propensity for mechanical twinning [266, 338, 339]. The activation of twinning during deformation has a large effect on texture evolution and flow stress due to lattice reorientation, e.g., the lattice will rotate by 86.3 ° through $\{10\bar{1}2\}$ twinning [65]. It has been observed that ~7% strain in twinning dominated deformation results in complete texture reorientation [66]. In addition to the effect on the orientation, mechanical properties and the microstructural evolution of deformed Mg alloys are also closely related to the twinning activity. The effect of twins on the mechanical properties of Mg alloys has been extensively studied, e.g. Barnet studied twinning and ductility in Mg alloys and concluded that the ductility of Mg alloys is associated with the activation of different twinning modes [74, 75].

When Mg alloys are deformed in a favourable direction for $\{10\bar{1}2\}$ twinning, the yield strength will be reduced in comparison to with that in more unfavourable directions [76]. In addition, because twins tend to propagate through parent grains, the boundaries between twins and parent grains act as sub-boundaries that induce Hall-Petch strengthening during deformation [77]. Therefore, in order to understand and effectively utilise the evolution of microstructure and texture induced by twinning in cold rolled AZ31 tubes, it is essential to obtain a comprehensive understanding of twinning modes and their impacts on processing and properties.

Twinning modes which include $\{10\bar{1}2\}\langle\bar{1}011\rangle$ extension twins, $\{10\bar{1}1\}\langle10\bar{1}\bar{2}\rangle$ contraction twins, $\{10\bar{1}1\}-\{10\bar{1}2\}$ and $\{10\bar{1}2\}-\{10\bar{1}1\}$ double twins have been observed in previous studies of deformed Mg alloys [62, 340]. $\{10\bar{1}2\}$ twinning is one of the most commonly activated deformation mechanisms in Mg alloy on account of the low critical resolved shear stresses (CRSS) for this twinning mode. The characteristics of these twins and their relationship with the deformation conditions have been extensively studied. The authors studied the relationships between the mechanical properties and the twinning modes, and found that extension twins and contraction twins were activated with the change processing parameters and had different effects on the mechanical properties. Ma *et al.* reported a two-shear mode mechanism for twinning in a strongly textured Mg alloy for the nucleation of $\{10\bar{1}1\}-\{10\bar{1}2\}$ double twins [60]. The initial texture of Mg alloys plays an important role in the formation of different twinning modes and the activation of $\{10\bar{1}2\}$ extension twinning is largely dependent on the strain directions [61]. Xin et al. studied the formation mechanism of multiple twinning modes and $\{10\bar{1}2\}-\{10\bar{1}1\}$ secondary twins in the rolling of AZ31 Mg alloys [62, 63]. They concluded that multiple twinning modes could be activated in grains with the same orientations and that the activation of these complex twins were in accordance with the prediction of an effective Schmid factor.

The CRSS for a given twinning mode is equal to the applied external stress multiplied by the Schmid factor. Therefore, twin variant selection in Mg alloys is frequently evaluated using the Schmid factor (SF). The SF distribution is dependent on the orientation of the parent grain/primary twins and the loading direction. It is widely accepted that $\{10\bar{1}2\}$ extension twins are favoured when there is a resolved extension strain parallel to the c-axis, while $\{10\bar{1}1\}$ contraction twinning is activated when there is a resolved contraction strain parallel to the c-axis. The grains in cold rolled tubes are deformed under a specific stress state in three directions, i.e. extension along elongation direction (ED) and contraction along the radial (RD) and tangential directions (TD). Most cold rolled tubes have grains with different orientations rather than a strongly textured microstructure. [341]. Therefore, a criterion

for the occurrence of different twinning modes must be established in order to obtain an understanding of twinning activity during cold rolling of AZ31 mini-tubes. In the present paper, a modified SF has been introduced and has been used to predict twinning activity during cold rolling of AZ31 Mg alloy mini-tubes.

Multiple and secondary twins were observed in Mg alloys deformed under plane strain conditions [342], which suggests that twinning activity may be more complex in the cold rolled tubes due to triaxial stresses.. Multiple twinning mechanisms significantly affect the evolution of microstructure and lead to subdivision of grains due to their growth and intersection. A number of studies have reported that most of the multiple and secondary twins are associated with non-Schmid behaviour [343, 344]. The occurrence of the twins is considered as a requirement for local strain accommodation between parent grains and twins or between primary twins and secondary twins. Jonas et al. [64] reported that almost half of $\{10\bar{1}1\}$ twins formed in tensile deformation of extruded Mg alloys were identified as non-Schmid twins due to their very low SF values and many potential twins with high SFs were not observed. Non-Schmid twins were also observed in the form of secondary twins, because less prismatic glide occurred at the grain boundaries than the amount required to form twins with high SF values [64]. Beyerlein et al. [249] found that most non-Schmid secondary twins are associated with stress concentrations at grain boundaries. The non-Schmid twins activated by strain accommodation were frequently identified as paired twins [345]. At least one of the paired twins had a high SF in the parent grain, so the occurrence of the non-Schmid twin with low SF was considered to accommodate the strain transferred from the former.

Most of the previous studies focused on the formation of twins in uniaxial deformation and only a few investigated twinning activity in the plane strain state, which is still not applicable to the characteristics of twins formed in cold rolled Mg tubes. The nucleation and growth mechanism of primary and secondary twins, the formation and interaction of multiple twins and the local strain accommodation at interfaces between the parent grain and twins remain unclear in the processing of cold rolled tubes. In addition, the cold rolled tubes have no strong texture, which is unlike most previous studies. It is of interest to understand the deformation mechanisms favourable for twinning under these conditions. This study aims to establish a comprehensive understanding for the evaluation of twinning activity in the cold rolling of AZ31 mini-tubes with consideration of the effects of both the SF and strain accommodation. In the present paper, the analysis of primary $\{10\bar{1}2\}$ extension twinning, primary and secondary $\{10\bar{1}1\}$ contraction twinning and $\{10\bar{1}2\} - \{10\bar{1}1\}$ double twins

were performed based on a grain-by-grain investigation in a large number of grains using electron backscatter diffraction (EBSD) analyses from cold rolled AZ31 tubes.

2. Experimental methods

The alloy used in the present paper was the commercial AZ31 (Mg-3% Al-1% Zn) alloy. The chemical composition is presented in Table 1. The material was received in the form of extruded tubes with an outside diameter of 7.7 mm and a wall thickness of 0.87 mm. An annealing process was performed at 420°C for 3 h in an air furnace to remove deformation structures and then air cooled as a homogenisation treatment. The annealed AZ31 tube was then rolled by a mill with three rollers (LD-8) at room temperature to an outside diameter of 7.2 mm and a wall thickness of 0.79 mm. According to the formula $\varepsilon = \frac{A_0 - A_1}{A_0} = \frac{t_0 \times (D_0 - t_0) - t_1 \times (D_1 - t_1)}{t_0 \times (D_0 - t_0)}$, (where, A_0 and A_1 are the initial and final cross-section area, t_0 and t_1 are the initial and final wall thickness, D_0 and D_1 are the initial and final outside diameter) [267], the strain for the cold rolled tube in the present study is 15%.

Table.1 Chemical composition of the AZ31 tubes (*wt. %*).

Mg	**Al**	**Zn**	**Mn**	**Cu**	**Fe**	**Ni**
Balance	2.70	0.71	0.20	0.008	0.007	0.001

EBSD mapping was carried out to obtain the microstructure and orientation data of the annealed and cold rolled tubes. The surfaces examined by EBSD were perpendicular to the radial direction and polished using 6 μm, 3 μm, 1 μm diamond paste and 0.02 m colloidal silica. Chemical polishing was performed to get rid of the thin layer affected by the prior mechanical polishing, thereby improving the quality of the EBSD patterns. The reagent is a solution of 5 ml nitric acid, 5 ml hydrofluoric acid and 90 ml distilled water. The EBSD investigations were carried out using a FEI field-emission gun scanning electron microscope at an accelerating voltage of 25 kV in order to meet the requirement for identifying secondary twins at a superior spatial resolution. The inverse pole figures were obtained from post treatments using the HKL® Channel 5 system. The microstructure did not exhibit significant differences over the tube cross sections probably due to the thinness of the tubes walls and the effects of the internal mandrel used for the cold rolling. Therefore, microstructures obtained from the central area of the tube cross-sections were used to investigate the twinning activity. Twinning activity from a total of 417 grains were identified in the present paper. Hereinafter, RD, ED and TD refer to the radial direction, elongation direction and tangential direction of the tube, respectively.

3. Results and discussion

3.1 Characteristics of twins in the cold rolled AZ31 tube

To identify the twinning modes and understand their orientation dependence, the twinning activity was investigated using inverse pole figures compiled from EBSD analyses. EBSD orientation maps present the angles between the c-axis of the twins/parent grains and the RD. The microstructure and texture of the annealed AZ31 tube, shown in Fig. 1a, reveal that the annealed tube is completely recrystallised. The grains in green or yellow illustrate orientations with the c-axes approximately aligned above 45 ° to the RD. The annealed tube has almost a half of the grains with their c-axes within 30 ° of the RD. Fig. 1 b shows the EBSD microstructure of different twin modes observed in the cold rolled tube with a processing strain of ε = 0.15. After cold rolling, most of these grains have a proportion of their area occupied by $\{10\bar{1}2\}$ and $\{10\bar{1}1\}$ twins and some of them have been re-oriented wholly by $\{10\bar{1}2\}$ twinning. Grain boundaries (GBs) are indicated by black lines, and $\{10\bar{1}2\}$ twin boundaries, $\{10\bar{1}1\}$ twin boundaries and $\{10\bar{1}2\}$–$\{10\bar{1}1\}$ double twin boundaries are indicated by blue, red and yellow lines, respectively. Generally $\{10\bar{1}2\}$ twin bands are broad-banded and lenticular-like, whilst $\{10\bar{1}1\}$ twin bands are narrow-banded and relatively straight. They have misorientation angles of 86 ° ± 3 °$\langle 1\bar{2}10\rangle$ and 56 ° ± 3 °$\langle 1\bar{2}10\rangle$, respectively. More than one twinning mode may be active in one grain, e.g., $\{10\bar{1}2\}$ twins and $\{10\bar{1}1\}$ twins were observed in grain G1 in Fig. 1b. However, for approximately 25% of the grains with their c-axes aligned within 30 ° of the RD (shown in green or blue), only $\{10\bar{1}2\}$ extension twins were observed.

The CRSS of $\{10\bar{1}1\}$ contraction twins is known to be around 76–153MPa, which is much higher than that of $\{10\bar{1}2\}$ extension twins (2–2.8 MPa) [346]. However, $\{10\bar{1}1\}$ contraction twins are favourable when a compression stress occurs parallel to the c-axis. According to the equation for the elastic strain energy $E = (c/r) \times \mu \times s^2$ (1), where c and r represent the thickness and length of the twin respectively; μ is the shear modulus; s is the twinning shear [346], a lower c/r value will result in a reduced elastic strain energy for $\{10\bar{1}1\}$ contraction twins. Therefore, $\{10\bar{1}1\}$ contraction twinning with small c has a propensity to occur in relatively large grains, where greater values of r can be reached than is the case for small grains. Contraction and double twins were only observed in relatively large grains due to the elastic strain energy. The mechanism of double twinning involves formation of $\{10\bar{1}2\}$ extension twins initially as the primary twins, then secondary $\{10\bar{1}1\}$

contraction twins nucleate and propagate within the primary twins [62, 347]. There is a relative large grain G2 in Fig. 1b with $\{10\bar{1}2\}$–$\{10\bar{1}1\}$ double twins, well-developed primary $\{10\bar{1}2\}$ extension twins (indicated by E1 and E2) with secondary contraction twins inside (indicated by C1' and C2'), which is consistent with the above mechanism of double twinning. The misorientation relationships between twin E1 and the parent grain, twin E1 and C1', and twin C1' and the parent grain are demonstrated in Fig. 2a, b and c, respectively. The twinning plane and twinning direction of the $\{10\bar{1}2\}$ extension twin E1 are identified as $\{10\bar{1}2\}$ and $\langle 10\bar{1}1\rangle$, indicated by black and dark green arrows in Fig. 2a. Similarly, the $\{10\bar{1}1\}$ plane and the $\langle 10\bar{1}2\rangle$ direction of the secondary contraction twin C1' are indicated in Fig. 2b. According to previous studies, the double twins have different misorientation angles to the parent grain orientations [340]. The E1-C1' double twin was identified as having a misorientation angle of 37.5 °$\langle 1\bar{2}10\rangle$, while the E2-C2' double twin has a misorientation angle of 66.5 °$\langle \bar{7}43\bar{2}\rangle$. In order to further clarify the different types of $\{10\bar{1}2\} - \{10\bar{1}1\}$ double twins. The distribution of misorientation angles associated with all the observed double twins is shown in Fig. 3. Most of the double twins in the cold rolled tubes have a misorientation of 37.5 °$\langle 1\bar{2}10\rangle$, while the second most frequently observed double twins have a misorientation of 30.1 °$\langle 1\bar{2}10\rangle$. Another misorientation angle of 66.5 °$\langle \bar{7}43\bar{2}\rangle$ was also observed, but with the least frequency.

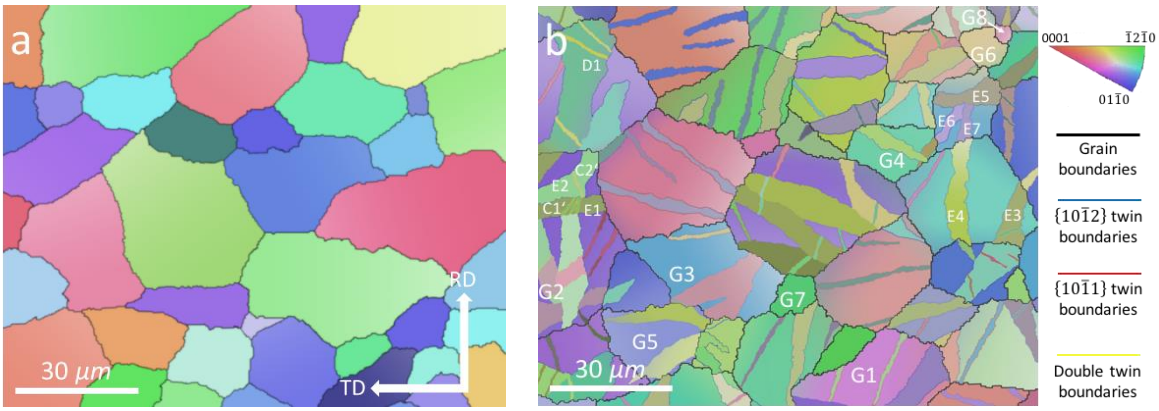

Fig. 1 Orientation maps of (a) the annealed AZ31 tube and (b) the cold rolled AZ31 tube with an ε = 0.15

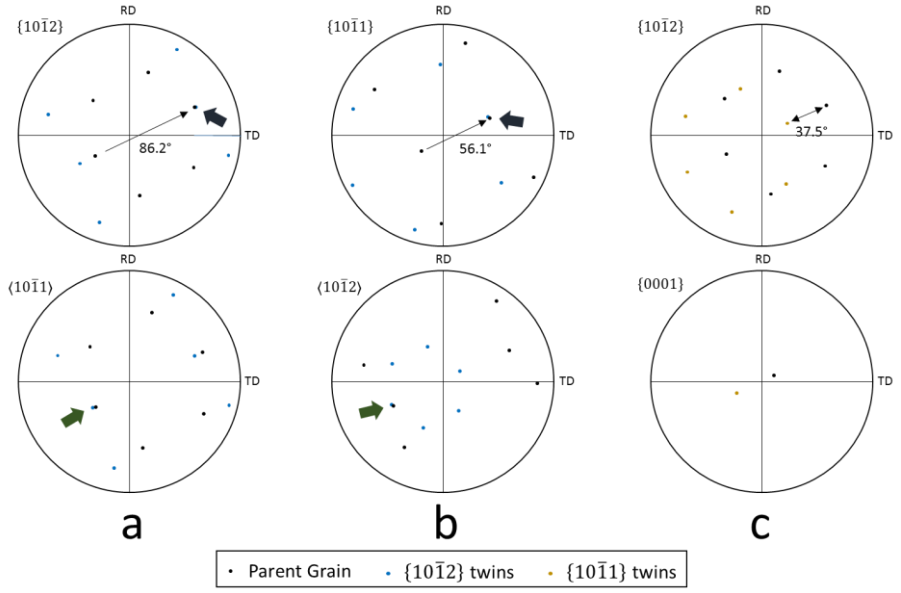

Fig. 2 The misorientation relationships between (a) the {10$\bar{1}$2}extension twin E1 and the parent grain, (b) E1 and the {10$\bar{1}$1}contraction twin C1′, (c) C1′ to the parent grain.

Although {10$\bar{1}$2} extension twins with large *c* value in equation (1) increase the elastic strain energy, their low CRSS and potentially large *r* value favour their activation in large grains in some cases. Therefore, {10$\bar{1}$2} extension twins were widely observed in relatively large grains as shown in Fig. 1 (b). The twin E3 has a misorientation of 86.24 °⟨11$\bar{2}$0⟩, which is a typical misorientation between the {10$\bar{1}$2} extension twin and the parent grain. The twin indicated by E4 is also identified as a {10$\bar{1}$2} extension twin associated with another variant. Compared with twins in relatively large grains, {10$\bar{1}$2} extension twins were observed in small grains exclusively, as shown in Fig. 1 (b). The corresponding twins are indicated by E5 to E7. Twinning orientation relationships between twins E5, E6 and the parent grain are demonstrated in Fig. 4, because E7 has the same orientation as E6. From the {0001} pole figure, the c-axis of the parent grain deviates from the RD by 73.5 °. The poles indicated by the black and blue arrows present the {10$\bar{1}$2} plane and ⟨1$\bar{2}$10⟩ axis of the extension twins E5 and E6 in relation to the parent grain, respectively. There is an extension strain component parallel to the c-axis during cold rolling, which favours the formation of {10$\bar{1}$2} extension twins.

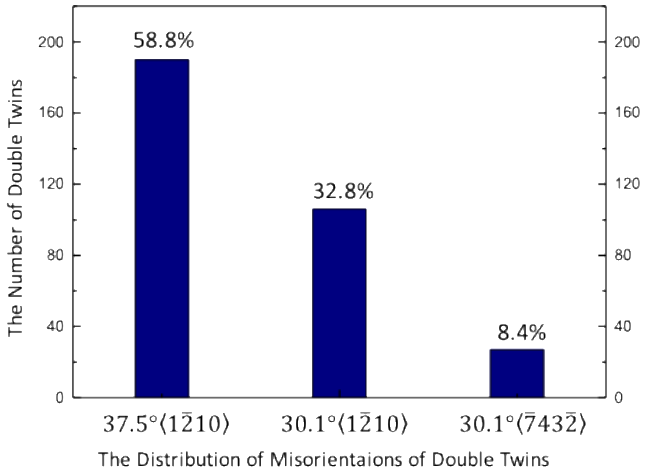

Fig. 3. The distribution of misorientation angles in the observed double twins

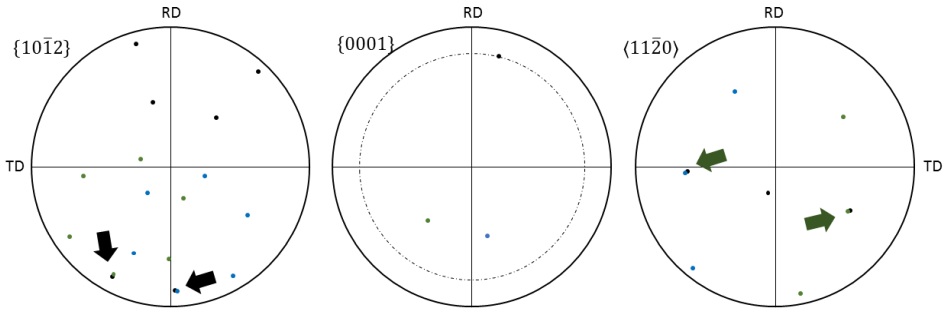

Fig. 4. Orientation relationships between $\{10\bar{1}2\}$ twins E5, E6 and the parent grain. The twinning planes and axes of E5 and E6 are indicated by black and green arrows

3.2 Modified Schmid factor

Twinning activity is commonly evaluated by a global SF defined as $m = \mathbf{COS}\,\varphi \times \mathbf{COS}\,\lambda$, where φ is the angle between the twinning plane normal and the external applied stress direction and λ is the angle between the twinning shear direction. A larger SF value for a given twinning mode indicates higher strain compatibility between the parent grains and the twins. This formula is mainly applicable for uniaxial deformations [178]. An effective SF for sheet rolling was defined as $m = 0.5 \times (\mathbf{COS}\,\varphi\, RD \times \mathbf{COS}\,\lambda\, RD - \mathbf{COS}\,\varphi\, ND \times \mathbf{COS}\,\lambda\, ND)$ by Tucker [348] and Dillamore [349] in investigations of fcc and bcc metals. The RD and ND in this formula refer to the rolling and normal directions in sheet deformation, which are different to those defined in the present paper. The effective

SF was used to investigate twinning activities in sheet rolling of Mg alloys, where the plane strain state was applied [340].

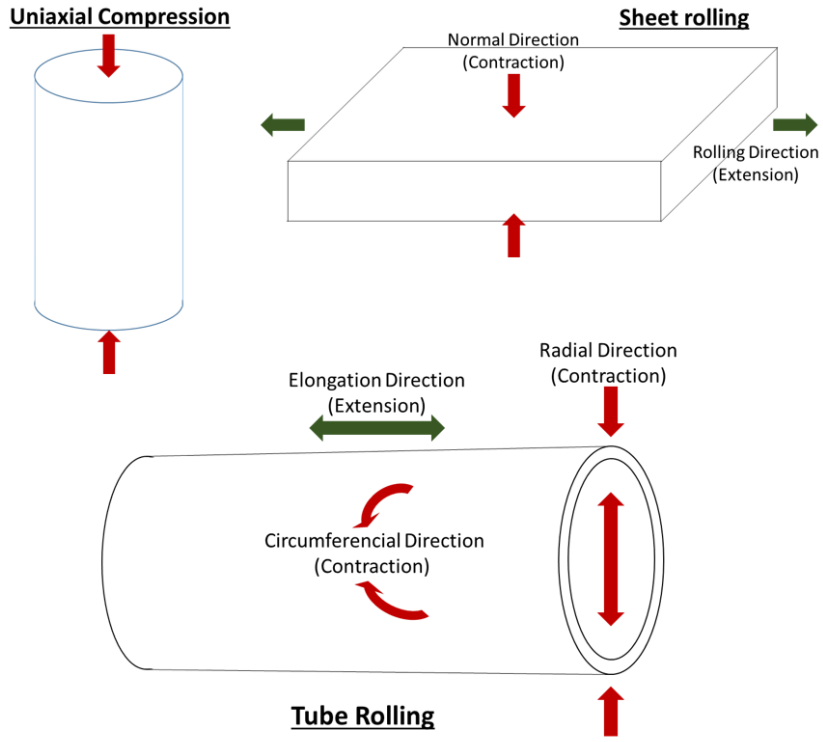

Fig. 5 The comparison of stress states in uniaxial deformation, sheet rolling and tube rolling

Fig. 5 illustrates the differing stress state in the processing of tubes in comparison with those of uniaxial deformation and sheet rolling. Compared with the plain stress state in sheet rolling, tube rolling involves a triaxial stress state, where a contraction stress is applied in the tangential direction. Therefore, a modified SF has been developed for this investigation to describe the twinning activity in the cold rolled tubes; $m_0 = 1/3 \times (\mathbf{COS}\,\varphi\, ED \times \mathbf{COS}\,\lambda\, ED - \mathbf{COS}\,\varphi\, RD \times \mathbf{COS}\,\lambda\, RD - \mathbf{COS}\,\varphi\, TD \times \mathbf{COS}\,\lambda\, TD)$. The external applied stress directions apply to ED, RD and TD in the above formula, respectively. The modified SF is defined as positive when the extension twin strain has a component corresponding to extension along ED, while it is negative when the contraction twin strain has a component corresponding to contraction along RD and TD. The SFs corresponding to the twinning variants were calculated on the assumption that the stress state of each grain coincides with specific external applied stress in the process of tube rolling. The $1/3$ in the formula is applied to normalise the modified SF values with the global ones.

In the present paper, 417 grains were investigated using the modified SF evolution in cold rolled AZ31 tubes, where $\{10\bar{1}2\}$, $\{10\bar{1}1\}$ and $\{10\bar{1}2\}-\{10\bar{1}1\}$ double twins were identified and detailed SF analyses for the twinning activity were performed. Fig. 6 shows the distributions of modified SF for primary $\{10\bar{1}2\}$ and $\{10\bar{1}1\}$ twins. The result reveals that about 72% of grains have a modified SF larger than 0.3 and 41% larger than 0.4 for $\{10\bar{1}2\}$ twins, whilst $\{10\bar{1}1\}$ twins have SFs larger than 0.4 in 62% of the grains. A SF rank diagram is shown in Fig. 7 for the grain G3 in Fig. 1b as an example. All the six SFs were calculated for the six primary twins which may form in G3. Rank 1 applies to the highest SFs and rank 6 applies to the lowest SFs. There is considerable variation in the SF value in a given rank due to the grain orientations. The lowest ranks may be associated with negative values in view of the nature of the modified SF. The SF depends on the initial relative orientation between the crystallographic orientation and the RD.

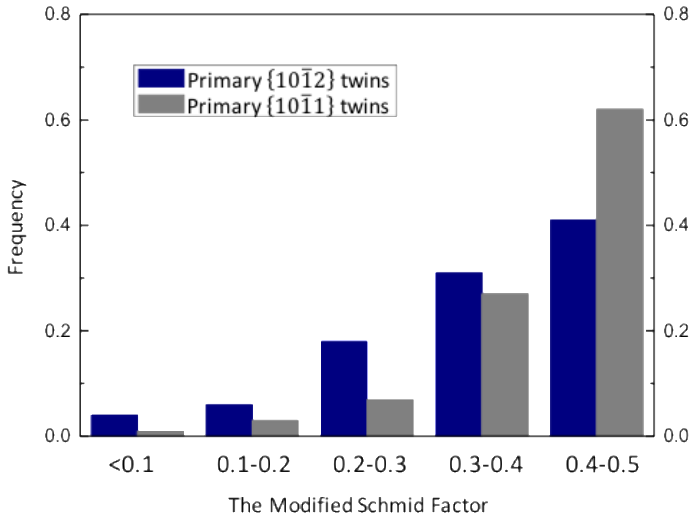

Fig. 6. Modified Schmid factor distributions of primary $\{10\bar{1}2\}$ and $\{10\bar{1}1\}$ twins in the cold rolled AZ31 tubes at an ε of 0.15

Both $\{10\bar{1}2\}$ twins and $\{10\bar{1}1\}$ twins were observed in the same grains after cold rolling as mentioned in the section 3.1. Modified SFs for activating $\{10\bar{1}2\}$ and $\{10\bar{1}1\}$ twins were calculated based on orientations of the 417 observed grains and the average of the maximum SFs are plotted in Fig. 8 in order to further understand the coexistence of $\{10\bar{1}2\}$ and $\{10\bar{1}1\}$ twinning activities. Only the maximum SFs are used in this calculation. This is reasonable because the highest SF variant is the most likely selected for $\{10\bar{1}2\}$ and $\{10\bar{1}1\}$ twinning (abnormal twins have been observed and will be discussed in the following section). According to the nature of the SF, the activation of $\{10\bar{1}2\}$ and $\{10\bar{1}1\}$ twins are less affected by the change of orientations around the c-axis in parent grains,

but they are largely affected by the c-axis orientations. Fig. 8 shows that both $\{10\bar{1}2\}$ twins and $\{10\bar{1}1\}$ twins were favoured in grains with their c-axes aligned 30-60 °to the RD during the process of cold rolling. This might be one reason for the observation of complex twinning in the cold rolled AZ31 tubes. The increased activity of $\{10\bar{1}2\}$ twins over $\{10\bar{1}1\}$ twins is due to the low CRSS of the former.

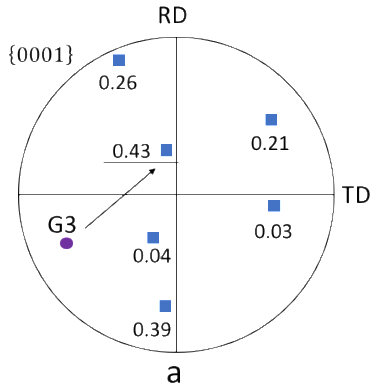

a

Rank	Modified Schmid factor
Rank 1	0.43
Rank 2	0.39
Rank 3	0.26
Rank 4	0.21
Rank 5	0.04
Rank 6	0.03

b

Fig. 7. (a) {0001} pole figure for the parent grain G3 shown in Fig. 1b, the six potential twin variants indicated by blue squares, the activated variant in G3 labelled by underline and the modified Schmid factors. (b) The Schmid factor rank in G3

All of the secondary twins were formed from primary twins. They were converted into second generation twins by further straining of the primary twins. Therefore, there are a large number of double twins observed due to the large strains imparted in the process of cold rolling. In order to understand the activation of double twins in the cold rolled AZ31 tubes, the following SF calculation was performed. According to the distribution of modified SFs for the activation of secondary $\{10\bar{1}2\}$ twins in the primary $\{10\bar{1}1\}$ twins (Fig. 9a), the $\{10\bar{1}1\}$ twinned areas are unfavourably oriented for secondary $\{10\bar{1}2\}$ twinning. Most of the area fraction has a SF value of less than 0.1 and so it is difficult to activate $\{10\bar{1}1\} - \{10\bar{1}2\}$ double twins. The $\{10\bar{1}2\} - \{10\bar{1}1\}$ double twin, D1, shown in Fig. 1b is discussed as an example. The orientation of the parent grain was determined and represented by a red square in Fig. 9(b). The orientation of the primary $\{10\bar{1}2\}$ twins were obtained by rotating the parent grains by 180 °around the normal direction of a given twinning plane and were represented by a blue square in Fig. 9b. The SFs for the primary $\{10\bar{1}2\}$ twins and secondary $\{10\bar{1}1\}$ twins were calculated based on the orientations of the parent grains and the primary $\{10\bar{1}2\}$ twins, respectively. The potential activation of primary $\{10\bar{1}2\}$ and secondary $\{10\bar{1}1\}$ twins can be evaluated by comparing their SF values in a given grain. Fig. 9c presents the comparison results of the SFs from 188 grains with $\{10\bar{1}2\} - \{10\bar{1}1\}$ double twins. It shows that approximately 59.6% of

the grains have the SF ratio of secondary $\{10\bar{1}1\}$ twins to primary $\{10\bar{1}2\}$ twins of over 2, and approximately 22.9% of grains have a ratio larger than 3. In all identified extension twins, the median SF for secondary $\{10\bar{1}1\}$ twins was 0.34. The level of the average SF value indicates that secondary $\{10\bar{1}1\}$ twinning was favourable in terms of their SF during the cold rolling of the AZ31 tubes. This is regarded as the primary reason for the activation of $\{10\bar{1}2\} - \{10\bar{1}1\}$ double twins in the cold rolled samples.

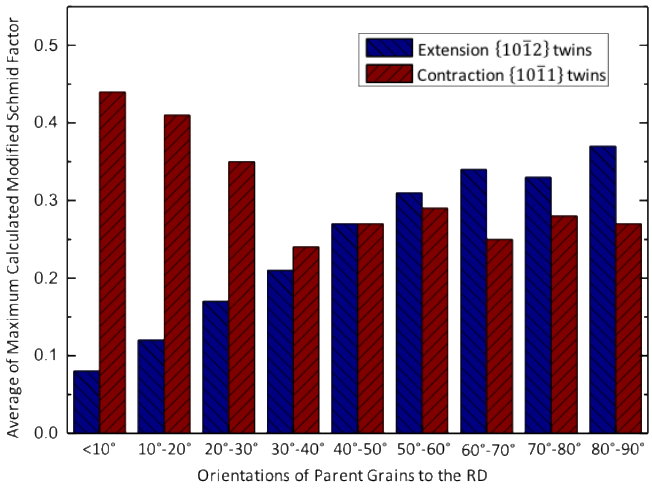

Fig. 8. The distribution of modified Schmid factor for activating $\{10\bar{1}2\}$ and $\{10\bar{1}1\}$ twinning in the different orientations of parent grains

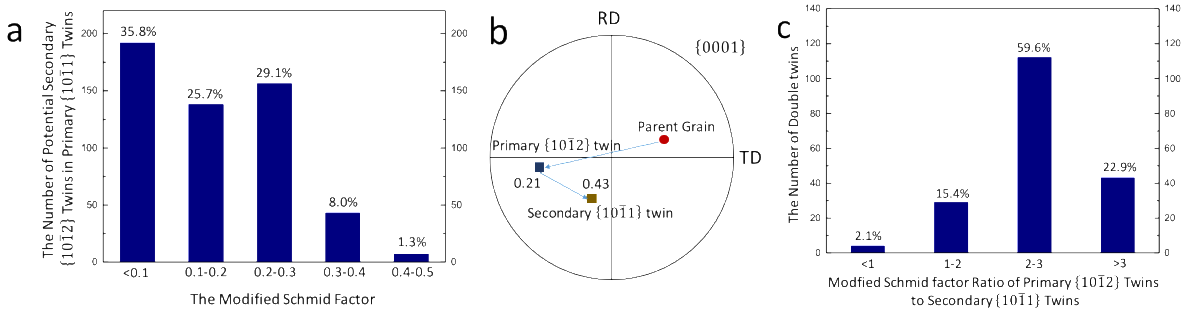

Fig. 9 (a) The distribution of modified Schmid factors for the activation of secondary $\{10\bar{1}2\}$ Twins in Primary $\{10\bar{1}1\}$ Twins. (b) The orientations of parent grain, primary $\{10\bar{1}2\}$ twin and corresponding secondary $\{10\bar{1}1\}$ twin in a double twin D1. (c) The distribution of modified Schmid factor ratio of primary $\{10\bar{1}2\}$ twins to secondary $\{10\bar{1}1\}$ twins

Some grains having only $\{10\bar{1}2\}$ twins were observed in the cold rolled AZ31 tubes, e.g. G4 and G5 in Fig 1b. Most of the c-axes of the grains are aligned within 60 °–90 °to the RD, and $\{10\bar{1}2\}$ twinning occurs with modified SF values ranging from 0.23 to 0.5. There are some grains aligned within 45 °–

60 °of the RD, which have low SFs for $\{10\bar{1}2\}$ twinning but high SFs for $\{10\bar{1}1\}$ twinning. However, the $\{10\bar{1}2\}$ twins were still observed in some of them. At the early stage of deformation, basal slip accumulated at GBs, leads to a high stress concentration [72]. The low CRSS for activating $\{10\bar{1}2\}$ extension twins then facilitates the nucleation of $\{10\bar{1}2\}$ twins, despite their low SFs. Different $\{10\bar{1}2\}$ extension twin variants may be activated in the same grain, but most of them have a high SF value, larger than 0.35, with the c-axes of their parent grains aligned within 80 °-90 °to the RD. This implies that the activation of different twin variants in a grain has a stronger orientation dependence than that for a single variant.

In some deformed grains, no obvious twins were identified, such as G6, G7 and G8 in Fig. 1b. Yang et al. [350] also reported a similar result by tracking a single grain through increasing strains. The grains were analysed in terms of the modified SF value. The results are plotted in Fig. 10 to show the distribution of the modified SF values for these twin free grains. Potential $\{10\bar{1}2\}$ extension twins have low SF values, ranging from 0.14 to 0.23, whereas the highest SF for $\{10\bar{1}1\}$ contraction twins was 0.44 which is a considerably higher value for the nucleation of twins. However, all of the twin free grains have areas smaller than 40 μm^2, with most grains having areas less than 24 μm^2, which is unfavourable for the activation of $\{10\bar{1}1\}$ twins in consideration of the elastic strain energy as detailed in section 3.1. Therefore, it is observed that these grains with relatively low SFs and small grain sizes of less than 40 μm^2 tend to remain twin free after cold rolling of the AZ31 tubes.

In the above analyses, the orientations of 417 grains were determined in the cold rolled tubes at a ε of 0.15. The modified SFs pertaining to 536 primary twins and 323 secondary twins were investigated. Approximately 30% of the grains had a single twin variant activated in the process of cold rolling. The activated twin variant had the first or second highest SF in most cases. The distribution of SFs reveals that almost half of these twins had relatively high SFs ranging from 0.3 to 0.5 depending on the grain orientations. However, in many grains, more than one variant was observed and these multiple twin variants did not show a high dependence on the SF ranking. Some of the twins had SF rankings of 3 or 4 with their values from 0.15 to 0.3. This shows that the SF is not the only aspect determining the activation of a given twin. Recent studies indicate that the variant selection in twin chains and multiple twins is also associated with the efficiency of twin transfer across twins and GBs [248, 347].

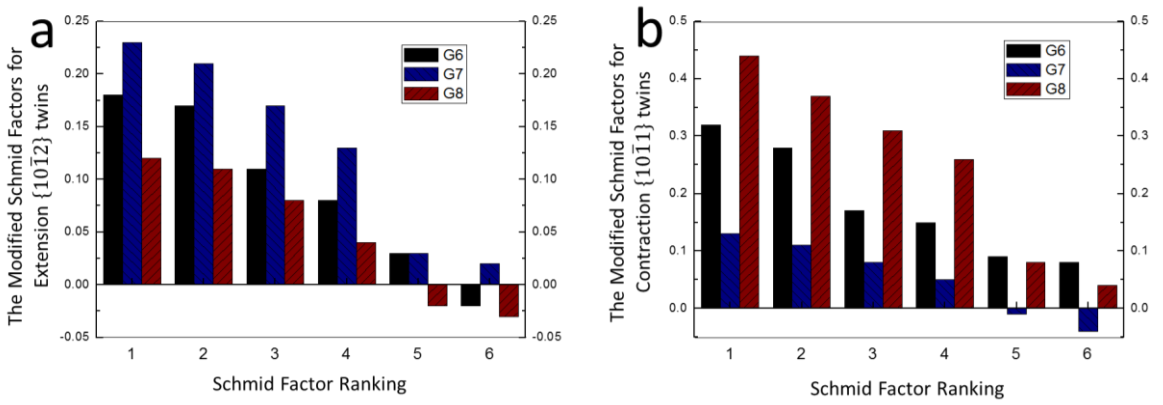

Fig. 10. The distribution of Modified Schmid Factors for (a) extension {10$\bar{1}$2} twins and (b) contraction {10$\bar{1}$1} twins in the untwinned grains G6, G7 and G8 in Fig. 1b.

3.3 Multiple twins

Fig. 11a shows a few twinned grains after cold rolling. The twins are generated with all twins being almost parallel except for twin E8, which is crossed by twin E9 in grain G10. The twin E8 is connected to twins E10 and E11 in the neighbouring grain, G11. The orientation relationship between the parent grains and twins are illustrated in Fig. 11b. Modified SFs for the twins are presented in Fig. 11c, which shows that all of the twins except for E8 are paired variants with SF rankings of 1 or 2. It is known that the six potential twin variants in Mg alloys can be grouped into three variant pairs. Each of those has similar SF values and a characteristic misorientation angle of approximately 7.4 °[351]. For example, twins E10 and E11 were activated as paired twin variants with the first and second highest SF values. Because grain orientations could be changed by dislocation slip, the SFs calculated based on the deformed grain orientations may deviate slightly from that of the activated twins. The paired twins with SFs either ranking 1 or 2 are considered to obey the Schmid law in this stage.

It is well known that the formation of twins involves shearing in parent grains. When twin nucleation initiates at a GB, the shear must be transmitted to the neighbouring grain. E8 (SF=0.24) in grain G10 is an example of a twin with a low SF value and a SF rank of 4, which shows that twins with low SF values may also be activated due to other factors. The efficiency of twin transfer across GBs can be described by a strain compatibility factor, $m_0 = \cos\psi \times \cos\kappa$, where ψ is the angle between the twinning plane normal of the two neighbouring grains, and κ is the angle between twinning shear direction of the two neighbouring grains [347]. The m_0 between neighbouring twins can be calculated using the orientation data from EBSD results. The calculation results show that the m_0 between E8 and E10 is 0.835, and m_0 = 0.871 between E8 and E11, indicating that the twin strain from E10 and

E11 can be effectively accommodated by E8. Therefore, the strain accommodation factor m_0 plays an important role in the activation of the non-Schmid twin E8.

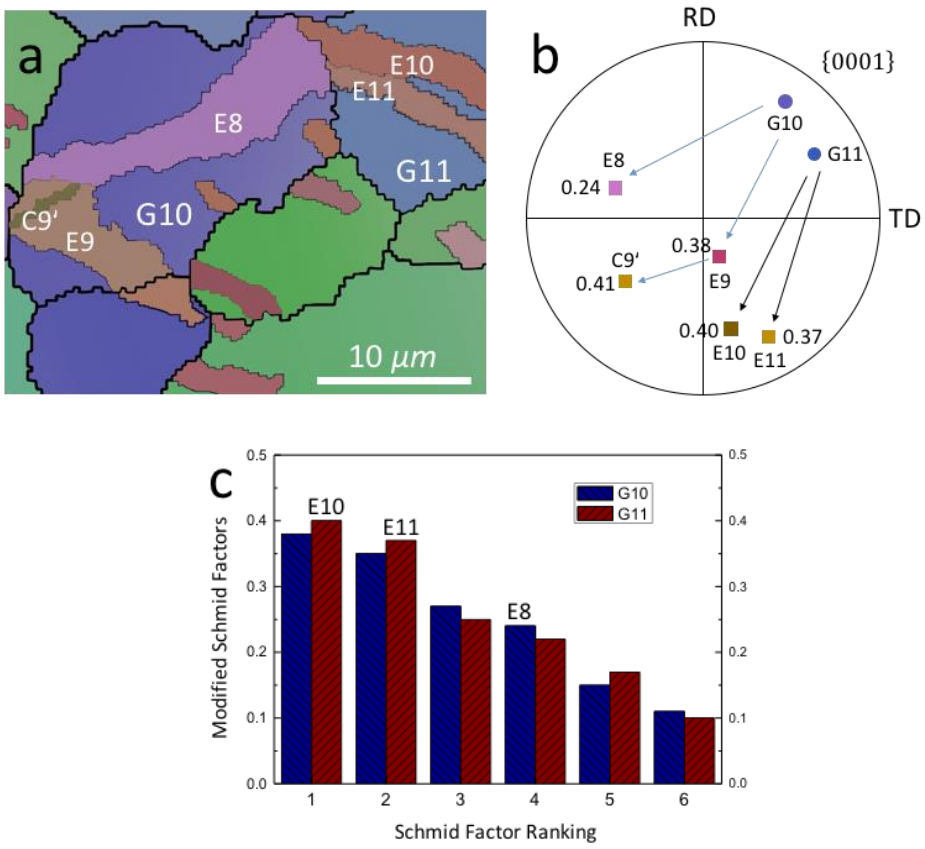

Fig. 11 (a) An example of multiple twins and non-Schmid twins in cold rolled tubes. (b) The misorientation relationships between the corresponding twins and parent grains. (c) Modified Schmid factors for the corresponding twins

Multiple twins may develop when the stress directions and the orientation of the parent grain are favourable for different twin variants. Twins E10 and E11 have a characteristic misorientation angle of 7.4 °for the paired variants. As mentioned earlier, the strain compatibility factor m_0 is an indicator of the efficiency of strain accommodation between two twins. However, the strain accommodation between the paired variants E10 and E11 was low (m_0 = 0.017). Therefore, twins E10 and E11 were considered to form independently rather than nucleate from the same point simultaneously. In view of the strain compatibility factor, m_0, these types of paired variants were not frequently observed in small grains despite their high SFs.

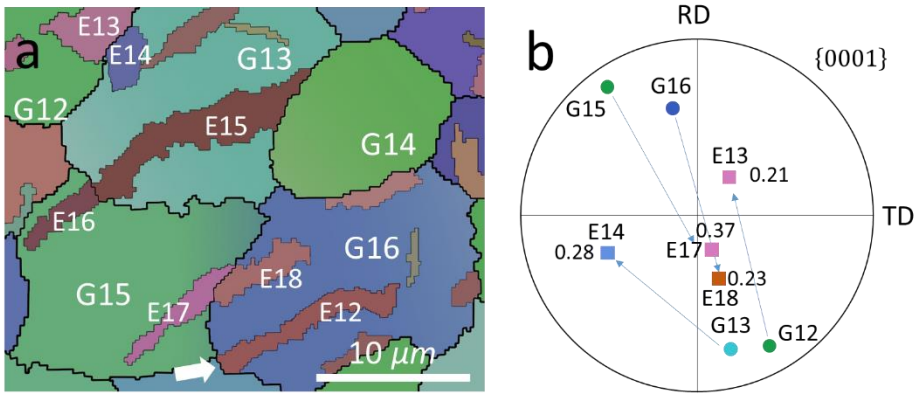

Fig. 12. (a) An example of non-Schmid twins in cold rolled tubes. (b) The misorientation relationships between the corresponding twins and parent grains

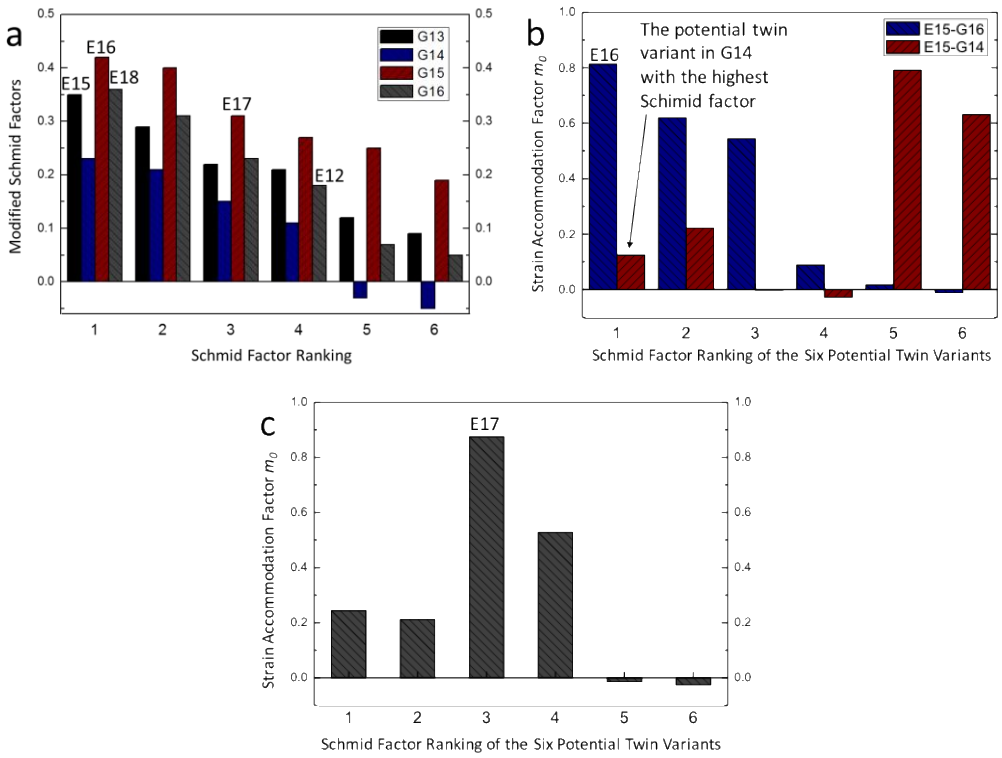

Fig. 13. (a) The modified Schmid factor ranking in G13, G14, G15 and G16. (b) Strain accommodation factor m_0 between E15 and the six potential variants in G16 and G14 in the order of Schmid factor ranking. (c) m_0 between E18 and the six potential variants in G1 and G15 in the order of Schmid factor ranking.

A secondary twin forms to accommodate strain at the twin intersection when a propagating twin intersects another. The propagating twin E8 and the secondary $\{10\bar{1}1\}$ twin C9′ were connected at the boundary between E8 and E9 as shown in Fig. 11a. The trace of the secondary $\{10\bar{1}1\}$ twin C9′

was parallel to the plane of the propagating twins. In addition, the high strain compatibility factor m_0 (0.878) indicates that the alignment of twinning plane and shear direction is of importance in the formation of the intersecting twins.

Fig. 12a displays a single twin E12 which does not intersect with other twins. Twin E12 had the fourth highest SF as indicated in table 2, which implies that there may be other factors affecting the variant selection of twins during the process of cold rolling. Twin E12 may nucleate at the GB indicated by the white arrow in Fig. 12a. The occurrence of the non-Schmid twin E12 was considered to be associated with the stress concentration accumulated at the GBs. Niezgoda et al. simulated the twin nucleation at GBs using a polycrystalline model and calculated stress concentrations [250]. Comparing the simulation results with the experimental data, they concluded that twins formed from GBs were associated with the stress concentration. More frequently, two twins in neighbouring grains nucleate simultaneously at GBs. For example, twin E13 had the modified SF of less than 0.3 as a non-Schmid twin, similarly twin E14 in grain G13 had a SF = 0.277 (Fig. 12b). Due to the similar thicknesses of E13 and E14, it is inferred that these two twins probably formed simultaneously at the G12-G13 GB. Fig. 12b indicates that the misorientation of the G12-G13 GB is very low. The formation of low angle grain boundaries is associated with the pile-up of dislocations and high stress concentrations. The two twins E13 and E14 formed from the G12-G13 GB were also favoured by the high efficiency of strain accommodation (m_0 = 0.891).

Twins E15 and E16, observed in Fig. 12a, exhibit a typical twin chain relationship across two neighbouring grains. Both of the twins have the highest SF among the six potential variants in the parent grains (Fig. 13a). The m_0 between E15 and E16 was also high, 0.813 (Fig. 13b). Therefore, the twin chain E15-E16 was favoured by both their SFs and the efficiency of strain accommodation. The previous case shows two paired twins with similar thicknesses and connected at a GB. High m_0 and low misorientation of boundaries are favourable for potential paired twins formed from the GBs. However, twinning is not activated in the neighbouring grain G14 through the transfer of shear strain from E15. The highest SF in G14 was calculated to have a relatively low value (SF=0.23). The m_0 between E15 and the variant with the highest SF in G14 is also very low. Consequently, twinning was not activated in the grain G14, and the twin chain was terminated at the GB. The shear strain transferred from E15 may be accommodated by slip. The slip-twin transfer mechanism in Mg and other hexagonal-close-packed materials, such as Zn and α-Ti, has been described in previous reports [352]. Fig. 13b demonstrates another twin chain across two grains. Twin chain E17-E18 was observed to involve two different twin variants. They connect at the GB between G15 and G16. Twin E18 had

the highest modified SF as indicated in Fig. 13a, whereas E17 had the third highest SF. The formation of twin E17 is probably induced by the twin E18 on the G15-G16 GB, due to the high stress concentration induced at the connection point, which is relieved by the activation of twinning in the neighbouring grain. E17 and E18 had small misorientations as shown in Fig. 12b, which result from the favourable twin-twin transfer and strain accommodation. Fig. 13c shows that E17 had the highest m_0 of 0.875 with respect to E18 and was much higher than that between E18 and the other five potential variants in G16 so that the stress concentration at G15-G16 GB and the shear strain from E18 could be relieved and accommodated efficiently. Therefore, strain accommodation at the GB played an important role in the activation of non-Schmid twins in this case.

4. Conclusion

The current study was concerned with twinning activity during cold rolling of AZ31 tubes. Three twinning modes, extension $\{10\bar{1}2\}$ twins, contraction $\{10\bar{1}1\}$ twins and double twins, were detected in the cold rolled tube at a ε of 0.15. The orientation data from EBSD were analysed in terms of the modified Schmid factor, as well as the accommodation strains. The main conclusions from the study are:

1. Extension $\{10\bar{1}2\}$ twins were most frequently observed in the cold rolled samples, because the selection of the twinning modes is associated their critical resolved shear stresses. When the two twinning modes had close and high Schmid factor values, $\{10\bar{1}2\}$ twinning was activated, whereas $\{10\bar{1}1\}$ twinning was activated when it had a high Schmid factor, exclusively. The dominant orientations of grains with c-axes 30 °-60 ° to the radial direction contribute to the complex twinning activity.
2. The modified Schmid factor for tube rolling is shown to be a pertinent parameter to predict the active twinning modes in the cold rolled AZ31 tube. Most of the $\{10\bar{1}1\}$ twins and some of the $\{10\bar{1}2\}$ twins obey the Schmid law exhibiting the highest or second highest Schmid factor values.
3. Twins with low Schmid factors were activated in the cold rolling of AZ31 tubes due to the influence of strain accommodation. Twins induced by stress concentrations at the grain boundaries or by the strain transferred from twins in neighbouring grains were observed. Secondary $\{10\bar{1}1\}$ twins can be activated at the intersection of primary $\{10\bar{1}2\}$ twins due to transfer of shear strain from one twin to the adjoining twin.

Chapter 4 Outcomes, Conclusions and Future Work

4.1. Outcomes and conclusions

4.1.1. Titanium alloy tubes

Several articles have been published during the candidature, which together represent a systematic study of the mechanical properties and evolution of microstructure in the processing of β Titanium and Magnesium alloy fine tubes. The results on the deformation of fine tubes fill a significant gap in the current literature and are applicable to the processing of metallic fine tubes composed of alloys with body-centred cubic and hexagonal close packed crystal structure.

The cold rolled and annealed biomedical β titanium alloy tubes with outside diameters (OD) from 3 mm to 8 mm have been investigated in this thesis. Profuse SIM α″ phase formed in the cold rolled tubes, and their volume fraction increased with increasing strain.

This research on the metastable beta titanium alloy has shown that the yield strength presents an inverted U–shaped curve with increasing strain ranging from 26% to 51% in annealed tubes. The ascending stage can be attributed to the increasing volume fraction of SIM α″ phase, while the growth of β grain size in the large deformed samples is believed to reduce the yield strength. The ductility decreased when the strain reached up to 51% in the annealed tubes, which is due to the increased proportion of low-angle grain boundaries according to the analysis using electron backscatter diffraction (EBSD).

The modulus of cold rolled tubes presents analogous superelastic characteristics – continuous reduction occurs during the elastic stage during tensile tests. Hence, the tangent modulus has been used in this thesis. The increasing proportion of the SIM α″ phase in the cold rolled tubes can be related to the varying tangent modulus: the reduction in the OD of the tubes from 8mm to 5.6 mm can reduce the tangent modulus both in the cold rolled and the annealed conditions, while the reduction in the OD from 5.6 mm increases the tangent modulus due to β texture evolution – from (100) and (110) to (211) on the observation plane parallel to the rolling direction. In view of the opposing effects of β phase rotation and the volume fraction of α″ phase, the varying orientation of α″ phase has been inferred to reduce the modulus when the OD was reduced.

The annealing process greatly enhanced the strain hardening behaviour and the ductility of the β titanium alloy tubes. For annealed tubes, double yielding phenomenon was observed during tensile

tests. The onset of martensitic phase transformation occurs around the first yield point, and stress-induced martensitic (SIM) α″ phase forms afterwards.

This thesis provided the evidence that both transformation induced plasticity and twinning induced plasticity were activated during cold deformation. The deformation products are $\{332\}\langle 113\rangle$ mechanical twins, primary and secondary SIM α″ phase. This thesis has provided the first reports on the synergistic deformation mechanisms contributing to the superior strain hardening rate and large ductility in the deformed metastable β titanium alloy fine tubes.

4.1.2. Magnesium alloy tubes

The processing of Mg-3Al-1Zn (AZ31) magnesium alloy tube was also investigated in this thesis via analyses of mechanical properties and twinning activity under different processing parameters. The two tube rolling parameters, ε the ratio in cross-sectional reduction and Q the ratio of wall-thickness to diameter reduction, has been used in this thesis.

The yield strength of AZ31 tubes increased with increasing ε, while it was reduced with an increase in Q. Another mechanical property, ductility decreased when ε and Q increased. This thesis shows that the formation of double twins contributed to the same tendency of strength and ductility with increasing Q.

The number of $\{10\bar{1}2\}$ extension twins increased with increasing ε until they were almost saturated when ε was above 16.5%. Then contraction/double twins and secondary twins propagated dramatically at high strain levels (≥16.5%) of ε. The $\{10\bar{1}2\}$ extension twins were the dominant deformation mechanism and overshadowed that of contraction and double twinning. Texture hardening and $\{10\bar{1}2\}$ extension twinning are the two dominant effects on the mechanical properties in the case of varying ε, whilst contraction and double twinning played a dominant role in the case of varying Q.

This thesis provided an integrated identification method for twinning activity in the cold rolling of AZ31 tubes. $\{10\bar{1}2\}$ was most frequently activated due to its low critical resolved shear stress. When $\{10\bar{1}2\}$ and $\{10\bar{1}1\}$ twinning have close Schmid factor values, the former will be activated, whereas the latter will be activated when it has a high Schmid factor exclusively. The dominant orientations

of grains with c-axes 30 °-60 °to the radial direction contribute to the complex twinning activity in the cold rolled AZ31 tubes.

A modified Schmid factor for the tube rolling has been proposed and been shown to be a pertinent parameter to predict the active twinning modes. However, Non-Schmid twins can be activated due to the complex stress state. Non-Schmid secondary $\{10\bar{1}1\}$ twins can be activated at the intersection of primary $\{10\bar{1}2\}$ twins due to the transfer of shear strain from one twin to the adjoining twin. Stress concentration at grain boundaries and the strain transferred from primary twins in neighbouring grains are ascribed to Non-Schmid primary twins.

4.2. Future work

4.2.1. Titanium alloy tubes

The two tube rolling parameters, ε and Q, were designed for the AZ31 magnesium tubes, and have been shown to be significant in the processing of AZ31 tube. They were not designed for the β titanium alloy tubes in this thesis, where the rolling and annealing process was only analysed via the varying strains. Therefore, it is expected that the two parameters will be applied to the β titanium fine tubes in future work, in order to supplement current understanding and optimise the processing parameters associated with tube rolling.

In this thesis, the mechanical properties were obtained from tensile tests, including modulus, yield strength, elongation and strain hardening behaviour. In addition to these properties, fatigue is of significance when considering the expected application for fine tube stent. It is believed that β titanium alloys have lower ratios of fatigue strength to yield strength in comparison with α+β type alloys [353]. The SIM α″ phase has been reported to be absent at the fracture surface during high-cycle fatigue tests [354], but a small amount of the SIM α″ phase was detected in low-cycle fatigue tests with a cycle strain above 2.5% [154]. The martensitic phase transformation appears to be related to the cyclical strains and stress in view of the metastable β phase is generally stable at an applied stress < 400 MPa. Therefore, future work should include cyclic tensile tests and crack propagation tests for the fine tubes.

Twinning planes were reported to act as crack initiation sites: the microcracks initiate at small voids at twin-matrix interfaces and grow to form cracks. Since profuse twinning can form in the current β

titanium samples, analysis of the relations between twinning and fatigue properties is also important when studying the fatigue properties. The microstructural observation (including SIM α″ and twins) using EBSD and Transmission electron microscopy (TEM) will be the focus in order to reveal the varying tendency of fatigue properties in the β titanium alloys.

The orientation of β and α″ phase has been analysed in this thesis involving the modulus, it is also associated with crack propagation and fracture. Therefore, when the fatigue properties are obtained, EBSD and TEM are expected to be used to reveal the relations between crack propagation and the orientation relationship of phases.

The influence of alloying elements (Nb, Sn, Zr and Mo) has also been considered in this thesis except for the role of oxygen, which also generally exists in these alloys. The oxygen in β titanium alloys acts as an interstitial element [42]. It can increase the β transit temperature and suppress the martensitic starting temperature. It has been reported that the β titanium alloy with low level oxygen plastically deforms via stress-induced phase transformation, while the alloy with high level oxygen deforms via {332}⟨113⟩ twinning mode [125]. Oxygen plays a significant role in stress-induced phase transformation and {332}⟨113⟩ mechanical twinning in cold rolling of tubes. Therefore, determining the oxygen content and analysis of the corresponding mechanical properties/microstructural evolution during deformation will be helpful to supplement current understanding.

4.2.2. Magnesium alloy tubes

The ductility of magnesium fine tubes is very limited, especially in the cold rolling condition. However, it has been reported that some combinations of twins have contributed to the improvement in ductility [54]. In this thesis, different twinning modes have been associated with the mechanical properties, including ductility, but the orientation of twins was also shown to contribute to the ductility and the occurrence of fracture. Twins identified using EBSD have been detailed in the current study, so the inverse pole figures presenting orientations of twins and parent grains can be simply obtained in future work. The influence of varying orientations of twins in the processing of fine tubes should be studied in combination with the fracture behaviour.

This thesis has shown that the rolling parameters, ε and Q, can influence nucleation and growth of the different types of twins. Thus, to further improve mechanical properties of magnesium fine tubes,

the design of fine and dense twin lamellae should be studied in future work. The twin boundaries was shown to generate a refinement hardening effect in magnesium tubes [266]. So the twin boundary hardening, spacing of twin lamellae and average twin size should be studied in future work.

The magnesium tubes used in this thesis are in the cold rolled condition, but thermal processing is necessary in the fabrication of fine tubes as described in the study of β titanium alloys. Park et al. [355] reported that annealing can suppress the detwinning activity in AZ31 alloy at a small strain. Further work could also involve thermal treatment, such as annealing at varying temperatures. This needs to be performed in order to study the stability of twins, twin growth and their influence on mechanical properties.

References

[1] Hermawan H, Dubé D, Mantovani D. Developments in metallic biodegradable stents. Acta Biomaterialia 2010;6:1693-7.
[2] Azaouzi M, Lebaal N, Makradi A, Belouettar S. Optimization based simulation of self-expanding Nitinol stent. Materials & Design 2013;50:917-28.
[3] Tian Y, Yu Z, Ong CYA, Kent D, Wang G. Microstructure, elastic deformation behavior and mechanical properties of biomedical β-type titanium alloy thin-tube used for stents. Journal of the Mechanical Behavior of Biomedical Materials 2015;45:132-41.
[4] Griza S, de Souza Sá DHG, Batista WW, de Blas JCG, Pereira LC. Microstructure and mechanical properties of hot rolled TiNbSn alloys. Materials & Design 2014;56:200-8.
[5] Grosdidier T, Philippe MJ. Deformation induced martensite and superelasticity in a β-metastable titanium alloy. Materials Science and Engineering: A 2000;291:218-23.
[6] Yang Y, Li GP, Cheng GM, Li YL, Yang K. Multiple deformation mechanisms of Ti–22.4Nb–0.73Ta–2.0Zr–1.34O alloy. Applied Physics Letters 2009;94:061901-1-3.
[7] Maeshima T, Ushimaru S, Yamauchi K, Nishida M. Effect of heat treatment on shape memory effect and superelasticity in Ti–Mo–Sn alloys. Materials Science and Engineering: A 2006;438–440:844-7.
[8] Azaouzi M, Makradi A, Belouettar S. Deployment of a self-expanding stent inside an artery: A finite element analysis. Materials & Design 2012;41:410-20.
[9] Kim HY, Ikehara Y, Kim JI, Hosoda H, Miyazaki S. Martensitic transformation, shape memory effect and superelasticity of Ti–Nb binary alloys. Acta Materialia 2006;54:2419-29.
[10] Kim HY, Hashimoto S, Kim JI, Inamura T, Hosoda H, Miyazaki S. Effect of Ta addition on shape memory behavior of Ti–22Nb alloy. Materials Science and Engineering: A 2006;417:120-8.
[11] Ping D, Mitarai Y, Yin F. Microstructure and shape memory behavior of a Ti-30Nb-3Pd alloy. Scripta Materialia 2005;52:1287-91.
[12] Kent D, Wang G, Yu Z, Dargusch MS. Pseudoelastic behaviour of a β Ti–25Nb–3Zr–3Mo–2Sn alloy. Materials Science and Engineering: A 2010;527:2246-52.
[13] Steinemann SG. Titanium' 84: Science and Technology. In: Lutjering G, Zwicker U, Bunk W, editors. Deutsche Gesellschaft Fur Metallkunde EV. Munich1985. p. 1373.
[14] Crapper DR, Mclachlan DR, Farnell B, Galin H, Karlik S, Eichhorn G, et al. Biological Aspects of Metals and Metals-Related Diseases. New York: Raven Press; 1993.
[15] Biesiekierski A, Wang J, Abdel-Hady Gepreel M, Wen C. A new look at biomedical Ti-based shape memory alloys. Acta Biomaterialia 2012;8:1661-9.
[16] Kim JI, Kim HY, Inamura T, Hosoda H, Miyazaki S. Shape memory characteristics of Ti–22Nb–(2–8)Zr(at.%) biomedical alloys. Materials Science and Engineering: A 2005;403:334-9.
[17] Ren Y, Wang F, Wang S, Tan C, Yu X, Jiang J, et al. Mechanical response and effects of β-to-α" phase transformation on the strengthening of Ti–10V–2Fe–3Al during one-dimensional shock loading. Materials Science and Engineering: A 2013;562:137-43.
[18] Kent D, Pas S, Zhu S, Wang G, Dargusch M. Thermal analysis of precipitation reactions in a Ti–25Nb–3Mo–3Zr–2Sn alloy. Applied Physics A: Materials Science & Processing 2012;107:835-41.
[19] Paladugu M, Kent D, Wang G, Yu Z, Dargusch MS. Strengthening of cast Ti–25Nb–3Mo–3Zr–2Sn alloy through precipitation of α in two discrete crystallographic orientations. Materials Science and Engineering: A 2010;527:6601-6.
[20] Yu Z, Zhou L. Influence of martensitic transformation on mechanical compatibility of biomedical β type titanium alloy TLM. Materials Science and Engineering: A 2006;438-440:391-4.
[21] Huang R, Lu S, Han Y. Role of grain size in the regulation of osteoblast response to Ti–25Nb–3Mo–3Zr–2Sn alloy. Colloids and Surfaces B: Biointerfaces 2013;111:232-41.
[22] Huang R, Han Y. Structure evolution and thermal stability of SMAT-derived nanograined layer on Ti–25Nb–3Mo–3Zr–2Sn alloy at elevated temperatures. Journal of Alloys and Compounds 2013;554:1-11.
[23] Kent D, Wang G, Dargusch M. Effects of phase stability and processing on the mechanical properties of Ti–Nb based β Ti alloys. Journal of the Mechanical Behavior of Biomedical Materials 2013;28:15-25.
[24] Hanada K, Matsuzaki K, Huang X, Chino Y. Fabrication of Mg alloy tubes for biodegradable stent application. Materials Science and Engineering: C 2013;33:4746-50.

[25] Erbel R, Di Mario C, Bartunek J, Bonnier J, de Bruyne B, Eberli FR, et al. Temporary scaffolding of coronary arteries with bioabsorbable magnesium stents: a prospective, non-randomised multicentre trial. The Lancet 2007;369:1869-75.
[26] Heublein B, Rohde R, Kaese V, Niemeyer M, Hartung W, Haverich A. Biocorrosion of magnesium alloys: A new principle in cardiovascular implant technology? Heart 2003;89:651-6.
[27] Farrar G, Blair JA, Altmann P, Welch S. Comparative plasma speciation of the aluminium model 'gallium-67' in Alzheimers disease, stroke dementia, downs syndrome, end-stage renal disease and controls. Neurobiology of Aging 1990;11:318.
[28] Phillipson M. The link between aluminium and Alzheimers—Not the whole story. Food and Chemical Toxicology 1988;26:76-7.
[29] Zeng R-C, Hu Y, Guan S-K, Cui H-Z, Han E-H. Corrosion of magnesium alloy AZ31: The influence of bicarbonate, sulphate, hydrogen phosphate and dihydrogen phosphate ions in saline solution. Corrosion Science.
[30] Hu J, Zhang C, Cui B, Bai K, Guan S, Wang L, et al. In vitro degradation of AZ31 magnesium alloy coated with nano TiO2 film by sol–gel method. Applied Surface Science 2011;257:8772-7.
[31] Premkumar M, Himabindu VS, Banumathy S, Bhattacharjee A, Singh AK. Effect of mode of deformation by rolling on texture evolution and yield locus anisotropy in a multifunctional β titanium alloy. Materials Science and Engineering: A 2012;552:15-23.
[32] Hao YL, Li SJ, Sun SY, Zheng CY, Yang R. Elastic deformation behaviour of Ti-24Nb-4Zr-7.9Sn for biomedical applications. Acta Biomater 2007;3:277-86.
[33] Niinomi M. Mechanical properties of biomedical titanium alloys. Materials Science and Engineering: A 1998;243:231-6.
[34] Xu W, Kim KB, Das J, Calin M, Eckert J. Phase stability and its effect on the deformation behavior of Ti-Nb-Ta-In/Cr β alloys. Scripta Materialia 2006;54:1943-8.
[35] Sun F, Zhang JY, Marteleur M, Gloriant T, Vermaut P, Laillé D, et al. Investigation of early stage deformation mechanisms in a metastable β titanium alloy showing combined twinning-induced plasticity and transformation-induced plasticity effects. Acta Materialia 2013;61:6406-17.
[36] Haghighi SE, Lu HB, Jian GY, Cao GH, Habibi D, Zhang LC. Effect of α″ martensite on the microstructure and mechanical properties of beta-type Ti－Fe－Ta alloys. Materials & Design 2015;76:47-54.
[37] Zhang Y, Kent D, Wang G, St John D, Dargusch M. Evolution of the microstructure and mechanical properties during fabrication of mini-tubes from a biomedical β-titanium alloy. Journal of the Mechanical Behavior of Biomedical Materials 2015;42:207-18.
[38] Kim HY, Ikehara Y, Kim JI, Hosoda H, Miyazaki S. Martensitic transformation, shape memory effect and superelasticity of Ti-Nb binary alloys. Acta Materialia 2006;54:2419-29.
[39] Hu Q-M, Li S-J, Hao Y-L, Yang R, Johansson B, Vitos L. Phase stability and elastic modulus of Ti alloys containing Nb, Zr, and/or Sn from first-principles calculations. Applied Physics Letters 2008;93:121902-1-3.
[40] Neelakantan S, San Martin D, Rivera-Díaz-Del-Castillo PEJ, Van Der Zwaag S. Plasticity induced transformation in a metastable β Ti-1023 alloy by controlled heat treatments. Materials Science and Technology 2009;25:1351-8.
[41] Tobe H, Kim HY, Inamura T, Hosoda H, Miyazaki S. Origin of {3 3 2} twinning in metastable β-Ti alloys. Acta Materialia 2014;64:345-55.
[42] Hanada S, Izumi O. Transmission electron microscopic observations of mechanical twinning in metastable beta titanium alloys. Metallurgical Transactions A 1986;17:1409-20.
[43] Oka M, Taniguchi Y. {332} Deformation twins in a Ti-15.5 pct V alloy. Metallurgical Transactions A 1979;10:651-3.
[44] Min XH, Emura S, Nishimura T, Tsuchiya K, Tsuzaki K. Microstructure, tensile deformation mode and crevice corrosion resistance in Ti-10Mo-xFe alloys. Materials Science and Engineering A 2010;527:5499-506.
[45] Bertrand E, Castany P, Péron I, Gloriant T. Twinning system selection in a metastable β-titanium alloy by Schmid factor analysis. Scripta Materialia 2011;64:1110-3.
[46] Zhao X, Niinomi M, Nakai M, Hieda J, Ishimoto T, Nakano T. Optimization of Cr content of metastable β-type Ti-Cr alloys with changeable Youngs modulus for spinal fixation applications. Acta Biomaterialia 2012;8:2392-400.

[47] Min XH, Tsuzaki K, Emura S, Sawaguchi T, Ii S, Tsuchiya K. {332}〈113〉 Twinning system selection in a β-type Ti–15Mo–5Zr polycrystalline alloy. Materials Science and Engineering: A 2013;579:164-9.
[48] Zhang Y, Kent D, Wang G, St John D, Dargusch M. An investigation of the mechanical behaviour of fine tubes fabricated from a Ti–25Nb–3Mo–3Zr–2Sn alloy. Materials & Design 2015;85:256-65.
[49] Chen F-K, Huang T-B. Formability of stamping magnesium-alloy AZ31 sheets. Journal of Materials Processing Technology 2003;142:643-7.
[50] Yang L-f, Mori K-i, Tsuji H. Deformation behaviors of magnesium alloy AZ31 sheet in cold deep drawing. Transactions of Nonferrous Metals Society of China 2008;18:86-91.
[51] Chao H-y, Sun H-f, Wang E-d. Working hardening behaviors of severely cold deformed and fine-grained AZ31 Mg alloys at room temperature. Transactions of Nonferrous Metals Society of China 2011;21, Supplement 2:s235-s41.
[52] Yang X, Okabe Y, Miura H, Sakai T. Effect of pass strain and temperature on recrystallisation in magnesium alloy AZ31 after interrupted cold deformation. Journal of Materials Science 2012;47:2823-30.
[53] Barnett MR, Nave MD, Bettles CJ. Deformation microstructures and textures of some cold rolled Mg alloys. Materials Science and Engineering: A 2004;386:205-11.
[54] Yoo MH. Slip, twinning, and fracture in hexagonal close-packed metals. Metallurgical Transactions A 1981;12:409-18.
[55] Ball EA, Prangnell PB. Tensile-compressive yield asymmetries in high strength wrought magnesium alloys. Scripta Metallurgica et Materiala 1994;31:111-6.
[56] Gharghouri MA, Weatherly GC, Embury JD, Root J. Study of the mechanical properties of Mg-7.7at.% Al by in-situ neutron diffraction. Philosophical Magazine A: Physics of Condensed Matter, Structure, Defects and Mechanical Properties 1999;79:1671-95.
[57] Wang YN, Huang JC. The role of twinning and untwinning in yielding behavior in hot-extruded Mg-Al-Zn alloy. Acta Materialia 2007;55:897-905.
[58] Koike J. Enhanced deformation mechanisms by anisotropic plasticity in polycrystalline Mg alloys at room temperature. Metallurgical and Materials Transactions A: Physical Metallurgy and Materials Science 2005;36:1689-96.
[59] Huber J, Hatherly M. NUCLEATION AND ANNEALING TEXTURE DEVELOPMENT IN ROLLED 70:30 BRASS. Zeitschrift fuer Metallkunde/Materials Research and Advanced Techniques 1980;71:15-20.
[60] Ma Q, El Kadiri H, Oppedal AL, Baird JC, Horstemeyer MF, Cherkaoui M. Twinning and double twinning upon compression of prismatic textures in an AM30 magnesium alloy. Scripta Materialia 2011;64:813-6.
[61] Jiang L, Jonas JJ. Effect of twinning on the flow behavior during strain path reversals in two Mg (+Al, Zn, Mn) alloys. Scripta Materialia 2008;58:803-6.
[62] Xin R, Wang M, Huang X, Guo C, Liu Q. Observation and Schmid factor analysis of multiple twins in a warm-rolled Mg–3Al–1Zn alloy. Materials Science and Engineering: A 2014;596:41-4.
[63] Xin R, Guo C, Xu Z, Liu G, Huang X, Liu Q. Characteristics of long {10-12} twin bands in sheet rolling of a magnesium alloy. Scripta Materialia 2014;74:96-9.
[64] Jonas JJ, Mu S, Al-Samman T, Gottstein G, Jiang L, Martin Ė. The role of strain accommodation during the variant selection of primary twins in magnesium. Acta Materialia 2011;59:2046-56.
[65] Wang YN, Huang JC. The role of twinning and untwinning in yielding behavior in hot-extruded Mg–Al–Zn alloy. Acta Materialia 2007;55:897-905.
[66] Xin Y, Wang M, Zeng Z, Huang G, Liu Q. Tailoring the texture of magnesium alloy by twinning deformation to improve the rolling capability. Scripta Materialia 2011;64:986-9.
[67] Meza-García E, Dobroň P, Bohlen J, Letzig D, Chmelík F, Lukáč P, et al. Deformation mechanisms in an AZ31 cast magnesium alloy as investigated by the acoustic emission technique. Materials Science and Engineering A 2007;462:297-301.
[68] Jonas JJ, Mu S, Al-Samman T, Gottstein G, Jiang L, Martin E. The role of strain accommodation during the variant selection of primary twins in magnesium. Acta Materialia 2011;59:2046-56.
[69] Bohlen J, Dobron P, Garcia EM, Chmelík F, Lukáč P, Letzig D, et al. The effect of grain size on the deformation behaviour of magnesium alloys investigated by the acoustic emission technique. Advanced Engineering Materials 2006;8:422-7.
[70] Liu X, Jonas JJ, Li LX, Zhu BW. Flow softening, twinning and dynamic recrystallization in AZ31 magnesium. Materials Science and Engineering: A 2013;583:242-53.

[71] Myshlyaev MM, McQueen HJ, Mwembela A, Konopleva E. Twinning, dynamic recovery and recrystallization in hot worked Mg-Al-Zn alloy. Materials Science and Engineering A 2002;337:121-33.
[72] Jiang L, Jonas JJ, Luo AA, Sachdev AK, Godet S. Influence of {10-12} extension twinning on the flow behavior of AZ31 Mg alloy. Materials Science and Engineering: A 2007;445–446:302-9.
[73] Barnett MR. Influence of deformation conditions and texture on the high temperature flow stress of magnesium AZ31. Journal of Light Metals 2001;1:167-77.
[74] Barnett MR. Twinning and the ductility of magnesium alloys: Part I: "Tension" twins. Materials Science and Engineering: A 2007;464:1-7.
[75] Barnett MR. Twinning and the ductility of magnesium alloys: Part II. "Contraction" twins. Materials Science and Engineering: A 2007;464:8-16.
[76] Park SH, Hong S-G, Lee CS. Enhanced stretch formability of rolled Mg–3Al–1Zn alloy at room temperature by initial {10–12} twins. Materials Science and Engineering: A 2013;578:271-6.
[77] Song B, Xin R, Chen G, Zhang X, Liu Q. Improving tensile and compressive properties of magnesium alloy plates by pre-cold rolling. Scripta Materialia 2012;66:1061-4.
[78] Knezevic M, Levinson A, Harris R, Mishra RK, Doherty RD, Kalidindi SR. Deformation twinning in AZ31: Influence on strain hardening and texture evolution. Acta Materialia 2010;58:6230-42.
[79] Rohatgi A, Vecchio KS, Gray IGT. A metallographic and quantitative analysis of the influence of stacking fault energy on shock-hardening in Cu and Cu–Al alloys. Acta Materialia 2001;49:427-38.
[80] Styczynski A, Hartig C, Bohlen J, Letzig D. Cold rolling textures in AZ31 wrought magnesium alloy. Scripta Materialia 2004;50:943-7.
[81] Fallone B, Wallace S, Gianturco C. Elastic characteristics of the self-expanding metallic stents. Invest Radiol 1988;23:370-6.
[82] Garg S, Serruys PW. Coronary Stents: Looking Forward. Journal of the American College of Cardiology 2010;56:S43-S78.
[83] Guildford A, Santin M, Phillips GJ. Cardiovascular stents. In: Black TGA, editor. Biomaterials and Devices for the Circulatory System: Woodhead Publishing; 2010. p. 173-216.
[84] Frotscher M, Nörtershäuser P, Somsen C, Neuking K, Böckmann R, Eggeler G. Microstructure and structural fatigue of ultra-fine grained NiTi-stents. Materials Science and Engineering: A 2009;503:96-8.
[85] Mani G, Feldman MD, Patel D, Agrawal CM. Coronary stents: A materials perspective. Biomaterials 2007;28:1689-710.
[86] Hanawa T. Materials for metallic stents. Journal of Artificial Organs 2009;12:73-9.
[87] Gy. Ring, E. Bognár, Dobránszky J. Coronary Stents Materials and Examinations of Surface and Expansion Features. Materials Science Forum 2007;537-538:449-55.
[88] O'Brien B, Carroll W. The evolution of cardiovascular stent materials and surfaces in response to clinical drivers: A review. Acta Biomaterialia 2009;5:945-58.
[89] Mechanical Properties of Nitinol Stents and Stent-grafts.
[90] Freiberg KE, Bremer-Streck S, Kiehntopf M, Rettenmayr M, Undisz A. Effect of thermomechanical pre-treatment on short- and long-term Ni release from biomedical NiTi. Acta Biomaterialia 2014;10:2290-5.
[91] Yuhua Li, Chao Yang, Haidong Zhao, Shengguan Qu, Xiaoqiang Li, Li Y. New Developments of Ti-Based Alloys for Biomedical Applications. Materials 2014;7:1709-800.
[92] Yang ZY, Zheng XH, Cai W. Martensitic transformation and shape memory effect of Ti–V–Al lightweight high-temperature shape memory alloys. Scripta Materialia 2015;99:97-100.
[93] Calin M, Helth A, Gutierrez Moreno JJ, Bönisch M, Brackmann V, Giebeler L, et al. Elastic softening of β-type Ti–Nb alloys by indium (In) additions. Journal of the Mechanical Behavior of Biomedical Materials 2014;39:162-74.
[94] Duerig TW, Tolomeo DE, Wholey M. An overview of superelastic stent design. Minimally Invasive Therapy & Allied Technologies 2000;9:235-46.
[95] Hanada S, Yoshio T, Izumi O. Plastic deformation mode of retainedβ phase inβ-eutectoid Ti-Fe alloys. Journal of Materials Science 1986;21:866-70.
[96] Kent D, Wang G, Yu Z, Ma X, Dargusch M. Strength enhancement of a biomedical titanium alloy through a modified accumulative roll bonding technique. Journal of the Mechanical Behavior of Biomedical Materials 2011;4:405-16.
[97] Zhang DC, Yang S, Wei M, Mao YF, Tan CG, Lin JG. Effect of Sn addition on the microstructure and superelasticity in Ti–Nb–Mo–Sn Alloys. Journal of the Mechanical Behavior of Biomedical Materials 2012;13:156-65.

[98] Zong Y, Yuan G, Zhang X, Mao L, Niu J, Ding W. Comparison of biodegradable behaviors of AZ31 and Mg–Nd–Zn–Zr alloys in Hank's physiological solution. Materials Science and Engineering: B 2012;177:395-401.
[99] Zomorodian A, Garcia MP, Moura e Silva T, Fernandes JCS, Fernandes MH, Montemor MF. Corrosion resistance of a composite polymeric coating applied on biodegradable AZ31 magnesium alloy. Acta Biomaterialia 2013;9:8660-70.
[100] Busk RS. Magnesium and Its Alloys. Handbook of Materials Selection: John Wiley & Sons, Inc.; 2007. p. 259-65.
[101] Peuster M, Wohlsein P, Brügmann M, Ehlerding M, Seidler K, Fink C, et al. A novel approach to temporary stenting: Degradable cardiovascular stents produced from corrodible metal - Results 6-18 months after implantation into New Zealand white rabbits. Heart 2001;86:563-9.
[102] Di Mario C, Griffiths H, Goktekin O, Peeters N, Verbist J, Bosiers M, et al. Drug-eluting bioabsorbable magnesium stent. Journal of interventional cardiology 2004;17:391-5.
[103] Zartner P, Cesnjevar R, Singer H, Weyand M. First successful implantation of a biodegradable metal stent into the left pulmonary artery of a preterm baby. Catheterization and cardiovascular interventions : official journal of the Society for Cardiac Angiography & Interventions 2005;66:590-4.
[104] Werkhoven RJ, Sillekens WH, Van Lieshout JBJM. Processing aspects of magnesium alloy stent tube. Magnesium Technology2011. p. 419-24.
[105] Sadeghpour S, Abbasi SM, Morakabati M. Deformation-induced martensitic transformation in a new metastable β titanium alloy. Journal of Alloys and Compounds 2015;650:22-9.
[106] Grosdidier T, Combres Y, Gautier E, Philippe MJ. Effect of microstructure variations on the formation of deformation-induced martensite and associated tensile properties in a β metastable Ti alloy. Metallurgical and Materials Transactions A 2000;31:1095-106.
[107] Hanada S, Masahashi N, Jung TK. Effect of stress-induced α″ martensite on Young's modulus of β Ti－33.6Nb－4Sn alloy. Materials Science and Engineering: A 2013;588:403-10.
[108] Yang Y, Li GP, Cheng GM, Wang H, Zhang M, Xu F, et al. Stress-introduced α″ martensite and twinning in a multifunctional titanium alloy. Scripta Materialia 2008;58:9-12.
[109] Laheurte P, Eberhardt A, Philippe MJ. Influence of the microstructure on the pseudoelasticity of a metastable beta titanium alloy. Materials Science and Engineering: A 2005;396:223-30.
[110] Liang SX, Yin LX, Che HW, Jing R, Zhou YK, Ma MZ, et al. Effects of Al content on structure and mechanical properties of hot-rolled ZrTiAlV alloys. Materials and Design 2013;52:246-50.
[111] Zhang SZ, Liu GF, Chen LQ, Qiu JX, Li HH, Xie GM. Effect of carbon on hot deformation behaviour and microstructural evolution of near-a titanium alloy Ti-5.6Al-4.8Sn-2Zr-1Mo- 0.35Si-0.7Nd. Materials Science and Technology 2011;27:1045-52.
[112] Chai YW, Kim HY, Hosoda H, Miyazaki S. Self-accommodation in Ti–Nb shape memory alloys. Acta Materialia 2009;57:4054-64.
[113] Zhang YW, Li SJ, Obbard EG, Wang H, Wang SC, Hao YL, et al. Elastic properties of Ti-24Nb-4Zr-8Sn single crystals with bcc crystal structure. Acta Materialia 2011;59:3081-90.
[114] Tahara M, Kim HY, Hosoda H, Nam TH, Miyazaki S. Effect of nitrogen addition and annealing temperature on superelastic properties of Ti-Nb-Zr-Ta alloys. Materials Science and Engineering A 2010;527:6844-52.
[115] Al-Zain Y, Kim HY, Hosoda H, Nam TH, Miyazaki S. Shape memory properties of Ti-Nb-Mo biomedical alloys. Acta Materialia 2010;58:4212-23.
[116] Fukui Y, Inamura T, Hosoda H, Wakashima K, Miyazaki S. Mechanical properties of a Ti-Nb-Al shape memory alloy. Materials Transactions 2004;45:1077-82.
[117] Kim JI, Kim HY, Inamura T, Hosoda H, Miyazaki S. Shape memory characteristics of Ti-22Nb-(2-8)Zr(at.%) biomedical alloys. Materials Science and Engineering A 2005;403:334-9.
[118] Kim HS, Kim WY, Lim SH. Microstructure and elastic modulus of Ti-Nb-Si ternary alloys for biomedical applications. Scripta Materialia 2006;54:887-91.
[119] Paradkar A, Kamat SV, Gogia AK, Kashyap BP. Effect of Al and Nb on the trigger stress for stress-induced martensitic transformation during tensile loading in Ti–Al–Nb alloys. Materials Science and Engineering: A 2008;487:14-9.
[120] Bhattacharjee A, Bhargava S, Varma VK, Kamat SV, Gogia AK. Effect of β grain size on stress induced martensitic transformation in β solution treated Ti-10V-2Fe-3Al alloy. Scripta Materialia 2005;53:195-200.

[121] Boyer R, Welsch G, Collings EW. Materials Properties Handbook: Titanium Alloys. ASM International 1994.
[122] Lovey FC, Torra V. Shape memory in Cu-based alloys: phenomenological behavior at the mesoscale level and interaction of martensitic transformation with structural defects in Cu-Zn-Al. Progress in Materials Science 1999;44:189-289.
[123] Li C, Chen JH, Wu X, Wang W, Van Der Zwaag S. Tuning the stress induced martensitic formation in titanium alloys by alloy design. Journal of Materials Science 2012;47:4093-100.
[124] Kuan TS, Ahrens RR, Sass SL. The Stress-induced omega phase transformation in Ti-V alloys. Metallurgical Transactions A 1975;6:1767-74.
[125] Wang XL, Li L, Xing H, Ou P, Sun J. Role of oxygen in stress-induced ω phase transformation and {332}<113> mechanical twinning in β Ti-20V alloy. Scripta Materialia 2015;96:37-40.
[126] Yang Y, Castany P, Cornen M, Prima F, Li SJ, Hao YL, et al. Characterization of the martensitic transformation in the superelastic Ti–24Nb–4Zr–8Sn alloy by in situ synchrotron X-ray diffraction and dynamic mechanical analysis. Acta Materialia 2015;88:25-33.
[127] Duerig TW, Terlinde GT, Williams JC. Phase transformations and tensile properties of Ti-10V-2Fe-3AI. Metallurgical Transactions A 1980;11:1987-98.
[128] Ishiyama S, Hanada S. Effect of Zr, Sn and Al addition on the mechanical properties of metastable β titanium alloys. Sumitomo Search 1993:41-7.
[129] Ishiyama S, Hanada S, Izumi O. Effect of Zr, Sn and Al additions on deformation mode and beta phase stability of metastable beta Ti alloys. ISIJ International 1991;31:807-13.
[130] Baker C. Shape memory behavior in ti-35 wt % nb alloy. J Met Sci 1971;5:92-100.
[131] Grosdidier T, Roubaud C, Philippe MJ, Combres Y. The deformation mechanisms in the β-metastable β-cez titanium alloy. Scripta Materialia 1997;36:21-8.
[132] Gil FJ, Planell JA. Behaviour of normal grain growth kinetics in single phase titanium and titanium alloys. Materials Science and Engineering A 2000;283:17-24.
[133] Banerjee D, Muraleedharan K, Strudel JL. Substructure in titanium alloy martensite. Philosophical Magazine A: Physics of Condensed Matter, Structure, Defects and Mechanical Properties 1998;77:299-323.
[134] Bertrand E, Castany P, Gloriant T. An alternative way to orient the parent phase in the cubic/orthorhombic martensitic transformation of titanium shape memory alloys. Scripta Materialia 2014;83:41-4.
[135] Chai YW, Kim HY, Hosoda H, Miyazaki S. Self-accommodation in Ti-Nb shape memory alloys. Acta Materialia 2009;57:4054-64.
[136] Buenconsejo PJS, Kim HY, Hosoda H, Miyazaki S. Shape memory behavior of Ti-Ta and its potential as a high-temperature shape memory alloy. Acta Materialia 2009;57:1068-77.
[137] Zafari A, Wei XS, Xu W, Xia K. Formation of nanocrystalline β structure in metastable beta Ti alloy during high pressure torsion: The role played by stress induced martensitic transformation. Acta Materialia 2015;97:146-55.
[138] Glavicic MG, Kobryn PA, Bieler TR, Semiatin SL. An automated method to determine the orientation of the high-temperature beta phase from measured EBSD data for the low-temperature alpha-phase in Ti-6Al-4V. Materials Science and Engineering A 2003;351:258-64.
[139] Jiang L, Jonas JJ, Mishra RK, Luo AA, Sachdev AK, Godet S. Twinning and texture development in two Mg alloys subjected to loading along three different strain paths. Acta Materialia 2007;55:3899-910.
[140] Bertrand E, Castany P, Gloriant T. Investigation of the martensitic transformation and the damping behavior of a superelastic Ti-Ta-Nb alloy. Acta Materialia 2013;61:511-8.
[141] Xing H, Sun J. Mechanical twinning and omega transition by <111> {112} shear in a metastable β titanium alloy. Applied Physics Letters 2008;93:031908.
[142] Hao YL, Li SJ, Prima F, Yang R. Controlling reversible martensitic transformation in titanium alloys with high strength and low elastic modulus. Scripta Materialia 2012;67:487-90.
[143] Liu JP, Wang YD, Hao YL, Wang HL, Wang Y, Nie ZH, et al. High-energy X-ray diffuse scattering studies on deformation-induced spatially confined martensitic transformations in multifunctional Ti–24Nb–4Zr–8Sn alloy. Acta Materialia 2014;81:476-86.
[144] Al-Zain Y, Kim HY, Koyano T, Hosoda H, Nam TH, Miyazaki S. Anomalous temperature dependence of the superelastic behavior of Ti-Nb-Mo alloys. Acta Materialia 2011;59:1464-73.
[145] Tahara M, Kim HY, Inamura T, Hosoda H, Miyazaki S. Lattice modulation and superelasticity in oxygen-added β-Ti alloys. Acta Materialia 2011;59:6208-18.

[146] Tahara M, Kim HY, Hosoda H, Miyazaki S. Cyclic deformation behavior of a Ti-26 at.% Nb alloy. Acta Materialia 2009;57:2461-9.
[147] Besse M, Castany P, Gloriant T. Mechanisms of deformation in gum metal TNTZ-O and TNTZ titanium alloys: A comparative study on the oxygen influence. Acta Materialia 2011;59:5982-8.
[148] Obbard EG, Hao YL, Talling RJ, Li SJ, Zhang YW, Dye D, et al. The effect of oxygen on α″ martensite and superelasticity in Ti-24Nb-4Zr-8Sn. Acta Materialia 2011;59:112-25.
[149] Kim JI, Kim HY, Hosoda H, Miyazaki S. Shape memory behavior of Ti-22Nb-0.5-2.0O(at %) biomedical alloys. Materials Transactions 2005;46:852-7.
[150] Abdel-Hady M, Fuwa H, Hinoshita K, Kimura H, Shinzato Y, Morinaga M. Phase stability change with Zr content in β-type Ti-Nb alloys. Scripta Materialia 2007;57:1000-3.
[151] Miyazaki S, Kim HY, Hosoda H. Development and characterization of Ni-free Ti-base shape memory and superelastic alloys. Materials Science and Engineering A 2006;438-440:18-24.
[152] Otsuka K, Ren X. Physical metallurgy of Ti-Ni-based shape memory alloys. Progress in Materials Science 2005;50:511-678.
[153] Hao YL, Li SJ, Sun SY, Zheng CY, Hu QM, Yang R. Super-elastic titanium alloy with unstable plastic deformation. Applied Physics Letters 2005;87:091906.
[154] Zhang SQ, Li SJ, Jia MT, Prima F, Chen LJ, Hao YL, et al. Low-cycle fatigue properties of a titanium alloy exhibiting nonlinear elastic deformation behavior. Acta Materialia 2011;59:4690-9.
[155] Hao YL, Niinomi M, Kuroda D, Fukunaga K, Zhou YL, Yang R, et al. Young's modulus and mechanical properties of Ti-29Nb-13Ta-4.6Zr in relation to α″ martensite. Metallurgical and Materials Transactions A: Physical Metallurgy and Materials Science 2002;33:3137-44.
[156] Srinivasu G, Natraj Y, Bhattacharjee A, Nandy TK, Nageswara Rao GVS. Tensile and fracture toughness of high strength β Titanium alloy, Ti-10V-2Fe-3Al, as a function of rolling and solution treatment temperatures. Materials and Design 2013;47:323-30.
[157] Shekhar S, Sarkar R, Kar SK, Bhattacharjee A. Effect of solution treatment and aging on microstructure and tensile properties of high strength β titanium alloy, Ti-5Al-5V-5Mo-3Cr. Materials and Design 2015;66:596-610.
[158] Kent D, Wang G, Wang W, Dargusch MS. Influence of ageing temperature and heating rate on the properties and microstructure of β Ti alloy, Ti–6Cr–5Mo–5V–4Al. Materials Science and Engineering: A 2012;531:98-106.
[159] Ivasishin OM, Markovsky PE, Matviychuk YV, Semiatin SL, Ward CH, Fox S. A comparative study of the mechanical properties of high-strength β-titanium alloys. Journal of Alloys and Compounds 2008;457:296-309.
[160] Fan J, Li J, Kou H, Hua K, Tang B, Zhang Y. Influence of solution treatment on microstructure and mechanical properties of a near β titanium alloy Ti-7333. Materials & Design 2015;83:499-507.
[161] Wang L, Lu W, Qin J, Zhang F, Zhang D. Influence of cold deformation on martensite transformation and mechanical properties of Ti-Nb-Ta-Zr alloy. Journal of Alloys and Compounds 2009;469:512-8.
[162] Zhang DC, Mao YF, Li YL, Li JJ, Yuan M, Lin JG. Effect of ternary alloying elements on microstructure and superelastictity of Ti-Nb alloys. Materials Science and Engineering A 2013;559:706-10.
[163] Kim JI, Kim HY, Inamura T, Hosoda H, Miyazaki S. Effect of annealing temperature on microstructure and shape memory characteristics of Ti-22Nb-6Zr(at%) biomedical alloy. Materials Transactions 2006;47:505-12.
[164] Christian JW, Mahajan S. Deformation twinning. Progress in Materials Science 1995;39:1-157.
[165] Wu XL, Liao XZ, Srinivasan SG, Zhou F, Lavernia EJ, Valiev RZ, et al. New Deformation Twinning Mechanism Generates Zero Macroscopic Strain in Nanocrystalline Metals. Phys Rev Lett 2008;100:100.
[166] Ogata S, Li J, Yip S. Energy landscape of deformation twinning in bcc and fcc metals. Phys Rev B 2005;71:71.
[167] Yang Y, Li GP, Wang H, Wu SQ, Zhang LC, Li YL, et al. Formation of zigzag-shaped {112}〈111〉β mechanical twins in Ti－24.5 Nb－0.7 Ta－2 Zr－1.4 O alloy. Scripta Materialia 2012;66:211-4.
[168] Yang Y, Wu SQ, Li GP, Li YL, Lu YF, Yang K, et al. Evolution of deformation mechanisms of Ti-22.4Nb-0.73Ta-2Zr-1.34O alloy during straining. Acta Materialia 2010;58:2778-87.
[169] Qu L, Yang Y, Lu YF, Feng L, Ju JH, Ge P, et al. A detwinning process of {332}<113> twins in beta titanium alloys. Scripta Materialia 2013;69:389-92.

[170] Kuramoto S, Furuta T, Hwang J, Nishino K, Saito T. EBSP analysis on microstructure of gum metal after plastic deformation. Nippon Kinzoku Gakkaishi/Journal of the Japan Institute of Metals 2005;69:953-61.
[171] Crocker AG. Twinned martensite. Acta Metallurgica 1962;10:113-22.
[172] Mantani Y, Takemoto Y, Hida M, Sakakibara A. Formation of α″ martensite and {332}<113> twin during tensile deformation in Ti-40 mass%Nb alloy. Nippon Kinzoku Gakkaishi/Journal of the Japan Institute of Metals 2002;66:1022-9.
[173] Oberson PG, Ankem S. Why Twins Do Not Grow at the Speed of Sound All the Time. Phys Rev Lett 2005;95:95.
[174] Rusakov GM, Litvinov AV, Litvinov VS. Deformation twinning of titanium β-alloys of transition class. Met Sci Heat Treat 2006;48:244-51.
[175] Ueji R, Tsuchida N, Terada D, Tsuji N, Tanaka Y, Takemura A, et al. Tensile properties and twinning behavior of high manganese austenitic steel with fine-grained structure. Scripta Materialia 2008;59:963-6.
[176] Sun F, Zhang JY, Marteleur M, Brozek C, Rauch EF, Veron M, et al. A new titanium alloy with a combination of high strength, high strain hardening and improved ductility. Scripta Materialia 2015;94:17-20.
[177] Bracke L, Verbeken K, Kestens L, Penning J. Microstructure and texture evolution during cold rolling and annealing of a high Mn TWIP steel. Acta Materialia 2009;57:1512-24.
[178] Godet S, Jiang L, Luo AA, Jonas JJ. Use of Schmid factors to select extension twin variants in extruded magnesium alloy tubes. Scripta Materialia 2006;55:1055-8.
[179] Yi S, Schestakow I, Zaefferer S. Twinning-related microstructural evolution during hot rolling and subsequent annealing of pure magnesium. Materials Science and Engineering A 2009;516:58-64.
[180] Dudamell NV, Ulacia I, Gálvez F, Yi S, Bohlen J, Letzig D, et al. Twinning and grain subdivision during dynamic deformation of a Mg AZ31 sheet alloy at room temperature. Acta Materialia 2011;59:6949-62.
[181] Min XH, Tsuzaki K, Emura S, Tsuchiya K. Enhancement of uniform elongation in high strength Ti-Mo based alloys by combination of deformation modes. Materials Science and Engineering A 2011;528:4569-78.
[182] Min XH, Tsuzaki K, Emura S, Tsuchiya K. Heterogeneous twin formation and its effect on tensile properties in Ti-Mo based β titanium alloys. Materials Science and Engineering A 2012;554:53-60.
[183] Zhao X, Niinomi M, Nakai M, Miyamoto G, Furuhara T. Microstructures and mechanical properties of metastable Ti-30Zr-(Cr, Mo) alloys with changeable Young's modulus for spinal fixation applications. Acta Biomaterialia 2011;7:3230-6.
[184] Furuhara T, Kishimoto K, Maki T. Transmission Electron Microscopy of {332}<113> Deformation Twin in Ti-15V-3Cr-3Sn-3Al Alloy. Materials Transactions, JIM 1994;35:843-50.
[185] Zhao X, Niinomi M, Nakai M, Hieda J. Effect of Deformation-Induced omega Phase on the Mechanical Properties of Metastable beta-Type Ti-V Alloys. MATERIALS TRANSACTIONS 2012;53:1379-84.
[186] Williams JC, de Fontaine D, Paton NE. The ω-phase as an example of an unusual shear transformation. MT 1973;4:2701-8.
[187] Marteleur M, Sun F, Gloriant T, Vermaut P, Jacques PJ, Prima F. On the design of new β-metastable titanium alloys with improved work hardening rate thanks to simultaneous TRIP and TWIP effects. Scripta Materialia 2012;66:749-52.
[188] Min X, Emura S, Meng F, Mi G, Tsuchiya K. Mechanical twinning and dislocation slip multilayered deformation microstructures in β-type Ti–Mo base alloy. Scripta Materialia 2015;102:79-82.
[189] Hao YL, Li SJ, Sun SY, Yang R. Effect of Zr and Sn on Young's modulus and superelasticity of Ti-Nb-based alloys. Materials Science and Engineering A 2006;441:112-8.
[190] Ma J, Karaman I, Maier HJ, Chumlyakov YI. Superelastic cycling and room temperature recovery of Ti74Nb26 shape memory alloy. Acta Materialia 2010;58:2216-24.
[191] Kocks UF, Mecking H. Physics and phenomenology of strain hardening: The FCC case. Progress in Materials Science 2003;48:171-273.
[192] Takesue N, Shimizu Y, Yano T, Hara M, Kuramoto S. Single-crystal growth of Ti-Nb-Ta-Zr-O alloys and measurement of elastic properties. Journal of Crystal Growth 2009;311:3319-24.
[193] Morris Jr JW, Hanlumyuang Y, Sherburne M, Withey E, Chrzan DC, Kuramoto S, et al. Anomalous transformation-induced deformation in <1 1 0> textured Gum Metal. Acta Materialia 2010;58:3271-80.

[194] Matsumoto H, Watanabe S, Hanada S. Beta TiNbSn alloys with low Young's modulus and high strength. Materials Transactions 2005;46:1070-8.
[195] Jung TK, Lee HS, Semboshi S, Masahashi N, Abumiya T, Hanada S. A new concept of hip joint stem and its fabrication using metastable TiNbSn alloy. Journal of Alloys and Compounds 2012;536:S582-S5.
[196] Tane M, Akita S, Nakano T, Hagihara K, Umakoshi Y, Niinomi M, et al. Peculiar elastic behavior of Ti-Nb-Ta-Zr single crystals. Acta Materialia 2008;56:2856-63.
[197] Inamura T, Hosoda H, Wakashima K, Miyazaki S. Anisotropy and temperature dependence of young's modulus in textured TiNbAl biomedical shape memory alloy. Materials Transactions 2005;46:1597-603.
[198] Lee SH, Todai M, Tane M, Hagihara K, Nakajima H, Nakano T. Biocompatible low Young's modulus achieved by strong crystallographic elastic anisotropy in Ti-15Mo-5Zr-3Al alloy single crystal. Journal of the Mechanical Behavior of Biomedical Materials 2012;14:48-54.
[199] Jung TK, Semboshi S, Masahashi N, Hanada S. Mechanical properties and microstructures of β Ti-25Nb-11Sn ternary alloy for biomedical applications. Materials Science and Engineering C 2013;33:1629-35.
[200] Hall EO. The deformation and ageing of mild steel: III Discussion of results. Proceedings of the Physical Society Section B 1951;64:747-53.
[201] Sen I, Tamirisakandala S, Miracle DB, Ramamurty U. Microstructural effects on the mechanical behavior of B-modified Ti-6Al-4V alloys. Acta Materialia 2007;55:4983-93.
[202] Wang C, Wang M, Shi J, Hui W, Dong H. Effect of microstructure refinement on the strength and toughness of low alloy martensitic steel. Journal of Materials Science and Technology 2007;23:659-64.
[203] Liu MY, Shi B, Wang C, Ji SK, Cai X, Song HW. Normal Hall-Petch behavior of mild steel with submicron grains. Materials Letters 2003;57:2798-802.
[204] Collings EW, Walter JL, Jackson MR, Sims CT. Alloying. ASM International 1988:257.
[205] Fan Z, Tsakiropoulos P, Smith PA, Miodownik AP. Extension of the Hall-Petch relation to two-ductile-phase alloys. Philosophical Magazine A 1993;67:515-31.
[206] Montecinos S, Cuniberti A, Sepúlveda A. Grain size and pseudoelastic behaviour of a Cu-Al-Be alloy. Materials Characterization 2008;59:117-23.
[207] Meyers MA, Vöhringer O, Lubarda VA. The onset of twinning in metals: A constitutive description. Acta Materialia 2001;49:4025-39.
[208] Stanford N, Carlson U, Barnett MR. Deformation twinning and the Hall-Petch relation in commercial purity Ti. Metallurgical and Materials Transactions A: Physical Metallurgy and Materials Science 2008;39 A:934-44.
[209] Meyers MA, Andrade UR, Chokshi AH. The effect of grain size on the high-strain, high-strain-rate behavior of copper. Metallurgical and Materials Transactions A 1995;26:2881-93.
[210] Lahaie D, Embury JD, Chadwick MM, Gray GT. A note on the deformation of fine grained magnesium alloys. Scripta Metallurgica et Materiala 1992;27:139-42.
[211] Barbier D, Gey N, Sébastien A, Humbert M. Grain size effect on the tensile behavior of a FeMnC TWIP steel in relation with the microstructure and texture evolutions. Ceramic Transactions2008. p. 79-86.
[212] Cerreta E, Yablinsky CA, Gray Iii GT, Vogel SC, Brown DW. The influence of grain size and texture on the mechanical response of high purity hafnium. Materials Science and Engineering A 2007;456:243-51.
[213] Barnett MR, Keshavarz Z, Beer AG, Atwell D. Influence of grain size on the compressive deformation of wrought Mg-3Al-1Zn. Acta Materialia 2004;52:5093-103.
[214] Hull D. Effect of grain size and temperature on slip, twinning and fracture in 3% silicon iron. Acta Metallurgica 1961;9:191-204.
[215] Yu Q, Shan ZW, Li J, Huang X, Xiao L, Sun J, et al. Strong crystal size effect on deformation twinning. Nature 2010;463:335-8.
[216] Marcinkowski MJ, Lipsitt HA. The plastic deformation of chromium at low temperatures. Acta Metallurgica 1962;10:95-111.
[217] Barnett MR. A rationale for the strong dependence of mechanical twinning on grain size. Scripta Materialia 2008;59:696-8.
[218] Capolungo L, Marshall PE, McCabe RJ, Beyerlein IJ, Tomé CN. Nucleation and growth of twins in Zr: A statistical study. Acta Materialia 2009;57:6047-56.
[219] Capolungo L, Beyerlein IJ. Nucleation and stability of twins in hcp metals. Phys Rev B 2008;78.
[220] Beyerlein IJ, Tomé CN. A probabilistic twin nucleation model for HCP polycrystalline metals. Proceedings of the Royal Society A: Mathematical, Physical and Engineering Sciences 2010;466:2517-44.

[221] McCabe RJ, Proust G, Cerreta EK, Misra A. Quantitative analysis of deformation twinning in zirconium. International Journal of Plasticity 2009;25:454-72.
[222] Jain A, Duygulu O, Brown DW, Tomé CN, Agnew SR. Grain size effects on the tensile properties and deformation mechanisms of a magnesium alloy, AZ31B, sheet. Materials Science and Engineering A 2008;486:545-55.
[223] Min X, Chen X, Emura S, Tsuchiya K. Mechanism of twinning-induced plasticity in β-type Ti–15Mo alloy. Scripta Materialia 2013;69:393-6.
[224] Sun F, Prima F, Gloriant T. High-strength nanostructured Ti-12Mo alloy from ductile metastable beta state precursor. Materials Science and Engineering A 2010;527:4262-9.
[225] Sun F, Hao YL, Nowak S, Gloriant T, Laheurte P, Prima F. A thermo-mechanical treatment to improve the superelastic performances of biomedical Ti-26Nb and Ti-20Nb-6Zr (at.%) alloys. Journal of the Mechanical Behavior of Biomedical Materials 2011;4:1864-72.
[226] Talling RJ, Dashwood RJ, Jackson M, Dye D. On the mechanism of superelasticity in Gum metal. Acta Materialia 2009;57:1188-98.
[227] Min XH, Emura S, Sekido N, Nishimura T, Tsuchiya K, Tsuzaki K. Effects of Fe addition on tensile deformation mode and crevice corrosion resistance in Ti-15Mo alloy. Materials Science and Engineering A 2010;527:2693-701.
[228] Min X, Chen X, Emura S, Tsuchiya K. Mechanism of twinning-induced plasticity in β-type Ti-15Mo alloy. Scripta Materialia 2013;69:393-6.
[229] Hanada S, Yoshio T, Izumi O. Effect of plastic deformation modes on tensile properties of beta titanium alloys. Transactions of the Japan Institute of Metals 1986;27:496-503.
[230] Weiss I, Semiatin SL. Thermomechanical processing of beta titanium alloys - An overview. Materials Science and Engineering A 1998;243:46-65.
[231] Sun F, Nowak S, Gloriant T, Laheurte P, Eberhardt A, Prima F. Influence of a short thermal treatment on the superelastic properties of a titanium-based alloy. Scripta Materialia 2010;63:1053-6.
[232] Ando D, Koike J, Sutou Y. The role of deformation twinning in the fracture behavior and mechanism of basal textured magnesium alloys. Materials Science and Engineering: A 2014;600:145-52.
[233] Stanford N, Geng J, Chun YB, Davies CHJ, Nie JF, Barnett MR. Effect of plate-shaped particle distributions on the deformation behaviour of magnesium alloy AZ91 in tension and compression. Acta Materialia 2012;60:218-28.
[234] Lou XY, Li M, Boger RK, Agnew SR, Wagoner RH. Hardening evolution of AZ31B Mg sheet. International Journal of Plasticity 2007;23:44-86.
[235] Koike J, Sato Y, Ando D. Origin of the Anomalous {10-12} Twinning during Tensile Deformation of Mg Alloy Sheet. MATERIALS TRANSACTIONS 2008;49:2792-800.
[236] Hong SG, Park SH, Lee CS. Role of {10-12} twinning characteristics in the deformation behavior of a polycrystalline magnesium alloy. Acta Materialia 2010;58:5873-85.
[237] Couret A, Caillard D. An in situ study of prismatic glide in magnesium-I. The rate controlling mechanism. Acta Metallurgica 1985;33:1447-54.
[238] Yoshinaga H, Obara T, Morozumi S. Twinning deformation in magnesium compressed along the C-axis. Materials Science and Engineering 1973;12:255-64.
[239] Barnett MR, Keshavarz Z, Beer AG, Ma X. Non-Schmid behaviour during secondary twinning in a polycrystalline magnesium alloy. Acta Materialia 2008;56:5-15.
[240] Cizek P, Barnett MR. Characteristics of the contraction twins formed close to the fracture surface in Mg–3Al–1Zn alloy deformed in tension. Scripta Materialia 2008;59:959-62.
[241] Agnew SR, Tomé CN, Brown DW, Holden TM, Vogel SC. Study of slip mechanisms in a magnesium alloy by neutron diffraction and modeling. Scripta Materialia 2003;48:1003-8.
[242] Gehrmann R, Frommert MM, Gottstein G. Texture effects on plastic deformation of magnesium. Materials Science and Engineering: A 2005;395:338-49.
[243] Yi SB, Davies CHJ, Brokmeier HG, Bolmaro RE, Kainer KU, Homeyer J. Deformation and texture evolution in AZ31 magnesium alloy during uniaxial loading. Acta Materialia 2006;54:549-62.
[244] Keshavarz Z, Barnett MR. EBSD analysis of deformation modes in Mg-3Al-1Zn. Scripta Materialia 2006;55:915-8.
[245] Liu WK, Karpov EG, Park HS. Classical Molecular Dynamics. Nano Mechanics and Materials: John Wiley & Sons, Ltd; 2006. p. 7-36.
[246] Barnett MR, Keshavarz Z, Nave MD. Microstructural features of rolled Mg-3Al-1Zn. Metallurgical and Materials Transactions A: Physical Metallurgy and Materials Science 2005;36:1697-704.

[247] Lou C, Zhang X, Duan G, Tu J, Liu Q. Characteristics of different {10-12} twin variants in magnesium alloy during room temperature dynamic plastic deformation. Journal of Materials Research 2013;28:1885-90.
[248] Jiang J, Godfrey A, Liu W, Liu Q. Identification and analysis of twinning variants during compression of a Mg-Al-Zn alloy. Scripta Materialia 2008;58:122-5.
[249] Beyerlein IJ, Capolungo L, Marshall PE, McCabe RJ, Tomé CN. Statistical analyses of deformation twinning in magnesium. Philosophical Magazine 2010;90:2161-90.
[250] Niezgoda SR, Kanjarla AK, Beyerlein IJ, Tomé CN. Stochastic modeling of twin nucleation in polycrystals: An application in hexagonal close-packed metals. International Journal of Plasticity 2014;56:119-38.
[251] Jiang XJ, Jing R, Ma MZ, Liu RP. The orthorhombic α″ martensite transformation during water quenching and its influence on mechanical properties of Ti-41Zr-7.3Al alloy. Intermetallics 2014;52:32-5.
[252] Koike J, Ohyama R. Geometrical criterion for the activation of prismatic slip in AZ61 Mg alloy sheets deformed at room temperature. Acta Materialia 2005;53:1963-72.
[253] Cizek P, Barnett MR. Characteristics of the contraction twins formed close to the fracture surface in Mg-3Al-1Zn alloy deformed in tension. Scripta Materialia 2008;59:959-62.
[254] Martin É, Capolungo L, Jiang L, Jonas JJ. Variant selection during secondary twinning in Mg-3%Al. Acta Materialia 2010;58:3970-83.
[255] Ando D, Koike J, Sutou Y. Relationship between deformation twinning and surface step formation in AZ31 magnesium alloys. Acta Materialia 2010;58:4316-24.
[256] Al-Samman T, Gottstein G. Room temperature formability of a magnesium AZ31 alloy: Examining the role of texture on the deformation mechanisms. Materials Science and Engineering A 2008;488:406-14.
[257] Wang B, Deng L, Guo N, Xu Z, Li Q. EBSD analysis of {10–12} twinning activity in Mg–3Al–1Zn alloy during compression. Materials Characterization 2014;98:180-5.
[258] Hong SG, Park SH, Lee CS. Strain path dependence of {10-12} twinning activity in a polycrystalline magnesium alloy. Scripta Materialia 2011;64:145-8.
[259] Barnett MR, Keshavarz Z, Beer AG, Atwell D. Influence of grain size on the compressive deformation of wrought Mg–3Al–1Zn. Acta Materialia 2004;52:5093-103.
[260] Xin Y, Wang M, Zeng Z, Nie M, Liu Q. Strengthening and toughening of magnesium alloy by {10-12} extension twins. Scripta Materialia 2012;66:25-8.
[261] Hyuk Park S, Hong S-G, Lee CS. In-plane anisotropic deformation behavior of rolled Mg–3Al–1Zn alloy by initial {10–12} twins. Materials Science and Engineering: A 2013;570:149-63.
[262] Karaman I, Sehitoglu H, Beaudoev AJ, Chumlyakov YI, Maier HJ, Tomé CN. Modeling the deformation behavior of Hadfield steel single and polycrystals due to twinning and slip. Acta Materialia 2000;48:2031-47.
[263] Song WQ, Sun S, Zhu S, Wang G, Wang J, Dargusch MS. Compressive deformation behavior of a near-beta titanium alloy. Materials and Design 2012;34:739-45.
[264] Jordon JB, Gibson JB, Horstemeyer MF, Kadiri HE, Baird JC, Luo AA. Effect of twinning, slip, and inclusions on the fatigue anisotropy of extrusion-textured AZ61 magnesium alloy. Materials Science and Engineering: A 2011;528:6860-71.
[265] Wang B, Xin R, Huang G, Liu Q. Effect of crystal orientation on the mechanical properties and strain hardening behavior of magnesium alloy AZ31 during uniaxial compression. Materials Science and Engineering A 2012;534:588-93.
[266] Song B, Guo N, Liu T, Yang Q. Improvement of formability and mechanical properties of magnesium alloys via pre-twinning: A review. Materials & Design 2014;62:352-60.
[267] Tenckhoff E. Deformation Mechanisms, Texture, and Anisotropy in Zirconium and Zircaloy1988.
[268] Xin Y, Zhou X, Liu Q. Suppressing the tension-compression yield asymmetry of Mg alloy by hybrid extension twins structure. Materials Science and Engineering A 2013;567:9-13.
[269] Reed-Hill RE, Robertson WD. The crystallographic characteristics of fracture in magnesium single crystals. Acta Metallurgica 1957;5:728-37.
[270] Hartt WH. The irrational habit of second-order {10-11}-{10-12} twins in magnesium. Trans Metall Soc AIME 1967;239.
[271] Hartt WH. Internal Deformation and Fracture of Second-order {10-11}-{10-12} Twins in Magnesium. Trans Metall Soc AIME 1968;242:1127-33.
[272] Ando D, Koike J. Relationship between deformation-induced surface relief and double twinning in AZ31 magnesium alloy. Nippon Kinzoku Gakkaishi/Journal of the Japan Institute of Metals 2007;71:684-7.

[273] Somekawa H, Mukai T. Fracture toughness in a rolled AZ31 magnesium alloy. Journal of Alloys and Compounds 2006;417:209-13.
[274] Somekawa H, Mukai T. Effect of texture on fracture toughness in extruded AZ31 magnesium alloy. Scripta Materialia 2005;53:541-5.
[275] Somekawa H, Mukai T. Effect of grain refinement on fracture toughness in extruded pure magnesium. Scripta Materialia 2005;53:1059-64.
[276] Somekawa H, Singh A, Mukai T. Fracture mechanism of a coarse-grained magnesium alloy during fracture toughness testing. Philosophical Magazine Letters 2009;89:2-10.
[277] Somekawa H, Nakajima K, Singh A, Mukai T. Ductile fracture mechanism in fine-grained magnesium alloy. Philosophical Magazine Letters 2010;90:831-9.
[278] Wu L, Jain A, Brown DW, Stoica GM, Agnew SR, Clausen B, et al. Twinning-detwinning behavior during the strain-controlled low-cycle fatigue testing of a wrought magnesium alloy, ZK60A. Acta Materialia 2008;56:688-95.
[279] Park SH, Hong SG, Lee CS. Role of initial {10-12} twin in the fatigue behavior of rolled Mg-3Al-1Zn alloy. Scripta Materialia 2010;62:666-9.
[280] Kaushik V, Narasimhan R, Mishra RK. Experimental study of fracture behavior of magnesium single crystals. Materials Science and Engineering A 2014;590:174-85.
[281] ASTM. Standard Test Methods for Determining Average Grain Size. West Conshohocken, PA2013.
[282] Guan L, Tang G, Jiang Y, Chu PK. Texture evolution in cold-rolled AZ31 magnesium alloy during electropulsing treatment. Journal of Alloys and Compounds 2009;487:309-13.
[283] Chino Y, Hoshika T, Lee J-S, Mabuchi M. Mechanical properties of AZ31 Mg alloy recycled by severe deformation. Journal of Materials Research 2006;21:754-60.
[284] Zhang L, Liu C-G, Wang H-Y, Nan X-L, Xiao W, Jiang Q-C. Twinning and mechanical behavior of an extruded Mg–6Al–3Sn alloy with a dual basal texture. Materials Science and Engineering: A 2013;578:14-7.
[285] Chino Y, Kimura K, Mabuchi M. Twinning behavior and deformation mechanisms of extruded AZ31 Mg alloy. Materials Science and Engineering: A 2008;486:481-8.
[286] Ion SE, Humphreys FJ, White SH. Dynamic recrystallisation and the development of microstructure during the high temperature deformation of magnesium. Acta Metallurgica 1982;30:1909-19.
[287] Al-Samman T, Molodov KD, Molodov DA, Gottstein G, Suwas S. Softening and dynamic recrystallization in magnesium single crystals during c-axis compression. Acta Materialia 2012;60:537-45.
[288] del Valle JA, Carreño F, Ruano OA. Influence of texture and grain size on work hardening and ductility in magnesium-based alloys processed by ECAP and rolling. Acta Materialia 2006;54:4247-59.
[289] Zhang Z, Rauch EF, Véron M. Twinning analyses in a magnesium alloy with tilting series scanning method using a TEM based orientation mapping system. Materials Letters 2013;111:192-6.
[290] Ranjbar Bahadori S, Dehghani K, Bakhshandeh F. Microstructure, texture and mechanical properties of pure copper processed by ECAP and subsequent cold rolling. Materials Science and Engineering: A 2013;583:36-42.
[291] Liang S, Sun H, Liu Z, Wang E. Mechanical properties and texture evolution during rolling process of an AZ31 Mg alloy. Journal of Alloys and Compounds 2009;472:127-32.
[292] Kim S-H, You B-S, Dong Yim C, Seo Y-M. Texture and microstructure changes in asymmetrically hot rolled AZ31 magnesium alloy sheets. Materials Letters 2005;59:3876-80.
[293] Ma Q, El Kadiri H, Oppedal AL, Baird JC, Li B, Horstemeyer MF, et al. Twinning effects in a rod-textured AM30 Magnesium alloy. International Journal of Plasticity 2012;29:60-76.
[294] Park SH, Hong S-G, Lee JH, Lee CS. Multiple twinning modes in rolled Mg–3Al–1Zn alloy and their selection mechanism. Materials Science and Engineering: A 2012;532:401-6.
[295] Mu S, Jonas JJ, Gottstein G. Variant selection of primary, secondary and tertiary twins in a deformed Mg alloy. Acta Materialia 2012;60:2043-53.
[296] Oppedal AL, El Kadiri H, Tomé CN, Kaschner GC, Vogel SC, Baird JC, et al. Effect of dislocation transmutation on modeling hardening mechanisms by twinning in magnesium. International Journal of Plasticity 2012;30–31:41-61.
[297] Miao Q, Hu L, Wang G, Wang E. Fabrication of excellent mechanical properties AZ31 magnesium alloy sheets by conventional rolling and subsequent annealing. Materials Science and Engineering: A 2011;528:6694-701.
[298] Jiang L, Jonas JJ, Luo AA, Sachdev AK, Godet S. Twinning-induced softening in polycrystalline AM30 Mg alloy at moderate temperatures. Scripta Materialia 2006;54:771-5.

[299] Collings EW, Gegel HL. A Physical Basis for Solid-solution Strengthening and Phase Stability in Alloys of Titanium. Scripta Mater 1973;7:437-43.
[300] Duerig TW, Albrecht J, Richter D, Fischer P. Formation and reversion of stress induced martensite in Ti-10V-2Fe-3Al. Acta Metallurgica 1982;30:2161-72.
[301] Mikulewicz M, Chojnacka K. Cytocompatibility of Medical Biomaterials Containing Nickel by Osteoblasts: a Systematic Literature Review. Biol Trace Elem Res 2011;142:865-89.
[302] Es-Souni M, Es-Souni M, Fischer-Brandies H. Assessing the biocompatibility of NiTi shape memory alloys used for medical applications. Anal Bioanal Chem 2005;381:557-67.
[303] Shabalovskaya S, Anderegg J, Van Humbeeck J. Critical overview of Nitinol surfaces and their modifications for medical applications. Acta Biomaterialia 2008;4:447-67.
[304] Malard B, Pilch J, Sittner P, Delville R, Curfs C. In situ investigation of the fast microstructure evolution during electropulse treatment of cold drawn NiTi wires. Acta Materialia 2011;59:1542-56.
[305] Undisz A, Fink M, Rettenmayr M. Response of austenite finish temperature and phase transformation characteristics of thin medical-grade Ni-Ti wire to short-time annealing. Scripta Materialia 2008;59:979-82.
[306] Kim HY, Satoru H, Kim JI, Hosoda H, Miyazaki S. Mechanical properties and shape memory behavior of Ti-Nb alloys. Materials Transactions 2004;45:2443-8.
[307] Xu W, Kim KB, Das J, Calin M, Rellinghaus B, Eckert J. Deformation-induced nanostructuring in a Ti–Nb–Ta–In β alloy. Applied Physics Letters 2006;89:031906.
[308] Ikeda M, Komatsu S-y, Sugimoto T, Kamei K. Reverse transformation of α″ and initial β decomposition in quenched Ti-Nb binary alloys. Nippon Kinzoku Gakkai-si 1989;53:664-71.
[309] Bhattacharjee A, Varma VK, Kamat SV, Gogia AK, Bhargava S. Influence of β grain size on tensile behavior and ductile fracture toughness of titanium alloy Ti-10V-2Fe-3Al. Metallurgical and Materials Transactions A 2006;37:1423-33.
[310] Guo S, Meng QK, Cheng XN, Zhao XQ. Deformation behavior of metastable β-type Ti–25Nb–2Mo–4Sn alloy for biomedical applications. Journal of the Mechanical Behavior of Biomedical Materials 2014;38:26-32.
[311] Al-Zain Y, Kim HY, Koyano T, Hosoda H, Nam TH, Miyazaki S. Anomalous temperature dependence of the superelastic behavior of Ti–Nb–Mo alloys. Acta Materialia 2011;59:1464-73.
[312] Cai M-H, Lee C-Y, Kang S, Lee Y-K. Fine-grained structure fabricated by strain-induced martensite and its reverse transformations in a metastable β titanium alloy. Scripta Materialia 2011;64:1098-101.
[313] He Y, Zhang W, Zhou H, Lu Y, Xi Z. Decomposition of orthorhombic martensite in TC21 alloy during aging treatment. Xiyou Jinshu Cailiao Yu Gongcheng/Rare Metal Materials and Engineering 2012;41:800-4.
[314] Filip R, Kubiak K, Ziaja W, Sieniawski J. The effect of microstructure on the mechanical properties of two-phase titanium alloys. Journal of Materials Processing Technology 2003;133:84-9.
[315] Akanuma T, Matsumoto H, Sato S, Chiba A, Inagaki I, Shirai Y, et al. Enhancement of athermal α″ martensitic transformation in Ti－10V－2Fe－3Al alloy due to high-speed hot deformation. Scripta Materialia 2012;67:21-4.
[316] Saito T, Furuta T, Hwang J-H, Kuramoto S, Nishino K, Suzuki N, et al. Multifunctional Alloys Obtained via a Dislocation-Free Plastic Deformation Mechanism. Science 2003;300:464-7.
[317] Geng F, Niinomi M, Nakai M. Observation of yielding and strain hardening in a titanium alloy having high oxygen content. Materials Science and Engineering: A 2011;528:5435-45.
[318] Li SJ, Cui TC, Hao YL, Yang R. Fatigue properties of a metastable β-type titanium alloy with reversible phase transformation. Acta Biomaterialia 2008;4:305-17.
[319] Hao YL, Li SJ, Sun SY, Yang R. Effect of Zr and Sn on Young's modulus and superelasticity of Ti–Nb-based alloys. Materials Science and Engineering: A 2006;441:112-8.
[320] Salem AA, Kalidindi SR, Semiatin SL. Strain hardening due to deformation twinning in α-titanium: Constitutive relations and crystal-plasticity modeling. Acta Materialia 2005;53:3495-502.
[321] Xu W, Wu X, Calin M, Stoica M, Eckert J, Xia K. Formation of an ultrafine-grained structure during equal-channel angular pressing of a β-titanium alloy with low phase stability. Scripta Materialia 2009;60:1012-5.
[322] Terlinde GT, Duerig TW, Williams JC. Microstructure, tensile deformation, and fracture in aged ti 10V-2Fe-3Al. Metallurgical Transactions A 1983;14:2101-15.
[323] Sauer C, Lütjering G. Influence of α layers at β grain boundaries on mechanical properties of Ti-alloys. Materials Science and Engineering: A 2001;319–321:393-7.

[324] Du Z, Xiao S, Xu L, Tian J, Kong F, Chen Y. Effect of heat treatment on microstructure and mechanical properties of a new β high strength titanium alloy. Materials & Design 2014;55:183-90.
[325] Wen M, Wen C, Hodgson P, Li Y. Fabrication of Ti–Nb–Ag alloy via powder metallurgy for biomedical applications. Materials & Design 2014;56:629-34.
[326] Bai XF, Zhao YQ, Zhang YS, Zeng WD, Yu S, Wang G. Texture evolution in TLM titanium alloy during uniaxial compression. Materials Science and Engineering: A 2013;588:29-33.
[327] Laheurte P, Prima F, Eberhardt A, Gloriant T, Wary M, Patoor E. Mechanical properties of low modulus titanium alloys designed from the electronic approach. Journal of the Mechanical Behavior of Biomedical Materials 2010;3:565-73.
[328] Ozaki T, Matsumoto H, Watanabe S, Hanada S. Beta Ti Alloys with Low Young's Modulus. Materials Transactions 2004;45:2776-9.
[329] Hayama AOF, Lopes JFSC, Gomes da Silva MJ, Abreu HFG, Caram R. Crystallographic texture evolution in Ti–35Nb alloy deformed by cold rolling. Materials & Design 2014;60:653-60.
[330] Matsumoto H, Watanabe S, Hanada S. Microstructures and mechanical properties of metastable β TiNbSn alloys cold rolled and heat treated. Journal of Alloys and Compounds 2007;439:146-55.
[331] Furuta T, Kuramoto S, Hwang J, Nishino K, Saito T. Elastic deformation behavior of multi-functional Ti-Nb-Ta-Zr-O alloys. Materials Transactions 2005;46:3001-7.
[332] Mahajan S, Chin GY. Formation of deformation twins in f.c.c. crystals. Acta Metallurgica 1973;21:1353-63.
[333] Gray G, T. Influence of Strain Rate and Temperature on the Structure. Property Behavior of High-Purity Titanium. J Phys IV France 1997;07:C3-423-C3-8.
[334] Salem AA, Kalidindi SR, Doherty RD. Strain hardening regimes and microstructure evolution during large strain compression of high purity titanium. Scripta Materialia 2002;46:419-23.
[335] Song SG, Gray GT. Influence of temperature and strain rate on slip and twinning behavior of zr. Metallurgical and Materials Transactions A 1995;26:2665-75.
[336] Salem AA, Kalidindi SR, Doherty RD. Strain hardening of titanium: role of deformation twinning. Acta Materialia 2003;51:4225-37.
[337] Lagerlöf KPD. On deformation twinning in b.c.c. metals. Acta Metallurgica et Materialia 1993;41:2143-51.
[338] Wang L, Huang G, Quan Q, Bassani P, Mostaed E, Vedani M, et al. The Effect of Twinning and Detwinning on the Mechanical Property of AZ31 Extruded Magnesium Alloy during Strain-path Changes. Materials & Design.
[339] Galindo-Nava EI. Modelling twinning evolution during plastic deformation in hexagonal close-packed metals. Materials & Design 2015;83:327-43.
[340] Luo JR, Godfrey A, Liu W, Liu Q. Twinning behavior of a strongly basal textured AZ31 Mg alloy during warm rolling. Acta Materialia 2012;60:1986-98.
[341] Zhang Y, Kent D, Wang G, StJohn D, Dargusch MS. The cold-rolling behaviour of AZ31 tubes for fabrication of biodegradable stents. Journal of the Mechanical Behavior of Biomedical Materials 2014;39:292-303.
[342] Song B, Xin R, Liang Y, Chen G, Liu Q. Twinning characteristic and variant selection in compression of a pre-side-rolled Mg alloy sheet. Materials Science and Engineering: A 2014;614:106-15.
[343] Beyerlein IJ, McCabe RJ, Tomé CN. Effect of microstructure on the nucleation of deformation twins in polycrystalline high-purity magnesium: A multi-scale modeling study. Journal of the Mechanics and Physics of Solids 2011;59:988-1003.
[344] Guo C, Xin R, Xu J, Song B, Liu Q. Strain compatibility effect on the variant selection of connected twins in magnesium. Materials & Design 2015;76:71-6.
[345] Barnett MR, Nave MD, Ghaderi A. Yield point elongation due to twinning in a magnesium alloy. Acta Materialia 2012;60:1433-43.
[346] Wu BL, Wan G, Zhang YD, Esling C. Twinning characteristics in textured AZ31 alloy under impact loading along specified direction. Materials Letters 2010;64:636-9.
[347] Guo C, Xin R, Ding C, Song B, Liu Q. Understanding of variant selection and twin patterns in compressed Mg alloy sheets via combined analysis of Schmid factor and strain compatibility factor. Materials Science and Engineering: A 2014;609:92-101.
[348] Tucker GEG. Comment on "Rolling textures in f.c.c. and b.c.c. metals". Acta Metallurgica 1964;12:1093-4.

[349] Dillamore IL, Roberts WT. Rolling textures in f.c.c. and b.c.c. metals. Acta Metallurgica 1964;12:281-93.
[350] Yang HJ, Yin SM, Huang CX, Zhang ZF, Wu SD, Li SX, et al. EBSD Study on Deformation Twinning in AZ31 Magnesium Alloy During Quasi-in-Situ Compression. Advanced Engineering Materials 2008;10:955-60.
[351] Nave MD, Barnett MR. Microstructures and textures of pure magnesium deformed in plane-strain compression. Scripta Materialia 2004;51:881-5.
[352] Wang L, Yang Y, Eisenlohr P, Bieler TR, Crimp MA, Mason DE. Twin nucleation by slip transfer across grain boundaries in commercial purity titanium. Metallurgical and Materials Transactions A: Physical Metallurgy and Materials Science 2010;41:421-30.
[353] Song X, Wang L, Niinomi M, Nakai M, Liu Y. Fatigue characteristics of a biomedical β-type titanium alloy with titanium boride. Materials Science and Engineering: A 2015;640:154-64.
[354] Zhang SQ, Li SJ, Jia MT, Hao YL, Yang R. Fatigue properties of a multifunctional titanium alloy exhibiting nonlinear elastic deformation behavior. Scripta Materialia 2009;60:733-6.
[355] Park SH, Lee JH, Huh YH, Hong SG. Enhancing the effect of texture control using {1 0-1 2} twins by retarding detwinning activity in rolled Mg-3Al-1Zn alloy. Scripta Materialia 2013;69:797-800.